Production, Characterization and Electrochemical Properties of Advanced Bulk Metallic Glasses for Hip Implant Applications

Master Thesis

Ali Tabeshian

NTNU
Norwegian University of
Science and Technology

Department of Materials Science and Engineering

Spring 2011

I hereby declare that this work has been carried out independently and in compliance with the examination regulations of the Norwegian University of Science and Technology, NTNU.

Ali Tabeshian

Stockholm, July 2011

Acknowledgment

This is the Master Thesis at the Norwegian University of Science and Technology (NTNU). The work submitted is my own and is based on experimental work carried out at NTNU, Trondheim, Royal Institute of Technology (KTH), Stockholm and Swerea KIMAB institute in Stockholm.

I would like to express my sincere gratitude to my supervisor Professor Ragnhild E. Aune for providing the theoretical framework for the project, and discussion of the results obtained in the experiments.

My deepest appreciation to Dan Persson, my supervisor in Swerea KIMAB Stockholm Sweden for his supervision and guidance in planning and performing the experimental works and analysis of the results obtained in the experiments.

I am grateful to Dr. Steven Savage and Dr. Shahid Akhtar to give me valuable information about my research and supporting me during my work.

I would like to extend my gratitude to professors A. Inoue and Y. Yokoyama of Tohoku University, Japan, whose contribution of $Zr_{55}Cu_{30}Ni_5Al_{10}$ BMG made this project possible.

I thank my family, friends and all of my colleagues in Swerea KIMAB for providing a suitable environment for me to complete my thesis work.

Last but certainly not least I wish to thank my wife Maryam for her love, support and care.

Ali Tabeshian

Stockholm, July 2011

Abstract

The aim of the present project was to investigate the possibilities of using a $Zr_{55}Cu_{30}Ni_5Al_{10}$ Bulk Metallic Glass (BMG) alloy as articulating surface in an artificial hip joint.

In order for a material to be used in human body as an implant, the foremost requirement is the acceptability by the human body. The implantations should not cause diseases or other complications for the patients. Moreover, the biomaterials should possess sufficient mechanical strength, high corrosion and wear resistance in harsh body environment with varying loading conditions.

There have been extensive research on the properties of stainless steel, Co-Cr-Mo alloys and Ti alloys regarding their bio-compatibility and they are currently being used as orthopedic implants, however less information is available for bulk metallic glasses. So, understanding the corrosion properties of BMGs is one of the key issues to evaluate their potential as biomaterials.

In the first phase of the project there was an attempt to develop a Zr-based BMG from pure elements in a vertical resistance furnace and quenching in liquid nitrogen. Afterwards, samples were examined by X-Ray diffraction and microscopically to investigate the presence of crystalline phases.

The second phase was electrochemical measurements to study the passivation behavior and the susceptibility to pitting corrosion for the crystalline $Zr_{55}Cu_{30}Ni_5Al_{10}$, amorphous $Zr_{55}Cu_{30}Ni_5Al_{10}$ BMG (received from Japan) and comparing the result with stainless steel and Co-Cr-Mo (F75). Investigations on corrosion properties were made in phosphate-buffered saline (PBS) with and without the addition of albumin fraction V, at a room temperature of 20 °C and body temperature (37°C) and in different pH values of 7.4 and 5.2. Running the experiment in lower pH shows the behavior of the implant against any probable inflation in the patient body.

The last phase was to investigate the interaction between the protein and surface of materials. For this purpose, FTIR spectroscopy and Electrochemical Impedance Spectroscopy (EIS) were carried out.

Keys words: Biomaterials, Bulk Metallic Glass, Crystalline $Zr_{55}Cu_{30}Ni_5Al_{10}$, Co-Cr-Mo alloy, Stainless steel, Polarization curve, FTIR, Impedance.

Table of Contents

1. Introduction

The hip is one of the largest weight bearing joints in a human body. The hip joint has two main parts. On the top of the thighbone there is a ball shaped part, which is the femoral head that fits into the acetabulum (rounded socket). The stability of this joint is provided by ligaments, bands of tissue that connect the femoral head to the acetabulum as shown in Figure 1.1.

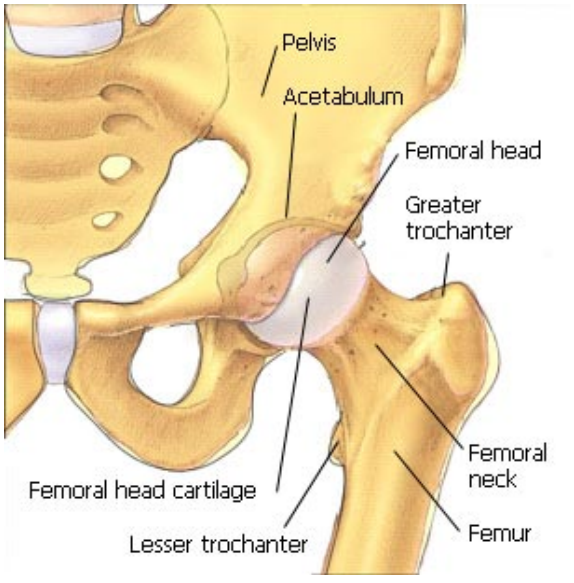

Figure 1.1: The hip joint structure [1]

A soft tissue called cartilage has covered the femoral head. Cartilage can wear as a result of different diseases. Without the presence of the cartilage, there is no protection between the bony surfaces of the femoral head (ball) and the acetabulum (socket). So, this can be a start of the rubbing these two parts against each other and they become rough eventually. This can even change the shape of the bone and causes a lot of pain especially during body movement (Fig 2.1).

Conditions that can lead to an unhealthy or painful hip include [2]:

• Rheumatoid arthritis: a chronic disease affecting primarily the lining of the joint results in destruction and deformity.

• Osteoarthritis: affects the joint surfaces of weight bearing areas of the joints. Although the exact reason of osteoarthritis is unknown, it is believed to be caused by abnormal wear and tear to the joint surfaces. Other factors that may contribute to osteoarthritis include age, sex, heredity and obesity.

• Other causes of deterioration of the hip include previous hip injury, metabolic bone disease, and abnormalities of growth.

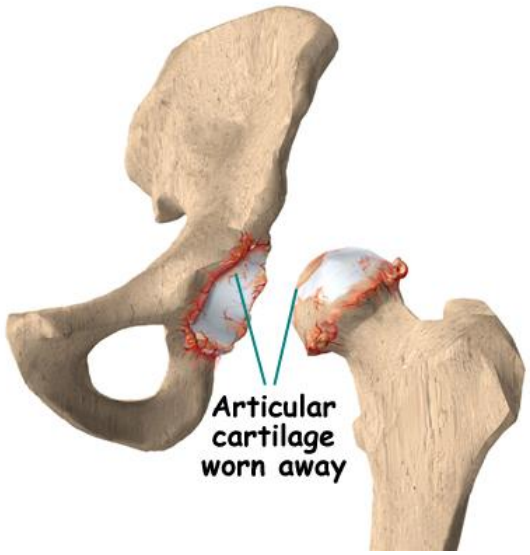

Fig 2.1: Articular cartilage worn away [3].

Total Hip Replacement (THR) has become a common surgery due to increase in the life expectancy and aging population of people. Moreover, about 20% of the hip injuries are caused by accidents.

According to the U.S. Department of Health and Human Services, from 1996 to 2006, total hip replacement discharges increased by one-third (to 19 per 10,000) population and it is predicted that this number will grow two times than the current value by 2030[4]. Canadian Joint Replacement Registry (CJRR) reported that in 2003 the age-standardized rate for women was 65.3 per 100,000 compared to 56.2 for men [5]. In the report from National Joint Registry, which shows the approximate number of 72,000 hip procedures in United Kingdom in 2008[6]. In Norway, the number of total hip joint replacements was about 7918 in 2008 [7] and 14105 total hip replacement in Sweden in 2007[8].

Hip implants are also important from the economic point of view for bio-medical industry. For example, For the United States, the biomaterials market has been estimated at about $9 billion as of the year 2000, with a growth rate of 20% per year [9]. Also, the cost of surgeries in Norway in 2008 was approximately 700 million NOK (*EUR* 88.9 million) per year and about 18% of this cost is related to revision surgeries [10]. Revision surgeries are necessary due to the failure of the hip implants and the chances drastically increase after 10-15 years [11]. On one hand, the revision surgery is very costly and on the other hand, it is really patient suffering. The rate of revision surgeries for orthopedic implants is about 7% after 10 years of service. With increase in the life expectancy and surgeries on younger patients due to accidents and sports related injuries, the rate of revision surgeries is increase significantly [9].

Nowadays, hip prostheses are mainly stainless steel, cobalt-chromium-molybdenum (CoCrMo), ceramics such as alumina and polymers such as Ultra High Molecular Weight Polyethylene (UHMWPE). Typically the stem and the femoral head are made of structurally strong metals or ceramics, while the acetabular cup very often is coated with UHMWPE for minimizing the friction. The main reasons for the hip failure and the reduction of the lifetime for different material systems are attributed to the generation of wear debris, autoimmune responses, surgical trauma, fracture and stress shielding [12].

Present metallic hip implants have some undesirable effects on the patient's body. Hypersensitivity to Ni (with relatively high fractions in some stainless steels) is common for about 14% of the people undergo hip replacement treatment. Also Co and Cr have adverse effects [13]. So, the need for prosthesis with improvements in biocompatibility and the average service time of at least 30 years should be the aim when developing new materials for hip joints.

Bulk metallic glasses are a new generation of amorphous materials with promising properties. Those compositions that lead to critical diameter exceeds 1 cm are considered to form bulk metallic glasses (BMGs) [14]. While they are electrically and optically metallic like ordinary

metals, the absence of crystals, boundaries, dislocations and vacancies give them physical, chemical and mechanical properties that may differ fundamentally from normal metals [14]. BMGs are believed to have improved properties with respect to the use as orthopedic implants [15]. One of the BMGs that may be suitable for the orthopedic purposes is the zirconium based BMGs [16].

Different Zr-based bulk metallic glasses such as: $Zr_{50}Cu_{40}Al_{10}$ [17], $Zr_{54}Ni_6Cu_{30}Al_{10}$ and $Zr_{70}Ni_{16}Cu_6Al_8$ [18] have been produced. But the biocompatibility of these alloys is not that much acceptable (due to the presence of Ni or Al).

The aim of this project is to test and characterized Zr-based BMG and compare the results to the common implant materials.

2. Theory

2.1 Ordinary orthopedic biomaterials

Although metallic materials, polymers, and ceramics are commonly used in orthopedics, it's the metals that have, over the years, uniquely provide the material properties such as high strength, ductility, fracture toughness, hardness, corrosion resistance, formability, and biocompatibility that are necessary for load-bearing applications required in fracture fixation and total joint arthroplasty (TJA) [9].

Despite the presence of wide range of metals, polymers and ceramics, only few of them are suitable for the orthopedic purposes. Knowledge of the material properties, usage and limitations of the present orthopedic biomaterials is necessary to improve their performance. The most common orthopedic biomaterials and their usages are mentioned in Table 2.1.

Table 2.1: The most common orthopedic biomaterials and their usages [9].

	Material	Usage
Metals	Ti alloy (Ti-6%Al –4%V)	Plates, screws, TJA components (nonbearing surface)
	Co–Cr–Mo alloy	TJA components
	Stainless steel	TJA components, screws, plates, cabling
Polymers	Poly(methyl methacrylate) (PMMA)	Bone cement
	Ultrahigh-molecular-weight polyethylene (UHMWPE)	Low-friction inserts for bearing surfaces in TJA
Ceramics	Alumina (Al_2O_3)	Bearing-surface TJA components
	Zirconia (ZrO_2)	Bearing-surface TJA components

There are some inherent problems with regard to the biocompatibility of three common alloys, which are being used as orthopedic applications.

The first alloy in the Table 2.1 is Ti alloy (Ti-6%Al –4%V), which is being used for orthopedic prosthesis. The biocompatibility of this alloy is excellent, especially, when the direct contact with the bone or tissue is required. Ti-6Al-4V's poor shear strength makes it undesirable for bone screws or plates. It also has poor surface wear properties and tends to seize when in sliding contact with itself and other metals [19]. Wear properties of titanium were reported by Galante and Rostoker [20]. Titanium and titanium alloys make a thin layer of titanium oxide on their surface, when they come into contact with oxygen either in the air or in the blood. The oxide layer is brittle and every time the surface rubs against another surface, some wear debris are being produced. On the other hand, a new oxide layer forms on the surface and this process continue as far as oxygen is present in the system and it produces an unending stream of titanium oxide particles [21]. Also aluminum that present in the alloy (about 6 %) has been linked to many neurodegenerative diseases such as Parkinsonism dementia and Alzheimer diseases [22].

Next alloys are Co–Cr–Mo alloy and Stainless steel, which are widely being used these days for hip implants. From the biocompatibility point of view, some metal ions have adverse biological reactions including Ni (relatively in high fractions in certain Stainless steel), Co (the base metal of the Co–Cr–Mo alloys), and Cr (contained in relatively high fraction in stainless steels and Co–Cr–Mo alloys). Also some people are allergic to Co and Cr, too [23]. Nickel, cobalt and chromium are known carcinogens in pure form, while Ni and Cr also form certain compounds that are found to be carcinogenic [24].

A new kind of metallic alloy system that have remarkable properties and may be used for orthopedic applications in future are the Bulk Metallic Glasses (BMGs).

2.2 Bulk Metallic Glass

Metallic glasses first discovered by Duwez in the California Institute of Technology's laboratory in 1959. The method was quenching the Au-Si from ~1300°C to the room temperature [25]. Afterwards, in early 1990s, bulk metallic glasses (BMGs) in metal-metal system such as La-, Mg-, Zr-based alloys were first prepared by quenching the liquids very fast [26-28].

Unlike traditional metals, which have a crystalline structure, amorphous metals are frozen liquids, which fail to crystallize during solidification from the molten state. Amorphous metals are electrically and optically metallic, like ordinary metals.

In 1995, three empirical component rules for the stabilization of a super cooled metallic liquid were proposed by Miller and Liaw. Those three rules are: (1) the multi-component system should consist of three or more elements, (2) atomic sizes of the main constituent elements should be different (more than ~12%), and (3) the elements should have negative heats of mixing [29].

In crystalline solids, atoms are arranged in a three dimensional lattice. . In some crystalline materials, the different elements prefer to reside on specific sites in the unit cell and thereby create ordered sublattices in the crystal. Glasses, including BMGs, do not have this long range order, so they are called amorphous. The structural model of glasses is dense random packing of atoms. The history of the production of BMGs can be found in the Table 2.2.

Table 2.2: Representative bulk metallic glass compositions including the critical diameter of the alloy that can be cast in amorphous state[14].

Base metal	Composition (atomic %)	Critical diam. (mm)	Production method	Year
Pd	$Pd_{40}Ni_{40}P_{20}$	10	fluxing	1984
	$Pd_{40}Cu_{30}Ni_{10}P_{20}$	72	Water quenching	1997
Zr	$Zr_{65}Al_{7.5}Ni_{10}Cu_{17.5}$	16	Water quenching	1993
	$Zr_{41.2}Ti_{13.8}Cu_{12.5}Ni_{10}Be_{22.5}$	25	Copper mold	1996
Cu	$Cu_{46}Zr_{42}Al_7Y_5$	10	Copper mold	2004
	$Cu_{49}Hf_{42}Al_9$	10	Copper mold	2006
Rare earth	$Y_{36}Sc_{20}Al_{24}Co_{20}$	25	Water quenching	2003
	$La_{62}Al_{15.7}Cu_{11.15}Ni_{11.15}$	11	Copper mold	2003
Mg	$Mg_{54}Cu_{26.5}Ag_{8.5}Gd_{11}$	25	Copper mold	2005
	$Mg_{65}Cu_{7.5}Ni_{7.5}Zn_5Ag_5Y_5Gd_5$	14	Copper mold	2005
Fe	$Fe_{48}Cr_{15}Mo_{14}Er_2C_{15}B_6$	12	Copper mold	2004
	$(Fe_{44.3}Cr_5Co_5Mo_{12.8}Mn_{11.2}C_{15.8}B_{5.9})_{98.5}Y_{1.5}$	12	Copper mold	2004
	$Fe_{41}Co_7Cr_{15}Mo_{14}C_{15}B_6Y_2$	16	Copper mold	2005
Co	$Co_{48}Cr_{15}Mo_{14}Er_2C_{15}B_6$	10	Copper mold	2006
Ti	$Ti_{40}Zr_{25}Cu_{12}Ni_3Be_{20}$	14	Copper mold	2005
Ca	$Ca_{65}Mg_{15}Zn_{20}$	15	Copper mold	2004
Pt	$Pt_{42.5}Cu_27Ni_{9.5}P_{21}$	20	Water quenching	2004

2.2.1 Formation of metallic glasses

It is important to have a practical overview about how to make a bulk metallic glass and prevent it from becoming crystalline upon heating and thermal processes. Four effects that can be useful for improvement of the thermal stability of BMGs are mentioned below[17]:

1. Close packing of constituent atoms.
2. Structural dissimilarity between the amorphous phase and crystallized phase(s).
3. Necessity of the long range diffusion of atoms during crystallization.
4. A large amount of the elastic strain energy yielded by crystallization in a glassy solid.

Turnbull et al. had different experiments regarding similarities between metallic and non metallic glasses and they found out that there is a glass transition for some metallic alloys due to quenching [30]. The glass forming ability (GFA) is the ratio of the transition temperature (T_g) over the liquidus temperature (T_m), which is called the reduced transition temperature of the alloy $T_{rg}=T_g/T_m$. If $T_g/T_m > 2/3$, nucleation is negligible and glassy phase can be obtained by slow cooling. On the other hand, if $T_g/T_m \sim 0.5$, as for many metallic alloys, amorphous phase can only be forms by rapid cooling ($> 10^6$ K/s) of the melt [31].

Generally in cooling a liquid, crystallization becomes thermodynamically possible below the liquidus temperature T_l, and is kinetically hindered below the glass-transition temperature T_g. Glass formation occurs when the gap between T_l and T_g is minimized, and is indicated by a high value of the reduced glass-transition temperature (T_{rg}). Higher values of T_{rg} are associated with lower critical cooling rates for glass formation. As T_g appears to be only weakly dependent on composition, local high values of T_{rg} are most simply indicated by depressions in T_l, and indeed glass-forming ability is particularly good at deep eutectics [14]. By reducing the quenching rate larger pieces of metallic glasses can be obyained. In the glass formation for new generation of alloys the role of intrinsic parameters such as the number of alloying elements, purity of alloying elements, atomic size (size difference) and composition have a more important roles in comparison with external factors such as the cooling rate. To increase the GFA in the bulk metallic glasses the number of alloying elements has to be as many as possible. This high number of alloying elements can destabilized the crystalline phase that can form during the quenching. This is called the “confusion principle” [32].

Considering the - temperature - transformation (TTT) diagram fast cooling and avoiding the “nose” of the TTT diagram, which is the start of the formation of the crystals, the result would be an amorphous material. Also, by changing the composition and introducing the chemical disorder, the nose can be shifted to the right which is for longer transformation time.

As the critical cooling rate for glass formation is reduced, a glass can be produced in large and thicker areas. As it was mentioned before, the compositions which their diameter exceeds 1 cm are considered as bulk metallic glasses (BMGs). The largest diameter which was produced fully glassy is 72 mm (the alloy is $Pd_{40}Cu_{30}Ni_{10}P_{20}$) [33].

According to Lin [34], in quenching molten alloys, a sample of typical dimension R and initial temperature T_m will require a total cooling time τ of the order of:

$$\tau : \ (R^2 / \kappa) \tag{2.1}$$

In equation 2.1, κ is the thermal diffusivity of the alloy. It is given by $\kappa = K / C$ where K is the thermal conductivity and C is the heat capacity per unit volume. The achieved cooling rate will be of the order of:

$$\dot{T} = \frac{dT}{dt} = \frac{(T_m - T_g)}{\tau} = \frac{K(T_m - T_g)}{CR^2} \tag{2.2}$$

$T_m - T_g \sim 400K$, $K \sim 0.1$ W/cm s^{-1} K^{-1} (typical of the molten alloys), and $C \sim 4$ J/cm^3 K^{-1} (also typical for the molten alloys), gives:

$$\dot{T}(K / s) = 10 / R^2(cm) \tag{2.3}$$

Therefore the maximum thickness of the amorphous alloy is determined by the critical cooling rate of the material [34].

Figure 2.1 shows the relation among R_c, maximum sample thickness (t_{max}) and reduced glass transition temperature (T_g/T_m) for newly developed bulk glassy alloys, together with the ordinary amorphous alloys [35].

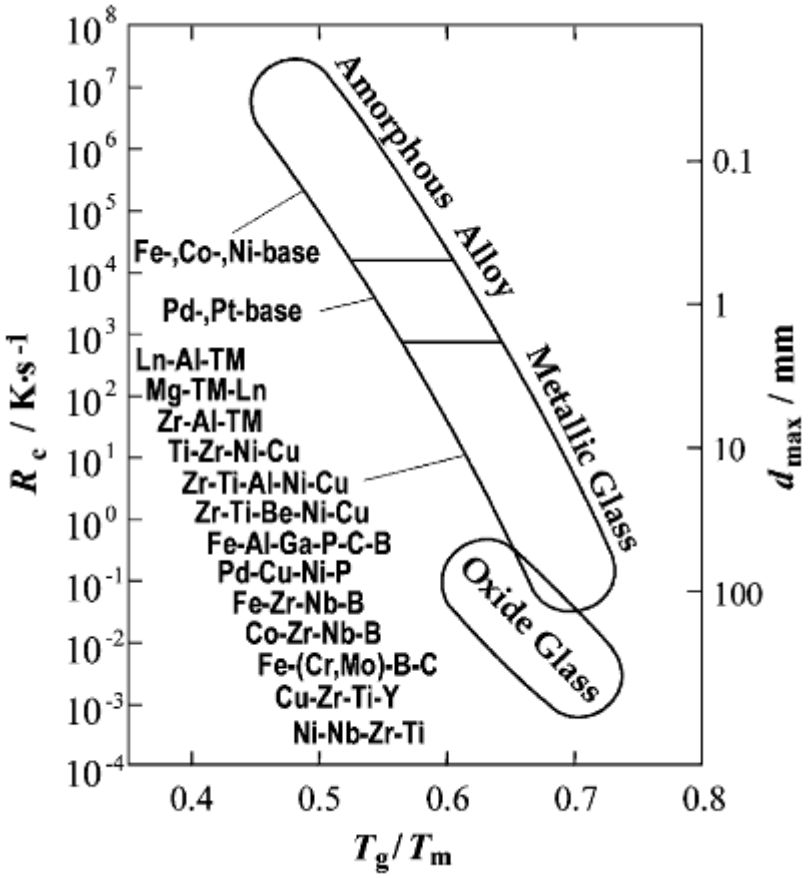

Figure 2.1: Relationship between the critical cooling rate for glass formation (R_c), maximum sample thickness for glass formation (d_{max}) and reduced glass transition temperature (T_g/T_m) for typical bulk glassy alloys. The data of amorphous alloys, previously reported Pd- and Pt-based glassy alloys and typical oxide glasses are also shown for comparison [35].

Structure

In 1960 Bernal considered the structure of the monatomic metallic liquids to be dense random packing [36]. Until now, different experiments has emphasized that densest packing is a key factor that the structure of metallic liquids and glasses are dependent on. Glass forming ability increases when the alloy's components have a negative heat of mixing. In many systems it is useful to analyze the structure in terms of solute centered clusters. The ratio of the solute atom at the center and of the solvent atoms around it determines that how many solvent atoms can fit in the coordination shield. The coordination number for the metallic glasses is mostly around 8 to 20 [14].

BMGs are being form by rapid cooling and decreasing the temperature limits the diffusivity, so the arrangement of the atoms in glasses would be without a long range configuration. The absence of the long rang order can be understood by analyzing the XRD diffraction pattern that shows no sharp Bragg peak (Fig 2.2).

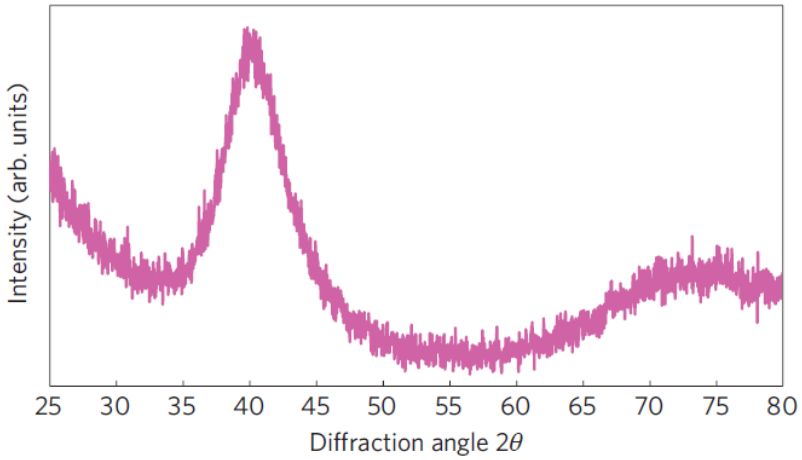

Figure 2.2: Amorphous structure of the $Pd_{79}Ag_{3.5}P_6Si_{9.5}Ge_2$ glass. X-ray diffraction analysis [37].

2.2.2 Mechanical performance of amorphous metals

Elasticity

Metallic glasses have liquid like structure with the structural length scale of the order of hundred atoms. Because of these criteria, they have very high strength and low elastic modulus [38].

Because of the low elastic modulus of bones, the low elastic modulus of the metallic glasses reduces the mismatch between the bone and the artificial prosthesis. Looking to the Figure 2.3, it can be seen that for certain strength, amorphous metal has significantly lower Young's modulus than any other crystalline biomaterials.

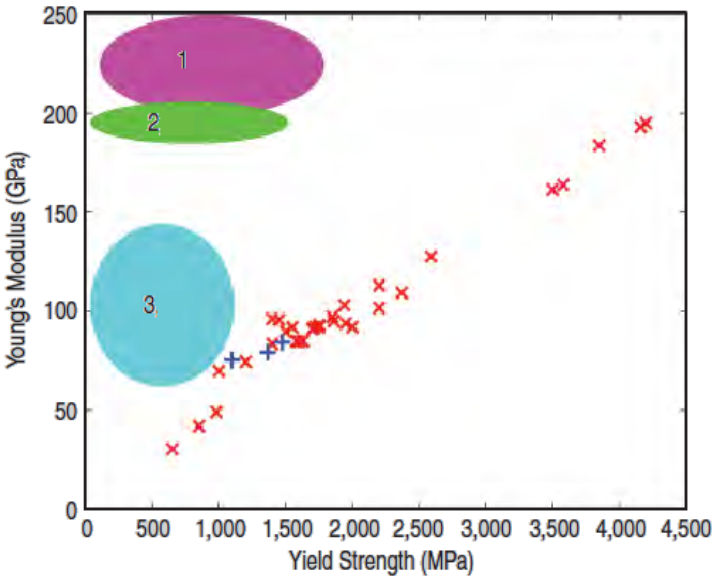

Figure 2.3: Young's modulus vs. yield strength data for amorphous metals (x) and ductile phase reinforced metals (+), shown together with data for stainless steels (2), Co-Cr based (1), and Ti based alloys (3) [13].

Hardness

A criterion that is related to the wear resistance capability of a material is the hardness. Since hardness is understood to be a measure of flow stress, it is connected to the material yield strength. Specifically, the Vickers hardness is expected to scale linearly with the material yield strength ($H_v \sim 3\sigma_y$). Having high yield strength, metallic glasses show better properties against deformation in comparison to the crystalline materials. Figure 2.4 shows the hardness of glassy metals as a function of yield strength along with data for conventional crystalline metallic biomaterials.

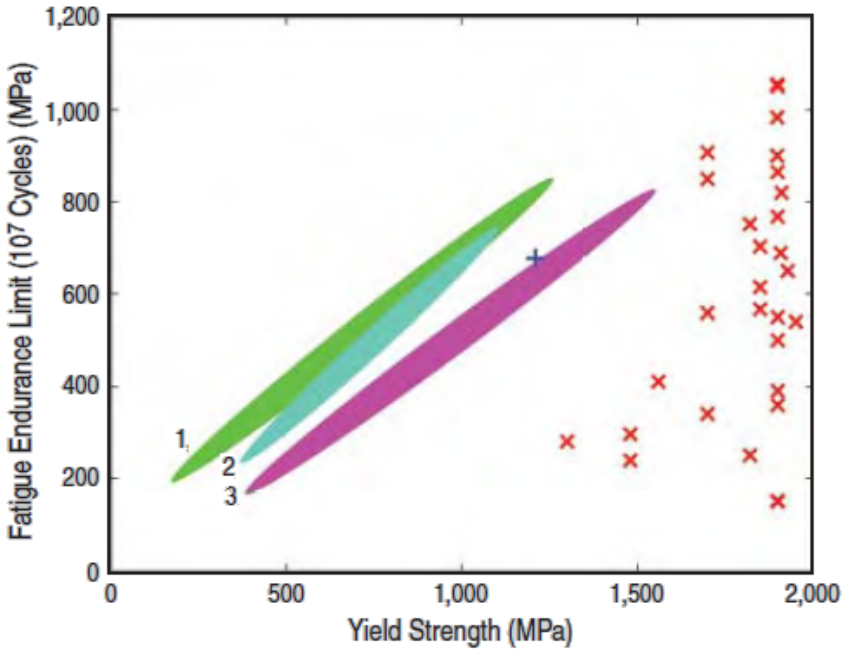

Figure 2.4: Fatigue endurance limit (stress-range based) vs. yield strength data for amorphous metals (x) and ductile-phase reinforced amorphous metals (+) shown together with data for stainless steels (1) Ti-based alloys (2) and Co-Cr-based (3) [13].

The wear resistance of metallic glasses has been found more than ceramics with the same hardness, which express that the mechanism of wear deformation in glassy metals is different from the brittle fracture criterion which is dominant for ceramic materials. The high wear resistance of metallic glasses due to their high hardness makes them a suitable choice for the load bearing prosthesis like the hip implants.

Fatigue

Fatigue endurance is important parameter for determining the lifetime of the load bearing implants. It is estimated that an average person who is not that much active applies several millions of cycles of stress on the hip joint per year [39]. Assuming that the hip implant should last about 20 to 30 years, the total rate would be approximately 10^8 loading cycles. Herein, the resistance of the material against cyclic loading is critical for having an acceptable life time for the hip implant. Figure 2.5 shows the fatigue endurance limit for some of the amorphous metals at 10^7 cycles against the corresponding yield strength.

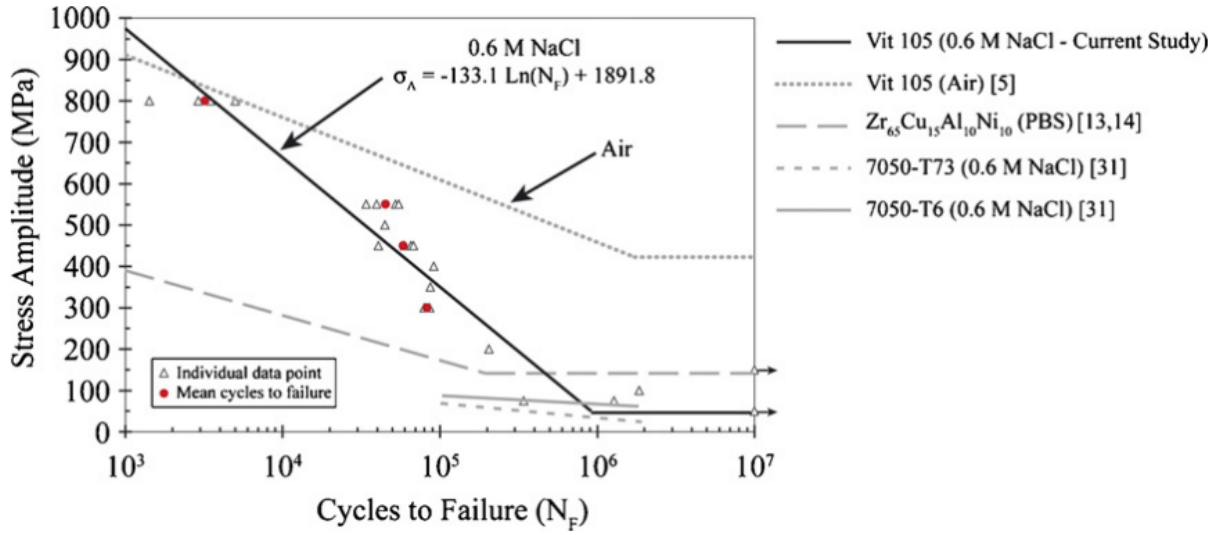

Figure 2.5: Plot of cycles to failure as a function of stress amplitude for the four-point bending of Vit 105 BMG in air and a naturally aerated, 0.6 M NaCl electrolyte at a frequency of 10 Hz and R= 0.1 [40].

Fatigue ratio is the ratio of the fatigue endurance limit to the material yield strength. Unlike the crystalline materials which have a consistent endurance limit and high fatigue ratio, the endurance limits of the Zr-based glasses are shown to be highly scattered and because of that the fatigue ratio changes from very small values (~ 0.1) to rather high (~ 0.5).

Fracture Toughness

Fracture toughness is a measure of load bearing capacity of a material before fracture, and it is a critical property that can determines the overall mechanical performance of a load bearing implants. Ceramics have good biological compatibility, but their low fracture toughness (K_{IC} ~ 10 MPa $m^{1/2}$) makes them an unsuitable choice for the hard tissue prosthesis. On the other hand, the fracture toughness of the metals is quite high (K_{IC} ~ 100 MPa $m^{1/2}$).

Lack of the microstructural mechanism, which can act as a barrier against the crack propagation in the amorphous metals, is a cause of having relatively low fracture toughness than the crystalline metals. Some amorphous metal alloys, however, tend to generate highly dense shear bands networks upon yielding that are able to self arrest in a manner that leads to higher toughness, near the values for the crystalline metals [13]. Therefore, glassy metals have fracture toughness values as low as for the brittle ceramics to high values comparable to engineering metals [41].

2.2.3 Biocompatibility of Bulk Metallic Glasses

Biocompatibility is the ability of a biomaterial to perform with an appropriate biological response. Biocompatibility has two different aspects, which are “host response” and the “material response.” The “host response” is defined as the local and systemic response of the living systems to the material, while the “material response” is the response of the material to the living system [42]. Figure 2.6 is an example of inappropriate biocompatibility.

Figure 2.6: The blue man (smurf man). The blue color of the skin is because of the adverse effect of the silver ions in his body [43].

The most basic material responses in load-bearing implant applications include corrosion or dissolution due to chemical attack, friction and wear, and failure due to plastic deformation, fracture, or fatigue. Typical host responses include tissue adaptation, which can be either positive (e.g., osseointegration) or negative (e.g., stress shielding), inflammation, allergic response, and carcinogenesis [42].

Due to high strength, hardness and fatigue resistance, metals show better mechanical response to biological systems than polymeric or ceramic materials. The commonly used materials for prosthesis are stainless steels, Co-Cr-based alloys, and Ti-based alloys. Although these metallic alloys are being used these days, they still have some inherent problems. For example, the stiffness of stainless steels and Co-Cr alloys compared to bones is very high. The Young’s modulus for of the Co-Cr based alloys is around 200-250 GPa while for the bone is 10-20 GPa.

Therefore, this big difference can cause an uneven load sharing between the bone and the prosthesis, which leads to bone resorption and then loosing the implant [44].

Another critical issue regarding currently used alloys is degradation products of these materials and the reaction of the reaction of tissues to them which can be followed by implant failure because of wear and corrosion.

Electrochemical corrosion can occur at the metal-implant surfaces. This has two different unwanted effects: the degradation can reduce the structural unity of the implant and the degradation products like metal ions can affect the host. There are different structural failure mechanisms related to corrosion such as stress- corrosion cracking, corrosion fatigue and fretting corrosion [45]. Approximately 14 % of people have hypersensitivity to Ni, also some people have hypersensitivity to Co and Cr. Nickel, Co and Cr are known carcinogenic in pure form, while Ni and Cr form certain compounds that are found to be carcinogenic. On the other hand, Al has been linked to several neurodegenerative diseases such as Parkinsonism dementia and Alzheimer's disease [13].

The use of BMGs as a material for biomedical applications have been suggested by many researchers [45-46] over the year as they have proven to have properties such as high strength and ductility, relatively low elastic modulus as well as high corrosion resistance. Homazava et al. [46] investigated the corrosion behavior of a Zr-based BMG with the composition $Zr_{58.5}Cu_{15.6}Ni_{12.8}$ $Al_{10.3}Nb_{2.8}$ (called the Vitreloy 106a alloy) and found that the corrosion rate for the alloy was very low. Additionally, the alloy showed a preferential dissolution of copper and aluminum, leaving nickel virtually undissolved in the BMG sample.

Liu et al. [47] have, however, reported fabricating nickel free Zr-based BMGs. Their results showed a biocompatibility similar to, and even higher than, that of the commonly used biomedical implant material Ti-6Al-4V. In addition, the wear properties were shown to surpass that of the titanium alloy, with significantly lower material loss during wear tests.

2.2.4 Corrosion behavior of amorphous metals

Investigation of the corrosion properties of the biomaterials is very critical because small amount of metallic ions or particles that are released in the body, even in very small scale such as ppb, can lead to hypersensitivity, cancer or other biological problems.

The oxidation of the material in the aqueous environment is called corrosion, which can be influenced by different parameters such as anions, cations, proteins and the dissolved oxygen content. Figure 2.7 is an example of a corrosion in hip implants.

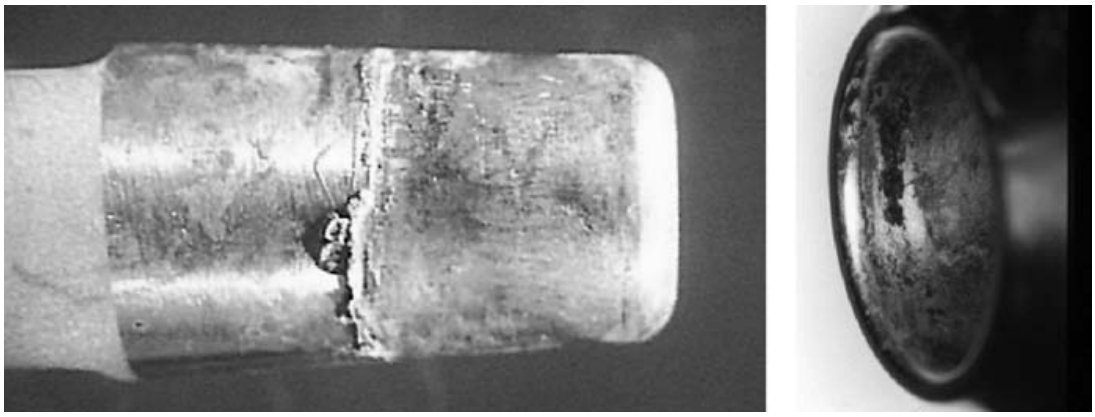

a) b)

Figure 2.7: (a) Modular junction taper connection of a total hip arthroplasty showing corrosion of the taper connections. (b) Macrograph of deposits of $CrPO_4$ corrosion particle products on the rim of a modular cobalt–chrome femoral head [9].

There are two main mechanisms for metal corrosion. The driving force for the first one is thermodynamic which causes oxidation and reduction according to the equation 2.4.

$$\Delta G = -nF\Delta E \tag{2.4}$$

Where *n* is the valence of the ion, *F* is the Faraday constant (96485 coulombs/mole electrons), and *E* is the voltage across the metal–solution interface. The reactivity of the metal or the tendency to form the oxide layer can be understood from the potential (E). As a conclusion, the more negative the potential of the metal in the solution, the more reactive it will be.

The other mechanism that can cause the corrosion is the kinetic barrier to corrosion such as surface oxide layer. The barrier preserves the metals by making a physical limitation. A good example of this mechanism is the formation of the passive film on the surface of the metal. According to the Figure 2.8 it can be seen that the barrier is like a dam in front of the ion exchange between metal and the solution. There are also other kinetic barriers such as polymeric coatings, but the most protective is the passive oxide film.

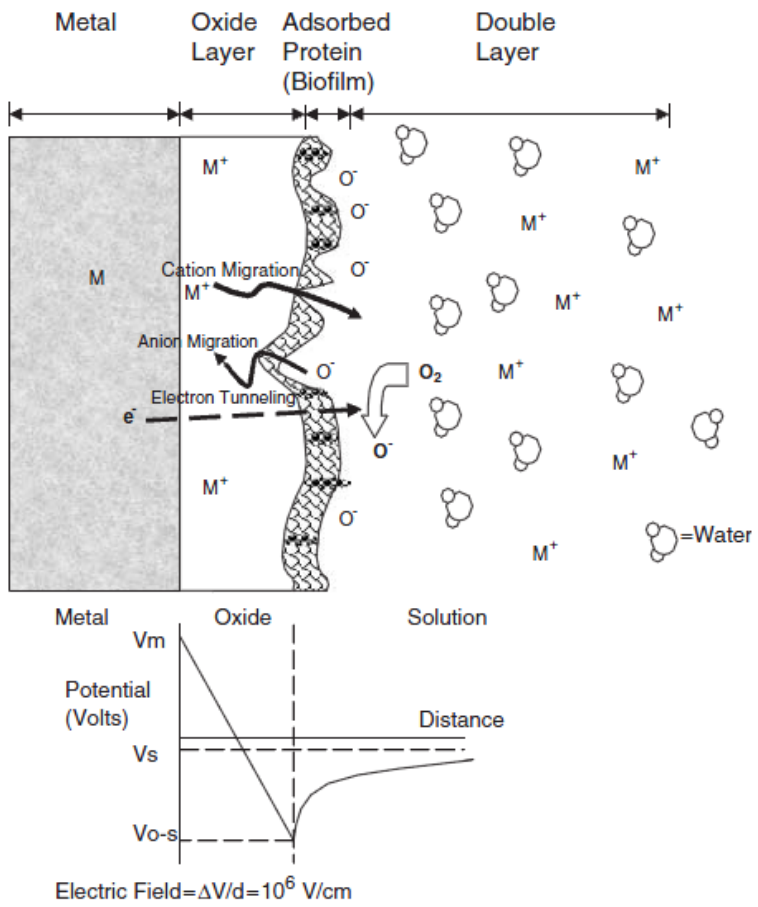

Figure 2.8: Schematic of the interface of a passivating alloy surface in contact with a biological environment [9].

The most important corrosion mechanism for metals is electrochemical dissolution. In the electrochemical reaction, electrons are being transferred from the metal surface to the aqueous electrolyte solution. Figure 2.9 illustrates the metal dissolution in the electrolyte solution.

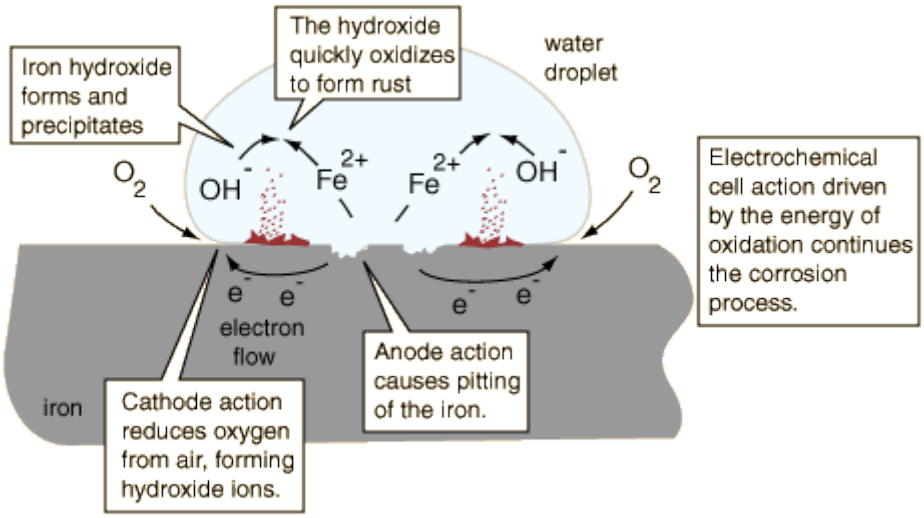

Figure 2.9: Schematic diagram of corrosion cells on iron [48].

The corrosion reaction is consists of two reactions, anodic and cathodic.

Anodic reaction, which is the release of the metallic ions (oxidation):

$$M \rightarrow M^{n+} + ne^{-} \tag{2.5}$$

The other reaction is the cathodic reaction that consumes the electrons produced in the first reaction (reduction):

- In neutral solution: $O_2 + 4H^{+} + 4e^{-} \rightarrow 2H_2O$ (2.6)
- In acidic solution: $2H^{+} + 2e^{-} \rightarrow H_2$ (2.7)

Generally, reduction of hydrogen happens under acidic condition and reduction of dissolved oxygen occurs in neutral or basic solutions [49].

It is a rule that in all corrosion procedures, the rate of the anodic reaction is equal to the rate of the cathodic reaction. Also, by changing the variables, the rate of the anodic and cathodic reaction can be changed and by using this principle, the rate of the corrosion can be determined.

2.3 Passivity

There are two different ways for preventing the material corrosion inside the human body. One is to use a noble metal such as platinum or gold, but this is an expensive solution and also they cannot bear the mechanical loading. The other solution is to use some materials which make a kind of oxide protective layer on the surface such as stainless steel, nickel, chromium, titanium and their alloys and recently application of bulk metallic glasses is suggested [50].

Passivity is transformation of the layer of metal to a form of stable oxide, which acts as a kind of a barrier that prevents the metals to be in direct contact with the environment. A passive film is in constant exchange of species with the electrolyte and consequently alters in thickness and composition with the environment [50]. The metal is insulated from solution and the film causes inhibition of the anodic dissolution process. Thus, corrosion could be retarded due to this passive film.

The stability of passive layer can be affected by biological species and the damage on passive layer can increase the rate of corrosion; the oxygen content in human body can vary in different situations that will affect the passive layer formation and passive layer breakdown and also released hydrogen which is the product of cathodic reaction can be one controlling factor, the bacteria can also develop hydrogen which influence the cathodic reaction [50].

Figure 2.10 shows a typical plot of current density versus potential. When a metal reaches its passive potential the current will decrease to a lower value than previous values instead of increasing to higher value. This phenomenon only could happen in metals with passive-active ability and the formation of the passive layer on the surface leads to decrease in the corrosion rate.

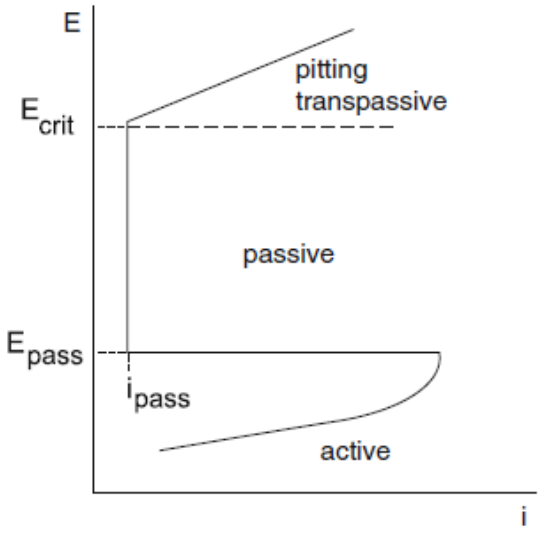

Figure 2.10: The idealized anodic polarization curve. Three different potential regions can be seen; the active, passive, and pitting or transpassive regions [51].

The passive behavior of metals can be used to protect them in the aggressive environments by different method such as applying a current to reach the potential above the E_p to keep the sample in the passive region (called anodic protection) and other method is the application of materials like aluminum, zinc and titanium, which form passive layer in that kind of environments [51].

The importance of the passive layer is very crucial in prosthesis from the structural and compositional point of view. The passive layer is in contact with the body cells. The structure of the protective layer is important because some defects in the surface could initiate a failure such as grain boundaries or non metallic inclusions. The passive layers must be non-porous and must fully cover the metal surface. They must have an atomic structure that limits the migration of ions and electrons across the metal oxide-surface interface [50].

The breakdown of the passive layer could also be caused by localized attacks: damaging species (chloride ions…) present, critical potential exceeded or rise of pH of the local environment... but also because of mechanical factors, such as fretting or stresses applied on the material. The performances of the passive layer is dependent on oxygen so its concentration should be controlled.

There are five primary structural and physical characteristics, which can become important in implant degradation processes [9]:

1. Oxide films in implants are very thin, mostly on the order of 5 Å to 70 Å, which depends on the potential of the interface and solution variables such as PH. If the interfacial potential becomes very negative or the pH of the solution is low enough, then the oxide films will no longer be thermodynamically stable and will undergo reductive dissolution.

2. Oxide films have the characteristics of semiconductors with a structure that has atomic defects, which determines the ability of ionic and electronic transport across films. Metal cations and oxygen anions require respectively, the presence of cationic or anionic vacancies in the oxide for transport of these species across the film. For having a needed control on it, spinels ($MgAl_2O_4$) seem to be an appropriate choice. Spinels are typically known to have higher strengths and better resistance to diffusion of ions compared to single metal ion oxides. So, having a high concentration of spinels in the oxide layer acts as a barrier for dissolution of a metal implant.

3. To investigate the adhesion between the metal and the oxide layer, the ratio of the "oxide specific volume" to metal alloy specific volume can be considered. If the mismatch between the oxide and metal is big, a lot of stresses will be generated at the interface.

4. The oxide layers have different morphology than a flat and smooth structure. Transmission electron microscopy (TEM) and atomic force microscopy (AFM) techniques have revealed that they are needle like or dome shape.

5. Mechanical factors such as fretting, micromotion or applied stresses may scratch or fracture oxide films. Hence, the mechanical stability of the oxide films, as well as the nature of their repassivation process, is central to the performance of oxide films in orthopedic applications.

2.4 Polarization curve

Polarization curve gives information about the corrosion behavior, which is the current variation as a function of applied potential. If the metals would not be able to make a passive film, a linear relation between E vs. log I can be observed. On the contrary, non linear curve is a representative of the passive metals. As can be seen in the figure 2.11, passive metals exist in different regions. From the passivity point of view, anodic curve is important, which is for corrosion resistance properties

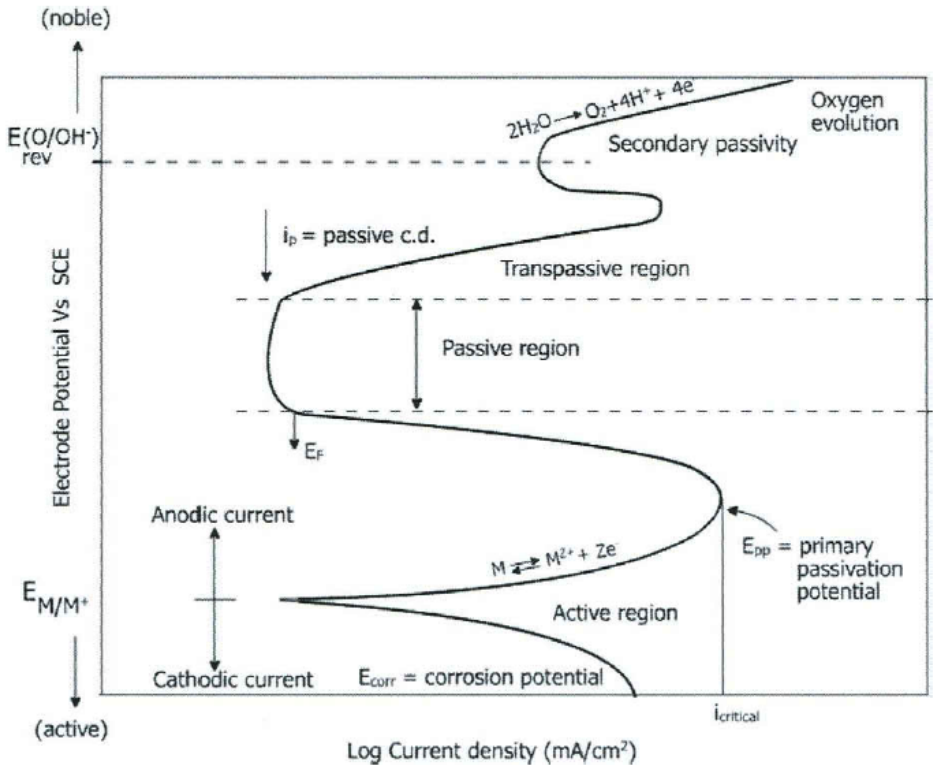

Figure 2.11: Polarization curve for a metal that undergoes an active to passive transition [52].

Figure 2.11 shows the anodic dissolution of a metal demonstrate an active-passive behavior. The hypothetical reversible potential of M is shown by $E_{(M/M^+)}$ and $E_{rev}^{(O/OH^-)}$ is for the reversible potential of the oxygen. The intersection of the anodic and cathodic curves in the active region gives E_{corr} which is the corrosion potential. The anodic curve has a Tafel behavior with the slope b_a. The maximum rate of corrosion is at the maximum current density called the critical current density ($i_{critical}$). The corresponding potential for the $i_{critical}$ is called the primary passive potential (E_{pp}).This potentials stands for transforming from active state to passive state. Start of the passivity causes a decrease in the current density (log i), due to formation of the oxide film on the metal surface. The decrease of the current density continuous until it reaches to a point that the potential becomes independent of the current density (flat potential E_F) and the current density remains constant. This represents the onset of the full passivity on the metal surface. The minimum current density required to maintain the passivity is called passive current density (i_p). At the i_p, the rate of the dissolution of metals remains constant and the oxide film begins to thicken.

2.5 Types of corrosion for implants

Artificial prosthesis for the bone surgery must have good corrosion properties especially to the body fluid with its NaCl content. Table 3 shows possible corrosion types in the implant alloys.

Table 2.3: Types of corrosion phenomenon in implant alloys [53].

TABLE 1. CORROSION PHENOMENA IN IMPLANT ALLOYS (POSSIBILITIES)

Type of corrosion	Initiating factors	Countermeasures
General surface corrosion	Corrosive medium	Selection of a stable-passive alloy
Pitting corrosion	Aerated medium containing chloride at a sufficiently high temperature	Alloying with elements counteracting pit formation, such as Cr, Mo, Ni; uniform surface finish
Crevice corrosion	Medium containing chloride, aeration difference in crevices between bone cement and metal or in different parts of tissue; combination of materials, for plates and screws largely differing in their electrochemical behaviour	Similar to those for pitting corrosion; avoidance of crevices and sharp notches
Stress corrosion cracking	Medium containg chloride + static tensile stresses + sensitive alloy	Pronounced tendency to passivation as a result of alloy selection and machining, low static tensile stressing; high tensile properties and toughness at same time
Fatigue corrosion	Aqueous medium + cycling tension/compression and/or torsional stresses + factors such as those for pitting corrosion	Prevention of surface notches and sudden changes of cross-section; pronounced tendency toward passivation, high fatigue strength
Galvanic corrosion	Combinations of materials differing electrochemically; high conductivity of medium	Matching of corrosion properties of materials used in composites

2.5.1 Uniform corrosion

Uniform of thinning of metal without any localized attack. This type of corrosion does not penetrate very deep inside as shown in Figure 2.12.

Figure 2.12: Uniform corrosion [54].

2.5.2 Galvanic corrosion

When two metals with different electrochemical potentials with the presence of a corrosive electrolyte are in contact with each other, the galvanic corrosion can occurs (figure 2.13).

Figure 1.13: Galvanic corrosion [54].

2.5.3 Crevice corrosion

This type is the localized form of corrosion which can be cause by deposition of dirt, mud, dust and other deposits on the metallic surface or by existence of voids, gaps and cavities between adjoining surfaces (figure 2.14). The occurrence of crevice corrosion is often associated with the adverse tissue reaction and a severe pain in the patient required removing the implant [55].

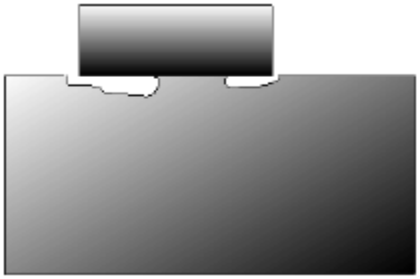

Figure 2.14: Crevice corrosion [54].

2.5.4 Pitting corrosion

It is a type of localized corrosion, when some parts of the metal surface corrode preferentially leading to formation of cavities or pits. Metals that form a passive film like aluminum and steels are more likely to this form of corrosion (figure 2.15). Also, pitting can be induced by cold working, which promotes formation of the second phase constituents along strain lines.

Figure 2.15: Pitting corrosion [54].

2.5.5 Stress Corrosion Cracking (SCC)

Whenever there is a conjoint action of stress and corrosion, stress corrosion can occur. In this phenomenon, static tensile stress, environment and sometimes, metallurgical condition leads to initiation and propagation of a crack until the failure (figure 2.16).

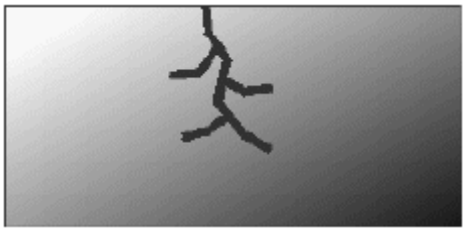

Figure 2.16: stress corrosion crack (SCC) [54].

2.5.6 Intergranular corrosion

The structure of metals and alloys is mostly crystalline. In this type of corrosion, there is a localized corrosion in the grain boundaries and it is very difficult to detect the Intergranular corrosion in the early stages (figure 2.17).

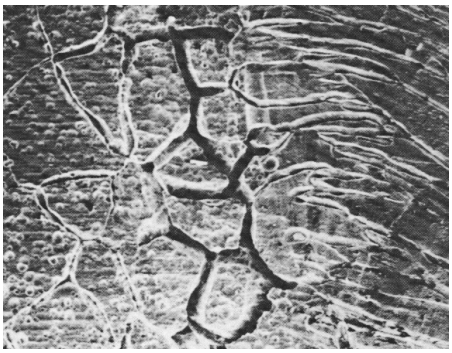

Figure 2.17: Intergranular corrosion [56].

2.6 Implant corrosion

2.6.1 Biological environment

The body is a harsh environment and metals and alloys should stand the oxygenate saline solution with salt content of about 0.9 % at pH ~ 7.4, and temperature of 37 ± 1 °C. When an implant is installed in the body, it is constantly in direct contact with the extracellular tissue fluid (figure 2.18). It can be said that all metallic implants, including the most corrosion resistance metals, undergo chemical or electrochemical dissolution at some finite rate, due to complex and corrosive environment in the human body. The body fluid is consist of water, complex compounds, dissolved oxygen and large amounts of sodium (Na^+) and chloride ions (Cl^-) and other electrolytes like bicarbonate and small amounts of potassium, calcium, magnesium, phosphate, sulphate and amino acids, proteins, plasma, lymph etc [57]. These ions have different functions such as maintenance of the body pH and participation in the electron transfer reactions. During the implant surgery and also a bit after that until the complete healing, the internal body environment is greatly disturbed such as disturbance of blood supply to the bones and variation in the ionic equilibrium and in some situations the pH can decrease down to ~ 5.3.

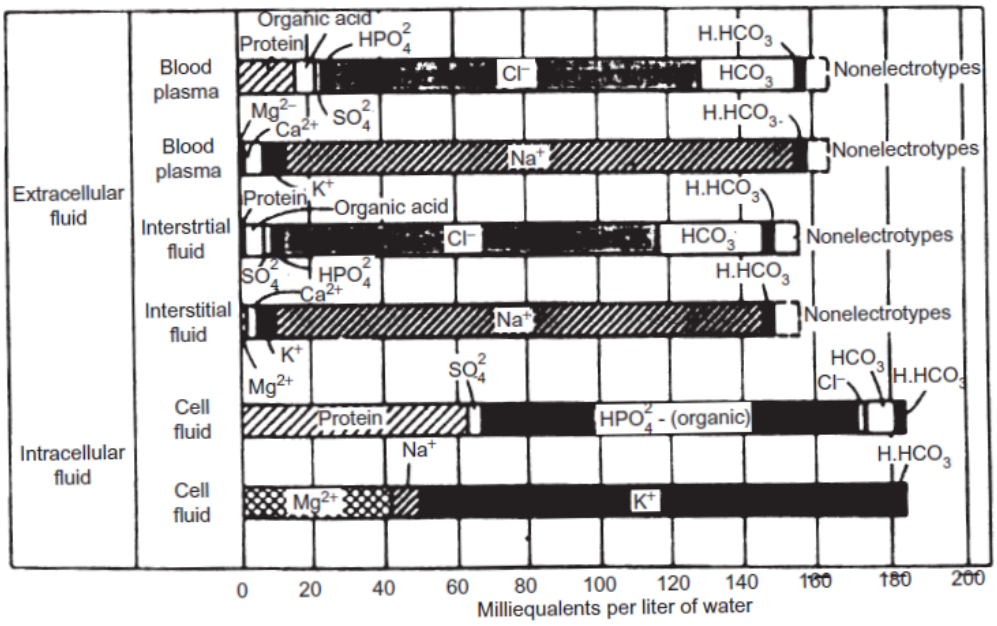

Figure 2.18: Ionic composition of blood plasma, interstitial fluid and intracellular fluid (Pholer 1986) [57].

Blood serum

An average human being has about 5.5 liters of blood in the body. 55% of the blood is made up of plasma, which constitutes the fluid part of the blood. The other 45% of the blood is composed of cells (erythrocytes (red blood cells) and leukocytes (white blood cells)) and platelets. The red blood cells constitute about 45% of whole blood and the white cells about 0.7%. Plasma contains water, proteins and inorganic salts like chlorides, as illustrated in Table 2.4:

Table 2.4: Composition of the plasma [58].

Element	Percentage
Water	90 %
Protein	8 %
Inorganic Ions	0.9 %
Organic substances	1.1 %

Proteins are responsible for transportation of insoluble substances, blood clotting, protection against infection and maintenance the pH stability of the blood. There are four different proteins in the plasma: serum globulin, serum albumin, fibrinogen and prothrombin. Serum globulin is produced by body immune system and the other three ones are produced by the liver.

60% of the total plasma proteins are made of albumin, which can pass through capillary walls because it is the smallest protein. Serum globulins make up 36% of the total plasma protein.

Table 2.5 shows the main inorganic ions present in the plasma. As an example, sodium allows keeping a constant blood pressure and ensuring the sufficient circulation of oxygen in the body and potassium helps the food digestion.

Table 2.5: Concentration of the inorganic ions presents in the plasma blood [58].

Ion	Symbol	Concentration (mmol/L)
Sodium	Na^+	135-146
Potassium	K^+	3.5-5.2
Calcium	C_2^+	2.1-2.7
Chloride	Cl^-	98-108
Hydrogen carbonate	HCO_3^-	23-31
Phosphate	PO_4^-	0.7-1.4

Synovial fluid

Synovial fluid is a stringy fluid present in the cavities of synovial joints (figure 2.19). Its responsibility is to reduce the friction between the articular cartilage and other tissues. In fact, this fluid serves the purpose of lubricating by allowing the bones to freely articulate and absorbing shocks. It also plays a role to nourish certain parts of the joint, to bring oxygen and other nutrients to the cartilage or other areas of the joint and finally to remove carbon dioxide and other waste products from the cartilage.

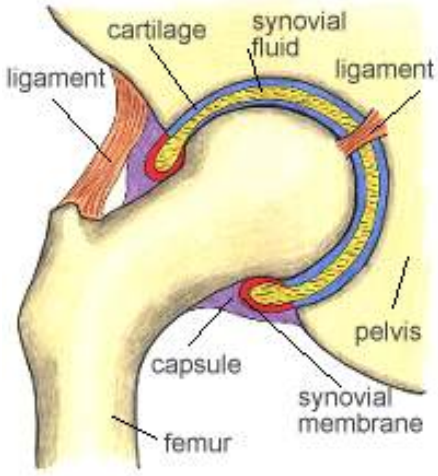

Figure 2.19: Articulated joint [59].

Proteins

Protein is a biological macromolecule composed of one or more chains of amino acids linked together by amide bonds. The protein folds on itself to form secondary structure, which is quantitatively the most important alpha (α) helix and beta (β) sheet structure.

Serum albumin and fibrinogen are the most present proteins due to their high concentrations in the body fluid. So, they should be considered important for the biocompatibility study.

The main responsibility of the albumin is to transport of the free fatty acids, which are insoluble in plasma without albumin. With concentrations ranging from 30 to 50 g/L, this protein is the major synovial protein. In case of an implanted biomaterial, albumin is the most adsorbed protein present because its concentration is significant in comparison to the others such as immunoglobulins and fibrinogens (Figure 2.21) [58].

Figure 2.20: X-ray crystallographic Structure of Human Serum Albumin [60].

Fibrinogen is involve in the blood coagulation cascade, where the protein's peptide fragments are ultimately cleaved by the enzyme thrombin to yield insoluble fibrin monomers that polymerize into an intricate cross-linking pattern that stabilizes the aggregated platelet plug at the injury site [61]. The concentration of fibrinogen is lower in comparison to albumin, typically ranging from 1.5 to 4.0 g/L.

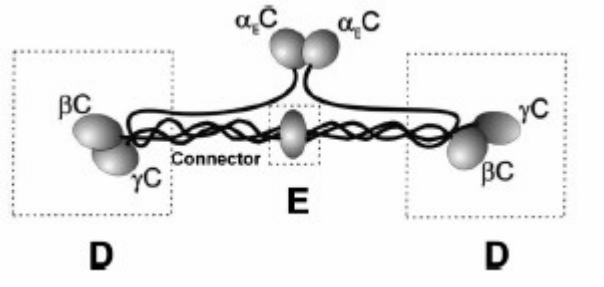

Figure 2.21: Fibrinogen molecule [62].

Fibrinogen is an elongated, symmetrical dimer, and its distinguishable regions include two hydrophobic outer domains (D domains) connected to a central globular hydrophobic domain (E domain) through two pairs of three non-identical α-helix coils (Aα, Bβ, and γ chains) [62].

2.7 Environment influence on implant corrosion

There are different environmental variables that can influence the corrosion behavior of the implants materials. From the other point of view, biological environment can be very harsh and can lead to failure earlier than expected. Here, some important criteria such as pH, surface preparation and temperature that have an effect on biomaterial performance are discussed.

2.7.1 pH

The pH of body fluids is different in each part: 7.15 -7.35 in blood, 7.0 in tissues, and 5.6 -7.6 in oral cavities [63]. However, infections or complications can change the pH more. The main purpose of pH is to have a kind of evaluation to see how much H^+ is available in the environment. The normal blood pH is considered to be around 7.4 and in case of infection it can decrease down to 5.2, due to the generation of acidic metabolic products. This change could have severe consequences on the materials corrosion behavior because the stability of the passive layer depends on the electrode potential and the pH of the solution, and also on the availability of oxygen. Consequently, it is compulsory to investigate the pH effect on corrosion properties before the use of biomaterials [58].

Figure 2.22 illustrates the Polarization curves of Zr65Al7.5Ni10Cu17.5 amorphous alloy in PCA with various pH levels and PBS (Phosphate Buffered Saline).

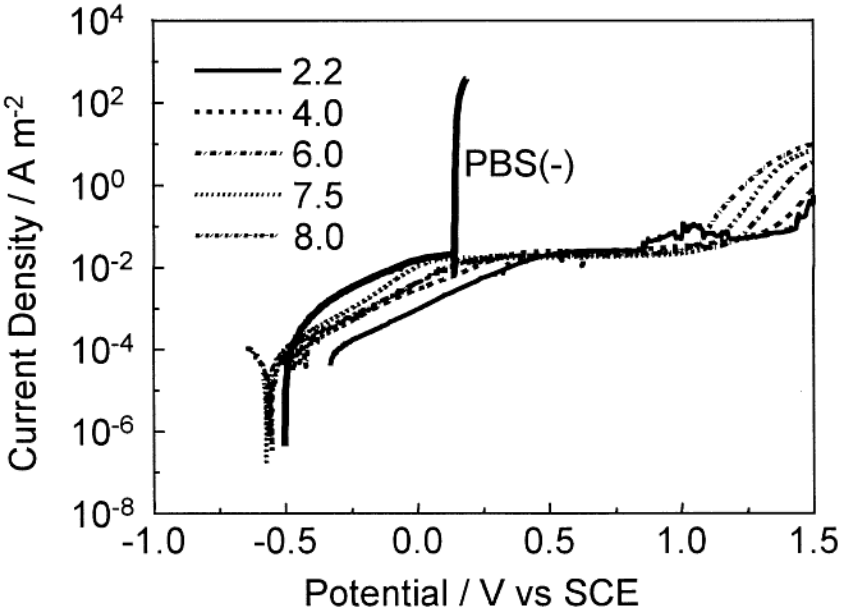

Figure 2.22: Polarization curves of Zr65Al7.5Ni10Cu17.5 amorphous alloy in PCA with various pH levels and PBS (Phosphate Buffered Saline) [63].

According to the curves, it seems that the current density at lower potentials was reduced with a decrease of pH. In the passive region, a stable domain could be noticed for all the curves: Consequently, the current density (i_{ps}) was not dependent on the pH. Otherwise, some observations could also be noted about the potential. E_{open} was higher for the lowest pH values, whereas E_{pit} was also influenced by the pH change because it was the same for all the attempts.

2.7.2 Surface perpetration

Orthopedic implants are supplied with surface finish ranging from rough grit-blasted to smooth, buffed or electropolished surfaces.

All existing implant metals and alloys depend on passive film for protection against corrosion. Scratching and other surface damages produced during implantation could also influence the subsequent corrosion rates [64]. Figure 2.23 shows that as it is expected, the sand blast treatment results in the highest corrosion rate and the electropolished specimen has the lowest rate.

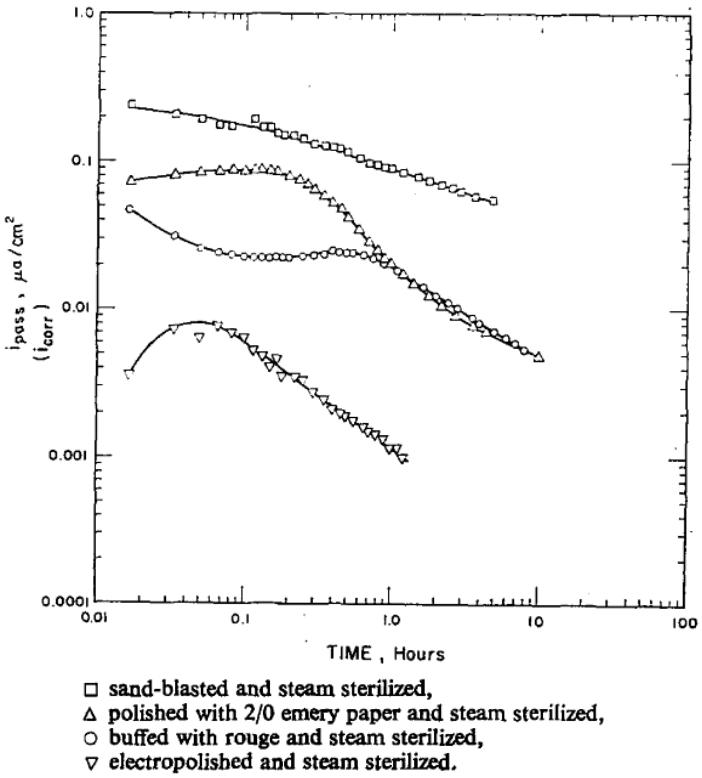

Figure 2.23: Effect of surface finish on the corrosion rate of the steam- sterilized type 316 stainless steel [64].

According to Revie and Greene [64], scratching and other minor surface damage have a little influence on the corrosion characteristics of implant alloys, however, electropolishing of implants is recommended.

2.7.3 Temperature

Temperature is important parameter as it can affect the corrosion properties. By increasing the temperature, the thickness of diffusion layer decreases whereas the critical current density ($i_{critical}$) increases. Also, temperature has effect on the solution and dissolution of materials. Moreover, temperature plays an important role in concentration of species or pH of the solvent. For instance, pure water can have a lower pH than 7 at a higher temperature. So, the temperature can change the pH a more toward the acidic values.

2.8 Suggestion for improvement of implant corrosion properties

a) Surface treatment [65]:

1. Shot peening or nitriding. It has been recently shown that nitriding can reduce the magnitude of fretting corrosion of Ti-6AI-4V devices (Maurer et al, 1993).
2. Implantation of ions (C, N, etc.) to harden the surface. This can improve the resistance to wear accelerated corrosion phenomenon (Buchanan et al, 1987).
3. Passivation, to thicken the protective oxide (Jacobs et al., 1998).
4. Electroplishing to remove surface roughness (Jacobs et al, 1998).

b) Quality control

1. Improved standards and quality control. The manufacturer should adopt the recommended metallurgical standards, fabricate the implants with care.
2. Improvements in design to minimize pits, crevices, large grain size, inclusions and porosity (Park and Lakes, 1992). Also, improved cleanliness has largely eliminated pitting (Black, 1988).
3. The carbon level to be less than 0.03 % has eliminated the risk of inter-crystalline corrosion that can happen when there is a chromium carbide precipitation at the grain boundary in stainless steel with carbon content above the mentioned value. (Park and Lakes, 1992).
4. Avoiding implantation of different types of metal in the same region (Atkinson and Jobbins, 1981).

c) Research and development

1. Development of alloy with good wear resistance and ability to repassivate at a high rate (to prevent fretting)
2. Using an alloy, which its open circuit potential or rest potential lies below the critical potential for pitting (Park and Lakes, 1992).

3. Experimental Work

The current project is focused in two different areas. One was the development of bulk metallic glass from pure elements and the other one was investigating the electrochemical behavior of the produced BMG and compare it with an amorphous bulk metallic glasses. He results are also compare with the most common material in hip joint implant, which is surgical grade Co-Cr-Mo alloy and stainless steel 316 LVM.

3.1 Materials

3.1.1 Surgical grade cast Co-Cr-Mo alloy

The most common material in hip joint implants is, surgical grade Co-Cr-Mo alloy (F75). The corrosion properties of F75 was measured and compared to crystalline and amorphous Zr-based bulk metallic glass. The surgical grade cobalt alloy was supplied by Sandvik AB in the shape of rod with diameter of 14 mm. The chemical composition of surgical grade Co-Cr-Mo F75 can be found in table 3.1.

Table 3.1: Chemical composition of Co-Cr-Mo alloy (F75).

Alloying element	Co	Cr	Ni	Mo	Fe	Mn	Ti	C	N	Si
wt%	Bulk	28.01	0.22	5.26	0.15	0.6	0.09	0.213	83 ppm	0.8

3.1.2 Stainless steel 316 LVM

Stainless steel 316 LVM has been used as an implant material for a long time. Presence of Cr in stainless steel improves corrosion resistance, Ni provides good surface finish and Mo gives high hardness and helps maintain a cutting edge. The stainless steel samples were in rod shape with the diameter of 16 mm and the material is provided by Sandvik AB. The composition of stainless steel 316 LVM is presented in table 3.2.

Table 3.2: Composition of stainless steel LVM 316

Alloying element	Wt %	Alloying element	Wt %
Fe	Bulk	Ni	14
Cr	17.5	Mo	2.8
Cu	< 0.1	N	< 0.10
C	< 0.0025	P	<0.0025
Mn	1.7	S	< 0.003
Si	0.6		

3.1.3 Amorphous bulk metallic glass

$Zr_{55}Cu_{30}Ni_5Al_{10}$ BMG was used in this survey. It was provided by Prof. A. Inoue and Prof. Y. Yokoyama at Tohoku University in Japan. To ensure the absence of crystalline regions x–ray diffraction measurements was performed at the Norwegian University of Science and technology. (M. Skjellrudssveen, M Sci Thesis NTNU, Trondheim, 2010). The XRD pattern is presented in Figure 3.1. The pattern does not contain any sharp peak, which indicates the lack of crystalline structure. The near neighbor distances in bulk metallic glass results in the diffuse peaks in 2θ = 38° and 2θ = 65° [66].

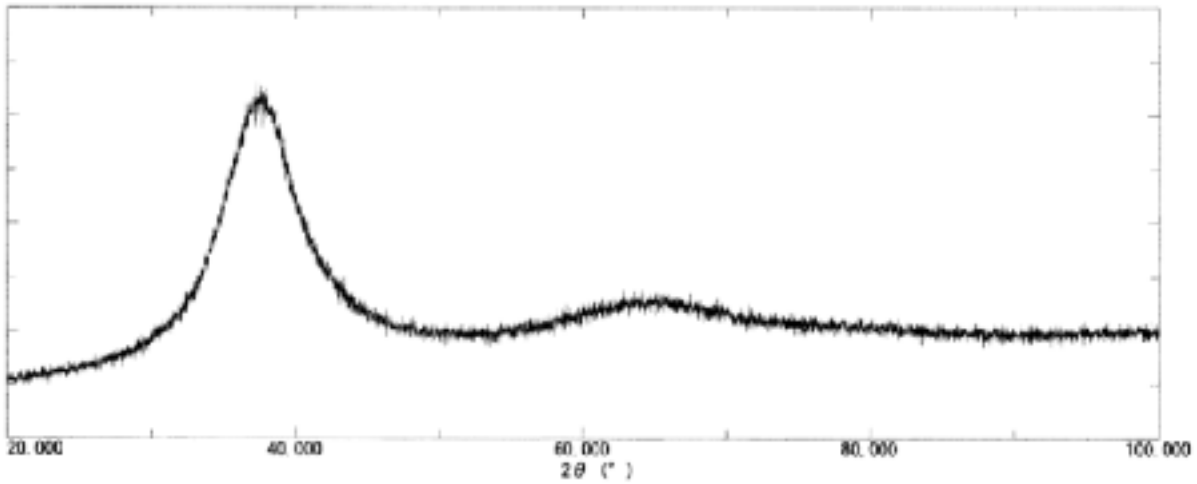

Figure 3.1: XRD pattern for Zr based bulk metallic glass (Cu/40 kV/150 mA). The vertical axis gives the intensity of the diffracted beam in arbitrary units (data from M. Skjellrudssveen, M Sci Thesis NTNU, Trondheim, 2010) [66].

3.2 BMG production

For the production of $Zr_{55}Cu_{30}Ni_5Al_{10}$ BMG, pure elements were used because it is very sensitive to impurities especially small amount of oxygen. The production was carried out in a vacuumed atmosphere and quenched in the liquid nitrogen.

Amorphous BMG samples, provided by Prof. A. Inoue and Prof. Y. Yokoyama at Tohoku University in Japan produced by cup-cap casting technique and there was an attempt to produce the same BMG with the facilities that was available in NTNU and in KTH. In order to produce $Zr_{55}Cu_{30}Ni_5Al_{10}$ BMG, specific amount of pure elements was placed in alumina crucible

with 3 cm diameter. In order to avoid oxygen in the sample, the crucible was placed in a vacuum quartz capsule, which had been flushed with argon gas (Figure 3.2). Moreover, argon gas was purged in the furnace during the experiment in order to protect the sample in case of any crack in quartz tube during the experiment.

Figure 3.2: Vacuum capsule with alumina crucible inside.

Three different capsules were made for different purposes. Inside one capsule there was BMG from Japan for re-melting and making a crystalline sample out of it. Inside the other one was pure elements to make a BMG and the in third capsule there was also pure elements to make a crystalline BMG sample.

In the next step capsule was placed in the vertical resistance furnace and heat it up until 1100 °C (Figure 3.3). There set of samples were produced i.e. BMG from pure elements (Crystalline and amorphous). For making the crystalline sample from amorphous BMG from Japan, the heating time was 4 hours and cooling rate was very low, about 5°C per minute and for amorphous BMG from pure elements the heating time was 20 hours and the sample was quenched in the liquid nitrogen. In order to produce crystalline BMG from pure elements same procedure was followed as for development of amorphous except the cool rate was slow (5°C per minute)

Figure 3.3: Vertical resistance furnace used for production of amorphous and crystalline BMG.

3.3 Electrochemical measurement

Electrochemical measurements were conducted to evaluate the corrosion behavior of the three different materials, Stainless steel 316, Co-Cr-Mo, crystalline and amorphous BMG. For the electrochemical experiments, all the variables were kept constant except temperature (25 °C and 37 °C, which is the body temperature), pH (7.4 and 5.2) and presence of albumin (a common protein in human body) in the phosphate buffered saline (PBS) solution. The aim was to investigate the occurrence of an infection in the body and compare it to the normal situation. Each experiment was repeated at least three times to ensure about the reproducibility of the result.

Figure 3.4 simply illustrate the electrochemical circuit and a picture of cell set up [66] and Figure 3.5 shows the electrochemical cell configuration. For more information about electrochemical equipment set-up, reader is referred to work done by Martin [58].

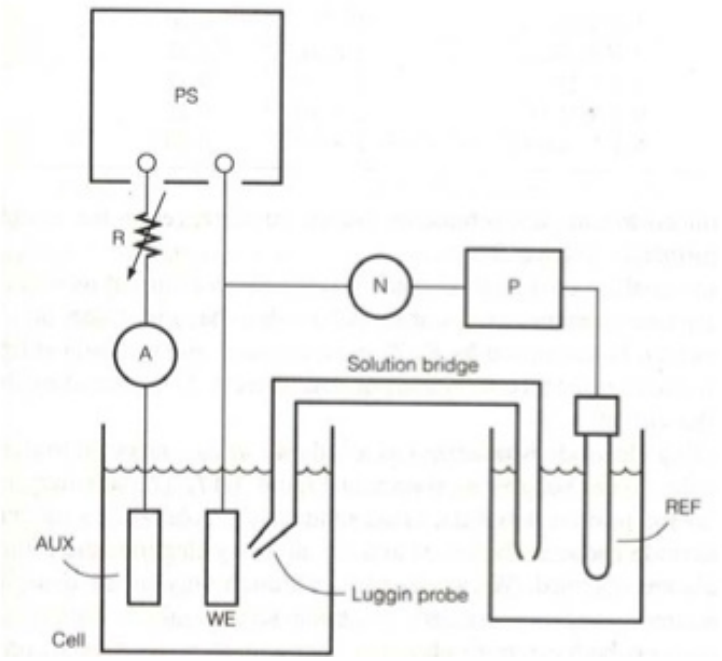

Figure 3.4: Schematic picture of the electrochemical circuit [66].

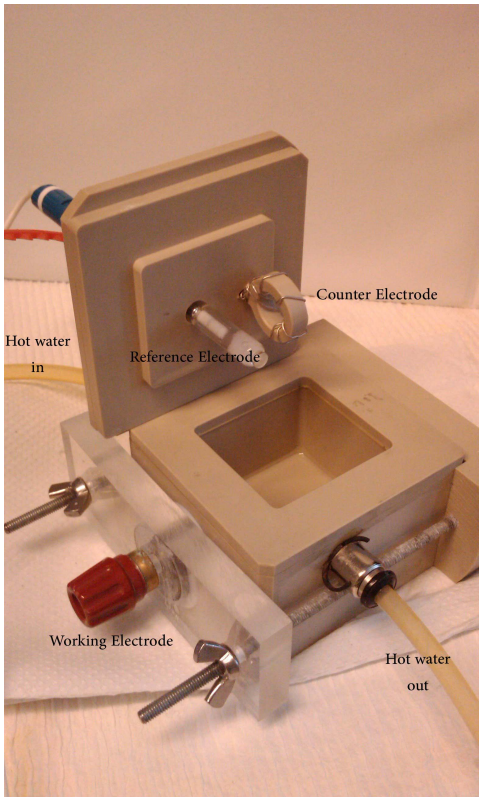

Figure 3.5: Electrochemical cell configuration

3.3.1 Sample preparation

Samples for electrochemical measurements were prepared by cutting, polishing and washing. All samples were cut into small pieces with the thickness of around 5 mm. The cutting speed was very low and cooling liquid was used to reduce the heat generation, which leads to change in the original microstructure. Then, grinding papers with different grades were used for 80, 160, 320, 400, 600, 1200, 2500 #SiC coarse and fine grinding. After final grinding step, samples were washed by water and ethanol 95%. To remove any grinding products on the surface of samples, the washed samples were placed in ethanol ultra sonic bath for 2 minutes and dried with the warm air.

3.3.2 Electrolyte

The electrolyte, which was used for electrochemical measurements, was Phosphate Buffered Saline (PBS) with the concentration of 0.05 M phosphate buffered and 0.15 M NaCl. The electrolyte consisted of 42.4 mM K_2HPO_4 (MERCK 99%), 7.6 mM KH_2PO_4 (MERCK 99%) and 0.15 M NaCl (MERCK 99%). High purity distilled water (Millipore-MPGP04001) was used to dilute the electrolyte. In order to reach the targeted pH (7.4 or 5.2) 1 M HCl and 1 M NaOH were used and the pH was measured with a pH-meter before and after the experiment.

On the other hand, for evaluating the effect of protein in the corrosion properties, albumin fraction V (MERCK 99%) with the concentration of 2 gram/liter was added to the PBS solution with pH 7.4 and 5.2. To restrict any foam formation and denaturation of the protein, shaking of the solution was avoided.

3.3.3 Measurement

The exposure time for the open circuit potential (OCP) was 1 hour in different solutions with Solartron Mobery potentiostat with the acquisition rate of 5 points per second. For further explanation about the electrochemical measurement and working with CorrWare software see reference [66].

Potentiodynamic polarization tests for the alloys performed with the same device in the solutions with the scan rate of 2 mV/sec. To remove any possible oxide on the surface, samples were cathodically polarized to -1.5 V vs SCE (Saturated Calomel Electrode) from the open circuit potential. Then the potential was swept from the same point -1.5 V vs SCE to 1.5 V vs SCE and the current was measured and log I versus E was registered. The maximum potential was 1.5 V vs SCE for the Co-Cr-Mo, because the break down in the passive layer at higher potentials. This value was 0.6 V vs SCE for both crystalline and amorphous BMGs. Some times to avoid any severe damage on sample; the potential increase was stopped manually. All the electro

chemical measurements performed with respect to the saturated calomel electrode (+0.2444 V vs. Standard Hydrogen Electrode, Radiometer analytical-Ref 401)

4.3 Pitting corrosion

Pitting corrosion is a localized form of corrosion by which cavities or "holes" are produced in the material. Pitting is considered to be more dangerous than uniform corrosion damage because it is more difficult to detect, predict and design against. The aim of this study was also to evaluate pitting corrosion tendencies in any of the materials.

4.3.1 Sample preparation

Sample preparation is similar to samples for electrochemical measurements except the last grinding paper was 4000 #SiC, because optical micrographs have to be taken after each test to see the pitting corrosion. So, to get a better quality in images, surface is important. Moreover, coarse surface can increase the tendency of pitting.

4.3.2 Electrolyte

The PBS solution used for study pitting corrosion assessment was the same used for electrochemical experiments without albumin and pH 7.4.

4.3.3 Measurement

The cell and software used in this experiment is the same as for the electrochemical measurement. All other adjustments are also the same as electrochemical measurement except the end point of the experiment was, when the cathodic current density reaches the value of 10^{-3} A/cm^2. By considering general polarization curve of the amorphous or crystalline BMG, it can be assumed that this current value is in the pitting region of the materials.

3.5 Fourier Transformation Infrared (FTIR)- spectroscopy

The aim of the FTIR-spectroscopy measurements was to investigate the adsorption of the protein on the material surface for different concentrations of albumin in the PBS solution. The experiments were carried out on surgical grade Co-Cr-Mo alloy, amorphous BMG and re-melted BMG with crystalline structure.

3.5.1 Sample preparation

The samples for FTIR-spectroscopy should be longer at least in one direction. Sample preparation is the same as for electrochemical measurement except that the grinding step was extended until 4000 #SiC, due to avoid rough surface finish and prevent infrared scattering, which can lead to noise in results.

3.5.2 Electrolyte

The PBS solution used for the FTIR-spectroscopy measurements was the same as electrochemical experiments. The only difference was the variation of albumin (0.005, 0.1, 0.6 and 2g/L), which was used in FTIR- spectroscopy.

3.5.3 Equipment

FTIR measurements were carried out in a reflection mode using a 78° incidence angle using a Varian 7000 spectrometer with a linearized narrow band MCT detector. The infrared light was p-polarized using a KRS-5 wire grid polarizer.

3.5.4 Measurement

For the spectrum acquisition, one average of 1000 scans was employed with a resolution of 8 cm^{-1}. All spectra were normalized against a background spectrum using a clean sample in order to eliminate as much as possible noise from the experimental device. A summary of the adjustments for the FTIR measurement can be seen in Table 3.3.

Table 3.3: FTIR spectrometer adjustment.

Spectrometer Brand	Varian 7000
Scan number	1000
Incidence angel (°)	78
Speed (KHz)	20
Resolution (cm^{-1})	8
Filter	5
UDR	2
Sensitivity	1
Wavelength domain (cm^{-1})	4500 to 600

After measuring the background spectrum of the clean samples, the sample was immersed in the solution with albumin. FTIR analyses were done for Co-Cr-Mo alloy, amorphous and crystalline BMG. Each experiment was repeated at least 3 times to be sure about the

reproducibility of obtained results. There were different solutions for this measurement; PBS with the pH of 7.4 with various concentration of albumin (0.005, 0.1, 0.6, 2 g/L) and PBS with the pH of 5.2 and albumin concentration of 2-g/L. The exposure time of samples for various solutions was 40 minutes. Afterward samples were carefully removed and rinsed twice with distilled water. Then, the samples were dried to remove the water trace on the surface as much as possible. Finally, the samples were placed on a holder inside the spectrometer for the measurement. Figure 3.6 shows inside the arrangement inside spectrometer, which consists of incidence angel regulator, Mirrors and sample holder.

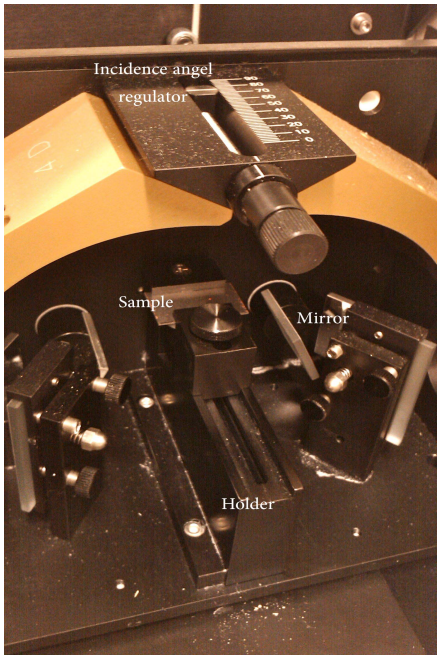

Figure 3.6: Inside FTIR spectrometer.

One small factor, which can affect the results, is the position of the samples. Each sample must be placed in the same position for background and main spectra measurement. Moreover the water spectrum had to be subtracted to avoid troubles caused by the water inside the spectrometer.

3.6 Electrochemical Impedance Spectroscopy (EIS)

Electrochemical impedance spectroscopy represents a very sensitive method for the in situ study of the adsorption of organic and biological molecules, as well as for the characterization of protein adsorption [71].

3.6.1 Sample preparation

Sample preparation is the same as for electrochemical measurement. Sample should be washed and dried with hot air. The delay time between polishing and using the sample in the cell is important and it should be constant for all experiments.

3.6.2 Electrolyte

The electrolyte, which was used for EIS, was Phosphate Buffered Saline (PBS) with the same composition as used for electrochemical measurements (chapter 3.3.2).

On the other hand, for evaluating the effect of protein, albumin fraction V (MERCK 99%) with the concentration of 2 gram/liter was added to the PBS solution with pH 7.4. To restrict any foam formation and denaturation of the protein, any shaking of the solution needs to be avoided.

3.6.3 Equipment

An Autolab PGSTAT 302 potentiostat with an FRA2 frequency response analyzer (Eco Chemie B.V.) was used for the EIS measurements.

3.6.4 Measurement

The amplitude of sinusoidal AC perturbation that applied to the sample was 10 mV. The sample surface area of 0.18 cm^2 the samples were exposed to the electrolyte. The measurements performed at open circuit potential. The frequency was varied between 10^5 and 10^{-2} Hz with 10 points/decade and current was between 10^{-2}-10^{-7} Amp. The set-up used a saturated calomel reference electrode (+0.2444 V vs. Standard Hydrogen Electrode, Radiometer analytical-Ref 401) and a platinum counter electrode. The amorphous Zr-based bulk metallic glass, stainless steel 316 LVM and Co-Co-Mo alloy F75 with the surface roughness of 2500 # SiC were used as working electrode.

4. Results and discussion

4.1 SEM images and XRD patterns of Zr-based alloys

4.1.1 BMG provided by Tohoku University in Japan

The SEM image of the amorphous bulk metallic glass that was made in Japan with cup-cap casting technique can be seen in the figure 4.1.

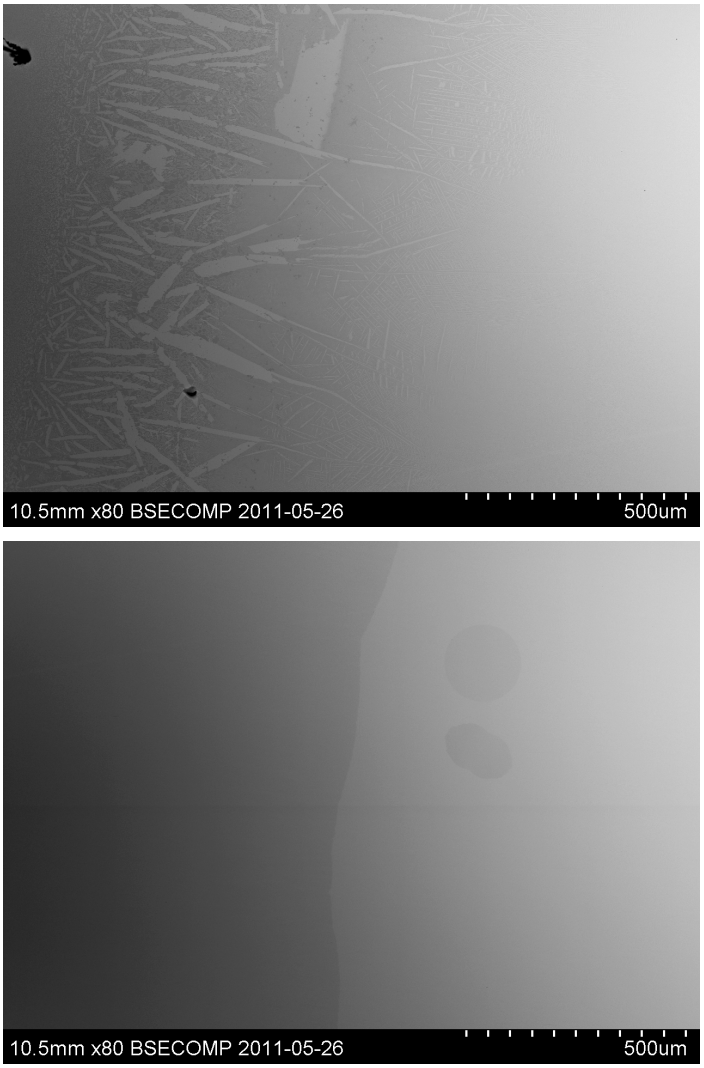

Figure 4.1: SEM image of the bulk metallic glass. (a) near the edge (b) the center of the sample.

Some needles and dendritic structure can be seen near the edge. Inside of the sample, it can be seen that needles disappear and amorphous structure becomes more evident. This result can be proven again with the XRD result of the same sample, which is presented in Figure 4.4. The crystalline region in the amorphous BMG is like a narrow band around the edge of sample with width of around 400-500 um.

Figure 4.2, shows the crystalline structure that was observed in BMG composed of, needles, dendrites and spheroids are clear and the composition of each phase is reported in the Table 4.1. This crystalline structure was observed just in the edge of the sample.

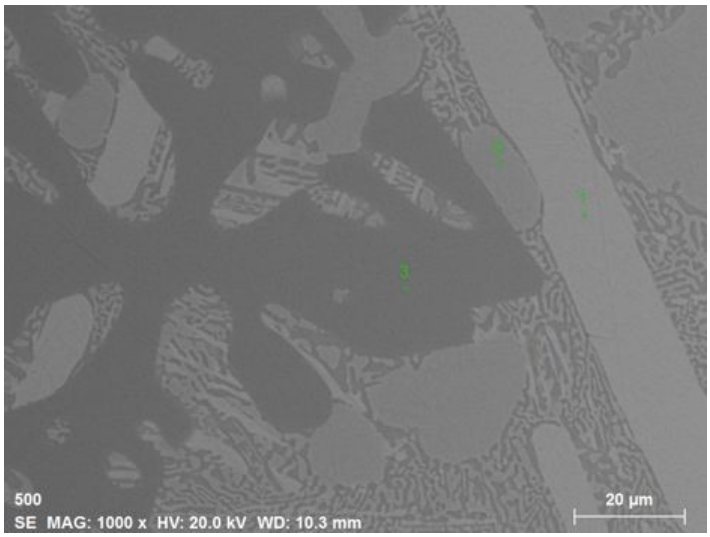

Figure 4.2: SEM image of the BMG from Tohoku University, Japan with 1000X magnification. Three different phases are clear; 1- Needle, 2- Spheroid, 3- Dendrite.

Table 4.1 gives the concentration of different elements of the three phases in the figure 4.2. Concentrations of phases were measured at various places and the results in the Table 4.1 are based on the average value.

Table 4.1: concentration of elements (wt%) in different phases.

	Zr	**Cu**	**Ni**	**Al**	**O**
1- Needle	71	22	2	0.5	4.5
2- Spheroid	58	31	6	1.5	3.5
3- Dendrite	62	24	2	7	5

Figure 4.3 is an image from inside of the BMG sample. It can be seen that there is no crystals in the central part and it is completely amorphous.

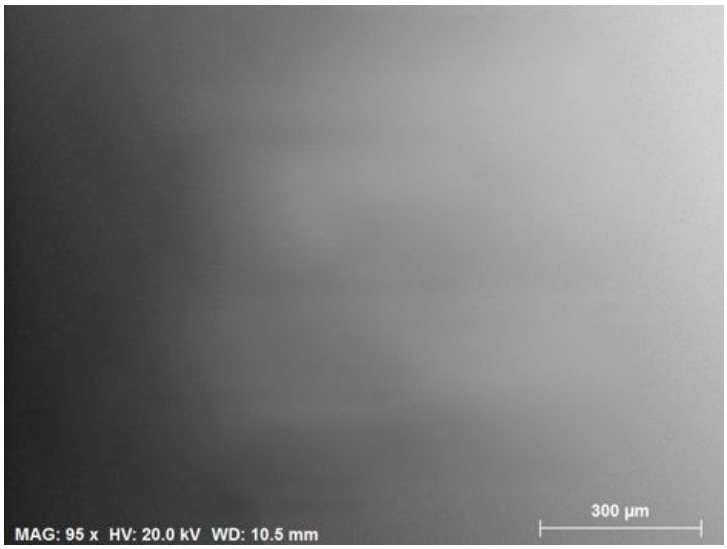

Figure 4.3: SEM image of the BMG from Tohoku University, Japan with 95X magnification (center of the sample).

Table 4.2: Concentration of elements (wt%) in amorphous phase.

	Zr	**Cu**	**Ni**	**Al**	**O**
Amorphous phase	64	25	4	3.5	3.5

BMG's are very sensitive even to very small amount of oxygen even in the order of 100 ppm, but in Table 4.2 it can be seen that there is 3.5wt% oxygen in the sample received from Japan.

To make sure about the amorphous nature of BMG sample, XRD pattern is given in the Figure 4.4. As it can be seen, the XRD pattern shows presence of some phases such as $CuZr_2$ and CuO in the sample

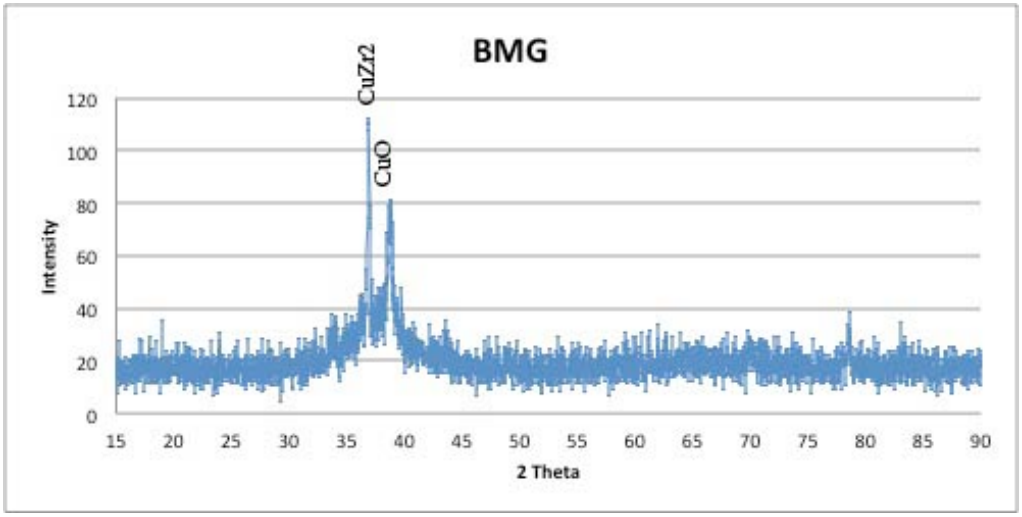

Figure 4.4: The X-Ray Diffraction (XRD) pattern (Cu/40 kV/150 mA) of the amorphous BMG sample provided by Tohoku University in Japan.

One explanation about this result is the purity of the sample or melting condition, which had some oxygen.

4.1.2 Crystalline BMG provided by Tohoku University in Japan

Another sample is the crystalline one with the same composition of the above bulk metallic glass that was provided from Japan. The crystalline structure of this sample can be seen in the figure 4.5. Three different phases, which are consisted of big needles, dendrites and spheroid, which are very clear in the Figure 4.6.

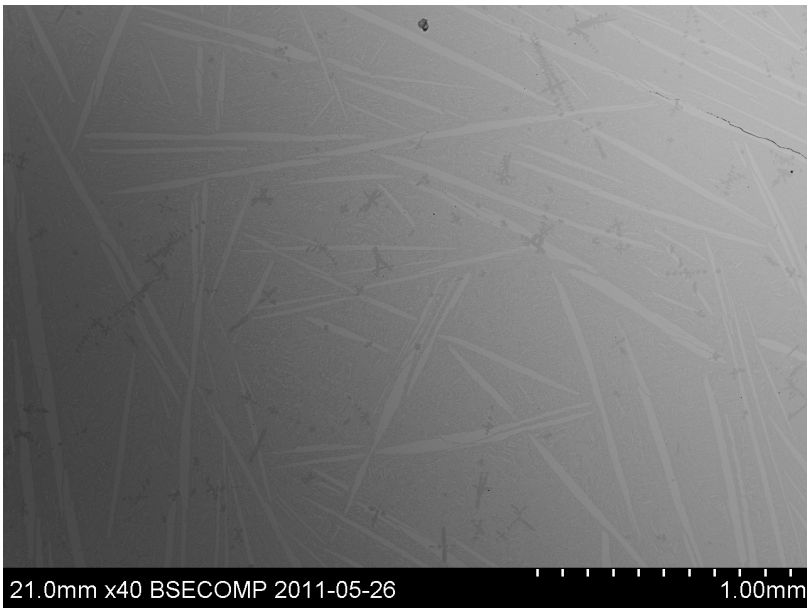

Figure 4.5: SEM image of the crystalline bulk metallic glass. Three different phases and big dendrites can be seen.

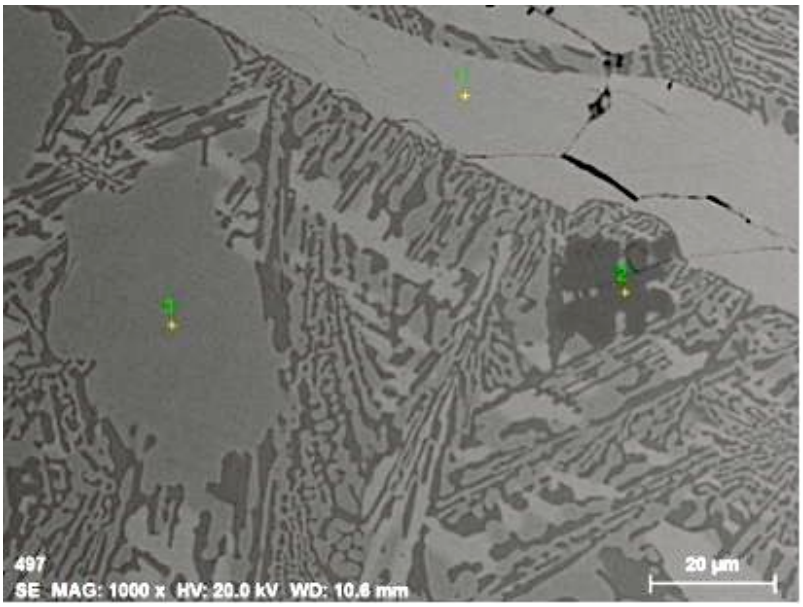

Figure 4.6: SEM image of the crystalline BMG made from BMG from Japan. Three different phases are clear; 1- needle, 2- dendrite, 3- spheroid.

Table 4.3 gives the concentration of different elements of the three phases in the figure 4.6. Concentrations of phases were measured in various places and the results in the Table 4.3 are the average.

Table 4.3: Concentration of elements (wt%) in different phases.

	Zr	Cu	Ni	Al	O
1- Needle	70	23	2	0.5	4.5
2- Dendrite	63	23.5	2	6.5	5
3- spheroid	58.5	31	5	2	3.5

As mentioned before, BMGs are very sensitive to oxygen and because of this, special condition was prepared not to let oxygen go inside the melt such as having a vacuumed capsule and flushing argon during melting, but even with these considerations about 4wt% of oxygen is present in the sample. By considering the Table 4.2, which shows that there is 3.5wt% oxygen in the preliminary BMG sample, it can be said that during remelting, not much oxygen has been introduced to the sample.

The X-Ray diffractogram recorded from the crystalline $Zr_{55}Cu_{30}Ni_5Al_{10}$ BMG is presented in Figure 4.7.

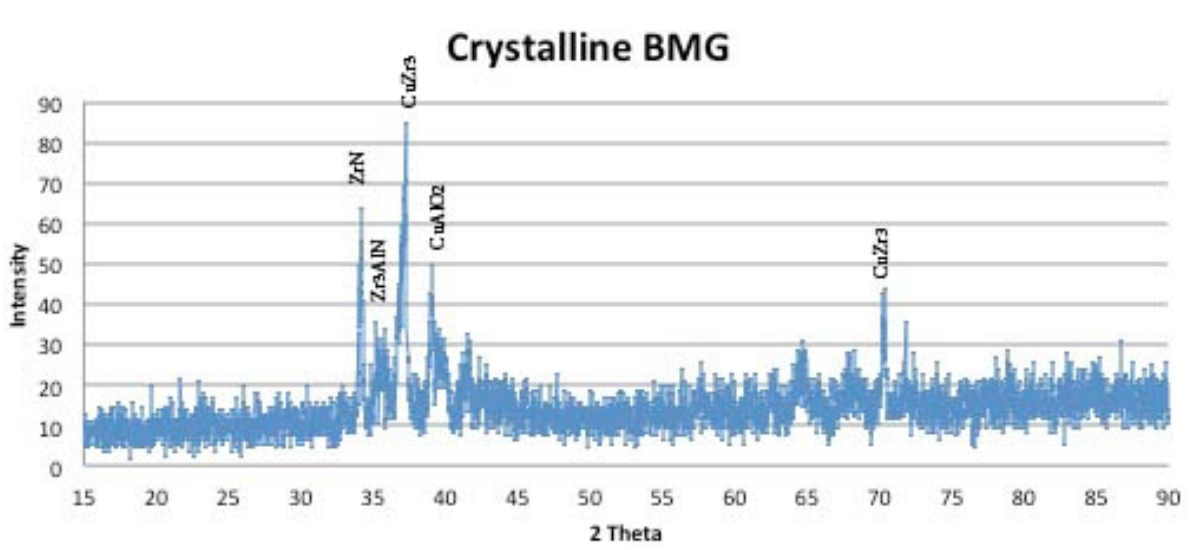

Figure 4.7: XRD pattern for crystalline Zr-based bulk metallic glass provided by Japan (Cu/40 kV/150 mA).

4.1.3 BMG produced in KTH

In order to develop the amorphous BMG sample, pure elements which was placed inside a vacuum capsule in advanced, were melted in the vacuumed vertical furnace up to 1100 °C for 5 hours and rapidly quench in the liquid nitrogen.

As it can be seen in the Figure 4.5, despite all the attempts for making an amorphous sample, dendrites and needles are clear.

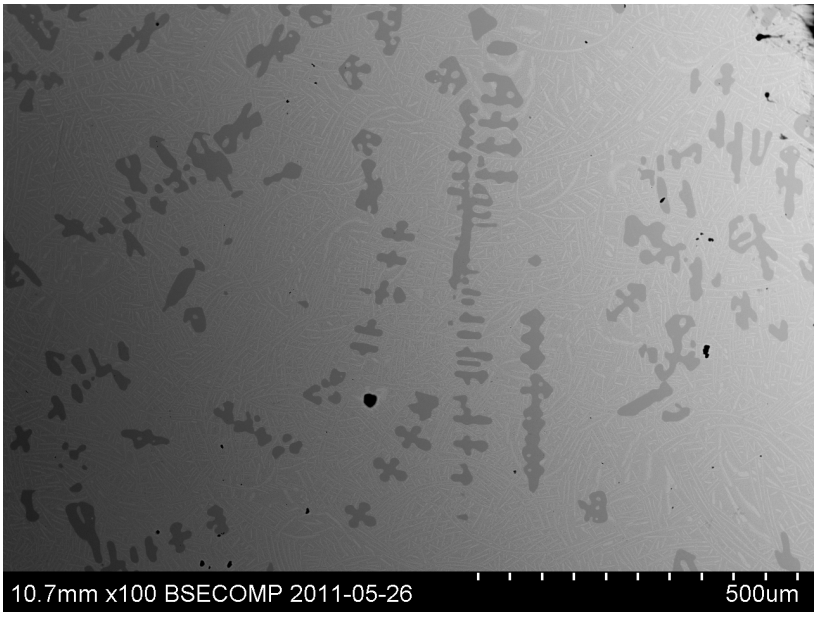

Figure 4.8: SEM image of the sample, which we tried to produce with amorphous structure. Dark grey dendrites and small needles can be seen.

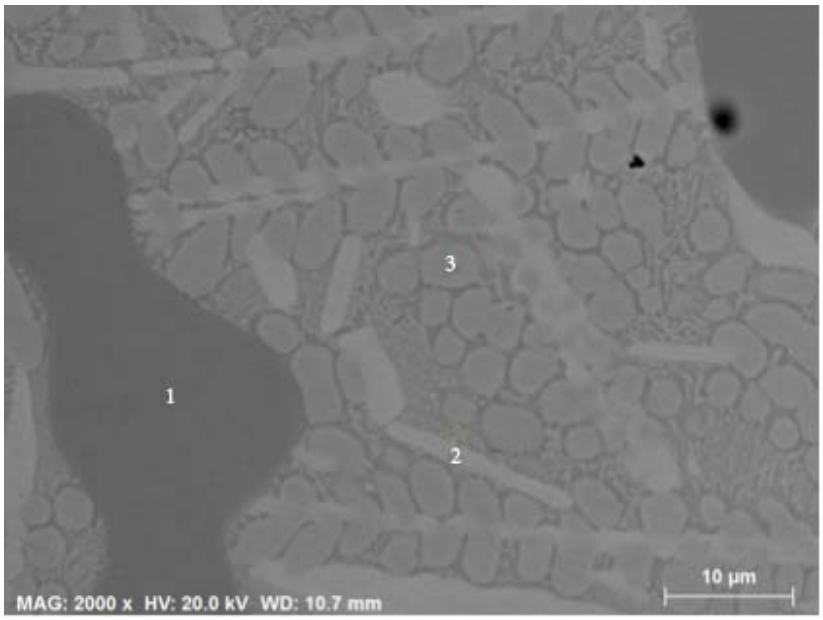

Figure 4.9: SEM image of the sample, which was tried to produce with amorphous structure. Three different phases are clear; 1- dendrite, 2- needle, 3- spheroid.

Table 4.4 gives the concentration of different elements of the three phases in the Figure 4.9. Concentrations of phases were measured in various places and the results in the Table 4.4 are based on the average value.

Table 4.4: concentration of elements (wt%) in different phases.

	Zr	**Cu**	**Ni**	**Al**	**O**
1- Dendrite	62	24	2.5	7	4.5
2- Needle	70	22	2.5	1	4.5
3- Spheroid	59	31	5	2	3

The X-Ray diffractogram recorded from the sample, which was tried to produce with amorphous structure, is presented in Figure 4.10. Four oxide peaks are clear in the XRD patter, which also shows that this procedure is very sensitive to oxygen.

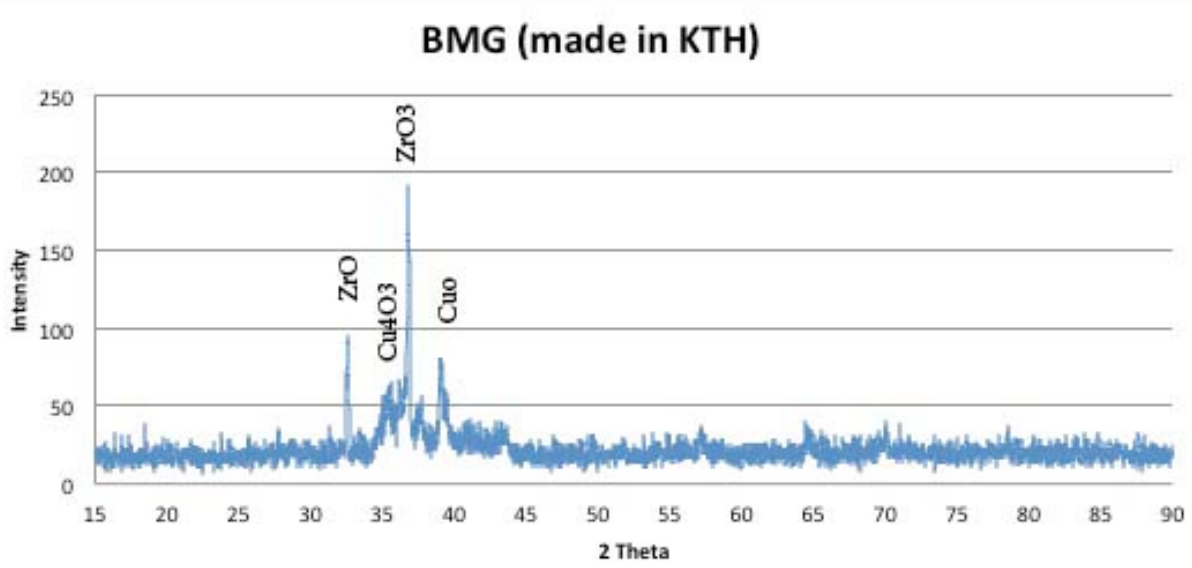

Figure 4.10: XRD pattern for the sample, which was tried to produce with amorphous structure (Cu/40 kV/150 mA).

4.1.4 Crystalline BMG produced in NTNU

This sample was made from the pure elements in the vacuum. Elements were put in the alumina crucible with diameter of 3cm and then the crucible was put in the vacuumed quartz capsule. Then the sample was heated up to 1100 °C for 20 hours and cooled down very slowly (5^{o}C per minute).

The crystalline structure of the BMG sample can be seen in the figure 4.11. Three different phases, which are consisted of big needles, dendrites and spheroid, that are very clearly shown in the figure 4.12 and in the Table 4.5 gives the concentration of different elements of the three phases in the figure 4.12. Concentrations of phases were measured in various places and the results in the Table 4.3 are based on the average value.

Dendrites and needles in this sample are bigger than that the crystalline one that was made from amorphous BMG from japan, but the compositions is similar.

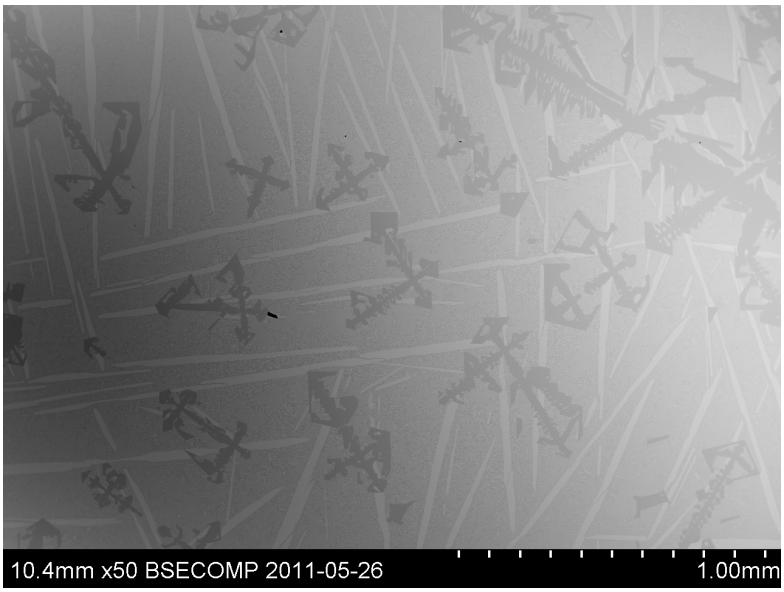

Figure 4.11: SEM image of the crystalline bulk metallic glass that was made in NTNU. Three different phases and big dendrites and needles can be seen.

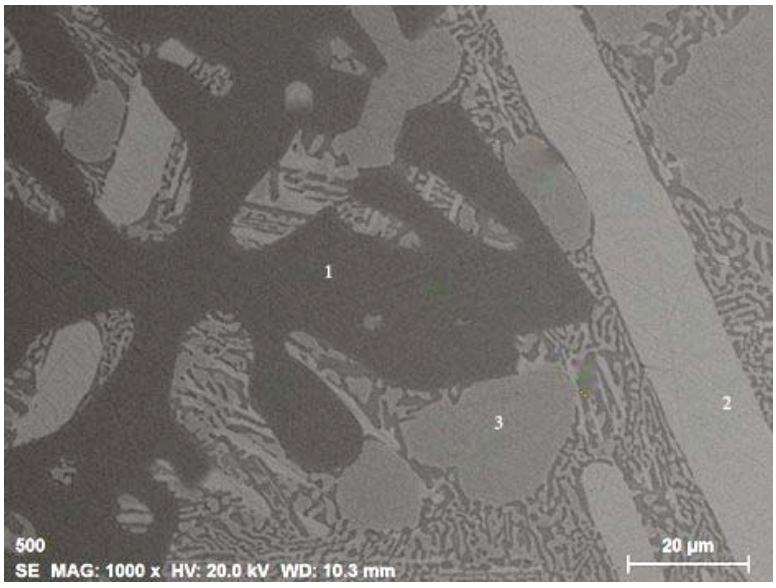

Figure 4.12: SEM image of the crystalline BMG made in NTNU. Three different phases are clear; 1- dendrite, 2- needle, 3- spheroid.

Table 4.5 gives the concentration of different elements of the three phases in the Figure 4.12. Concentrations of phases were measured at various places and the results in the Table 4.5 are based on the average values. As mentioned before, the result for the concentrations of elements is comparable to the results from the crystalline BMG made from BMG from Japan.

Table 4.5: concentration of elements (wt%) in different phases.

	Zr	Cu	Ni	Al	O
1- Dendrite	71	22	2	0.5	4.5
2- Needle	58.5	31	5.5	1.5	3.5
3- spheroid	62	24	2.5	6.5	5

The X-Ray diffractogram recorded from the crystalline sample made in NTNU, is presented in Figure 4.13.

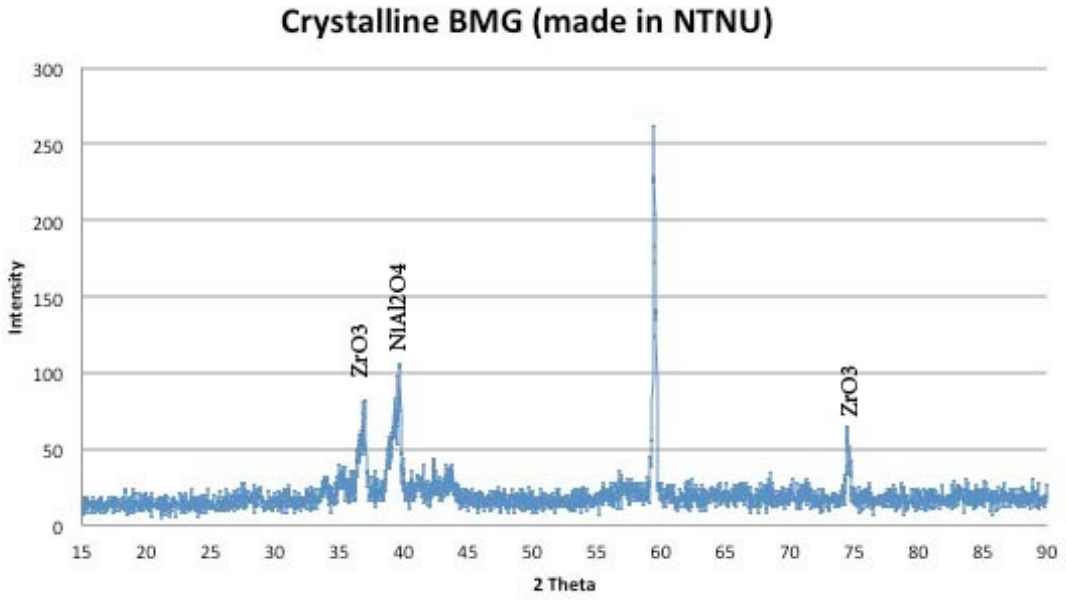

Figure 4.13: XRD pattern for the crystalline sample, which was made in NTNU (Cu/40 kV/150 mA).

There is one peak in $2\theta = 59$ that was not in the database.

4.2 Electrochemical measurement

To have a good understanding of the electrochemical behavior of the biomaterials, two different measurement techniques were employed in this project.

The first measurements were Open Circuit Potential (OCP) in order to reach a steady state condition before performing polarization measurements. The time evolution of the OCP also gives some information about the formation of the passive film on the sample's surface by increasing the potential.

The polarization measurements also tell about corrosion tendency of the samples. Indeed, polarization curve allows determining critical parameters associated with passive film breakdown and repassivation: corrosion potential, pitting potential, breakdown potential, corrosion current and passive current.

OCP measurements and polarization curve acquisitions for Co-Cr-Mo, stainless steel 316, crystalline and amorphous BMG, were obtained under varying conditions of temperatures, pH and presence of protein in the electrolyte. That is to say, in the electrochemical measurements, only the amorphous BMG from Japan and the crystalline BMG from remelting the BMG from Japan were used for experiments.

4.2.1 Temperature effect

One of the goals of this research was to investigate if the change of temperature has any effect on the corrosion properties of the biomaterials. Change in the temperature results in change of the thickness of the passive film, which results in decrease or increase of the corrosion resistance. Therefore, the same experiment was carried out for all materials at room temperature (20 °C) and body temperature (37°C) with and without the presence of albumin.

4.2.1.1 Co-Cr-Mo

Open circuit potential (OCP)

Figure 4.14 shows the curve of the OCP measurement for the Co-Cr-Mo alloy without albumin at 20°C and 37°C. The two curves are similar with exception of about 60 mV difference in the onset. Moreover, with the increase of the potential value is steady. It seems that the OCP value was slightly lower for temperature close to the body temperature.

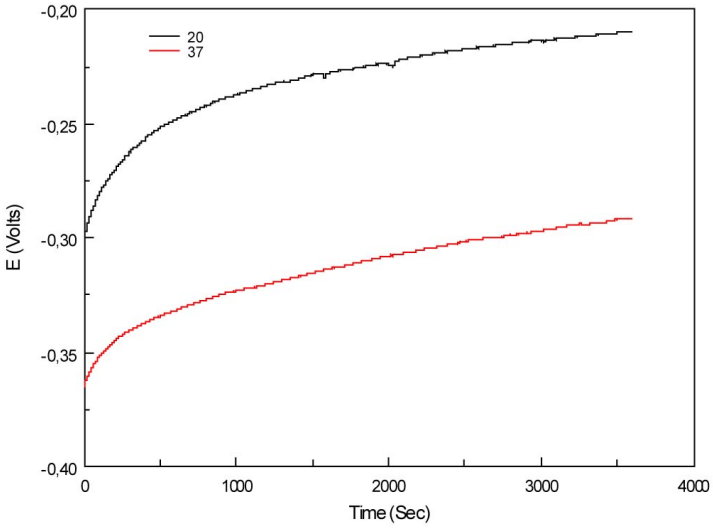

Figure 4.14: Effect of temperature on OCP value of surgical grade Co-Cr-Mo grade F75. Experimental conditions: pH=7.4; PBS; T=20°C and T=37°C.

In order to confirm the trend about the temperature effect, the experiment was repeated with the presence of 2 g/L albumin in the electrolyte (Figure 4.15). The resulting curves shows, the OCP value was higher for the experiment carried out at 37°C than the one done at room temperature.

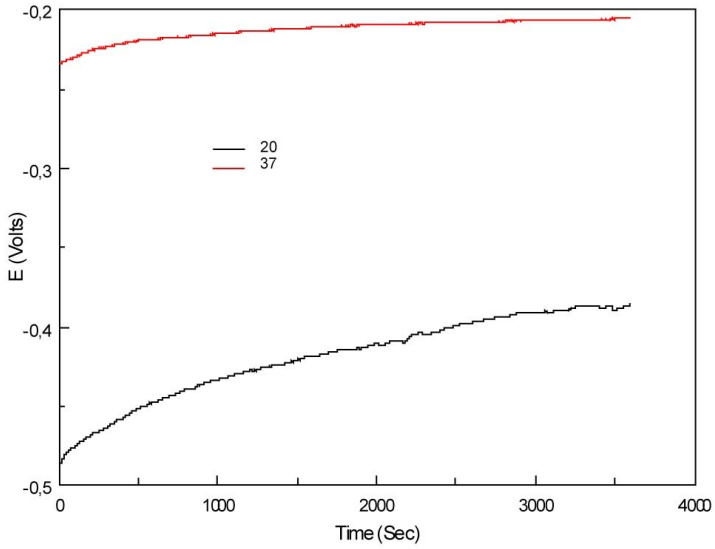

Figure 4.15: Effect of temperature on OCP value of surgical grade Co-Cr-Mo grade F75. Experimental conditions: pH=7.4; PBS with albumin addition (2 g/L); T=20°C and T=37°C.

Based on these results it is evident that the presence of albumin interferes with the temperature effect on the OCP experiments. From these results, it seems that albumin presence and higher temperature have opposite effects and change in the OCP curve. These

observations are in contrast to the results in previous work [58]. Further experiments are needed in order to understand the effect of temperature on corrosion behavior more conclusively.

Polarization Curve

Cyclic polarization measurements were performed at pH=7.4 without albumin at 20°C and 37°C, as shown in Figure 4.16. Increase in temperature may cause i_{corr} rise (there is a slight increase in the achieved plots too). Even if the i_{corr} variation between the two curves is minor. Furthermore, passive region is almost the same at both temperatures. Also an activation peak can be seen quite clearly in this figure. After the activation peaks the current will is stabilized in the passive region with a passive current of 1.4 x10-5 A/cm^2. After reaching the transpassive region a second peak can be seen which could be the result of oxidation of Co^{3+} to Co^{6+} in presence of phosphate ions in the electrolyte [69].

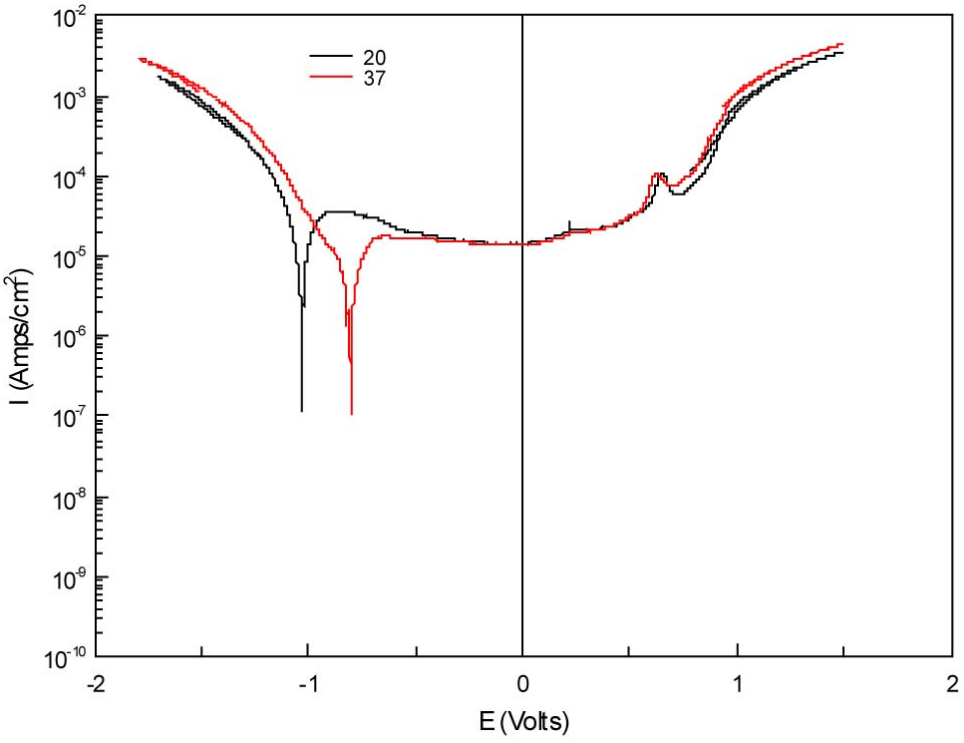

Figure 4.16: Effect of temperature on the polarization curve of surgical grade Co-Cr-Mo grade F75. Experimental conditions: pH=7.4; PBS; T=20°C and T=37°C.

The experiment was also carried out in presence of protein, as shown in Figure 4.17. The pattern of the two curves is not as smooth. Still the activation peak is distinguishable and the

peak for oxidation of Co^{3+} to Co^{6+} in presence of phosphate ions can bee seen for 37°C. This result is good agreement with the result in reference 58.

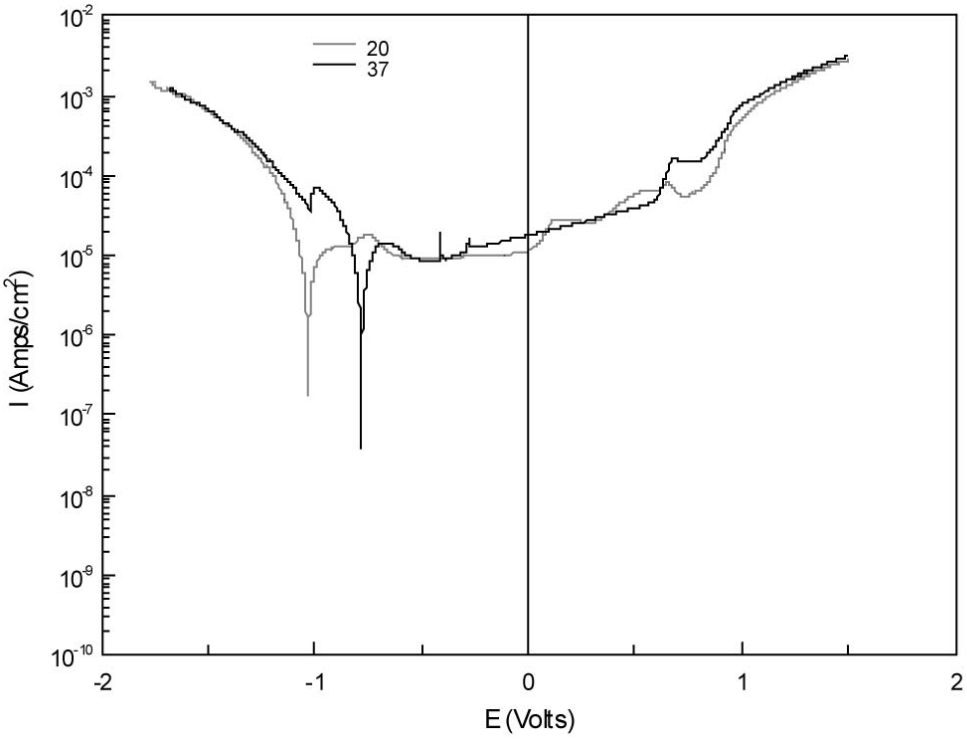

Figure 4.17: Effect of temperature on the polarization curve of surgical grade Co-Cr-Mo grade F75. Experimental conditions: pH=7.4; PBS with 2g/L albumin; T=20°C and T=37°C.

By comparing the results for the Figures 4.16 and 4.17, it can be argued that increase of the temperature results in increase of the corrosion potential (in this case the increase with temperature change is about 0.2 volts). On the other hand, increase in temperature leads to decrease in corrosion current density for around 0.5 A/cm^2. Also, there is not much difference in passive region.

4.2.1.2 Amorphous Bulk Metallic Glass (BMG)

Open circuit potential (OCP)

Figure 4.18 shows the curve of the OCP measurement for the amorphous zirconium based bulk metallic glass without albumin at 20°C and 37°C. The two curves are similar with exception of about 45 mV difference in the onset between them. The curve for 37°C dose not change that much during the experiment and it is almost constant with very small variations. Also, It seems that the OCP value was slightly lower for temperature close to the body temperature.

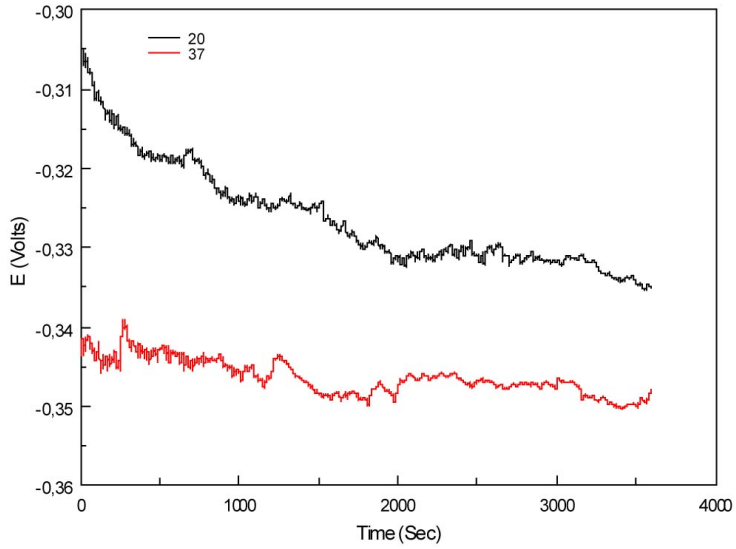

Figure 4.18: Effect of temperature on OCP value of bulk metallic glass. Experimental conditions: pH=7.4; PBS; T=20°C and T=37°C.

In order to confirm the regarding effect of temperature, the experiment was repeated with the presence of 2 g/L albumin in the electrolyte (Figure 4.19). According to the curves, the OCP value was lower for the experiment carried out at 37°C than the one done at room temperature.

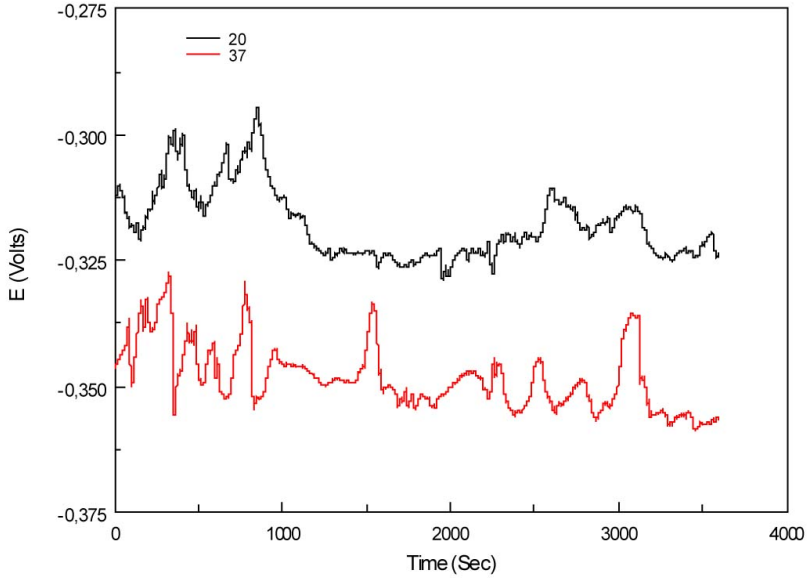

Figure 4.19: Effect of temperature on OCP value of bulk metallic glass. Experimental conditions: pH=7.4; PBS with albumin addition (2 g/L); T=20°C and T=37°C.

By considering the results, presented in Figures 4.18 and 4.19, it can be seen that for zirconium based bulk metallic glass, the OCP trend is almost constant Also with or without presence of

albumin, OCP is lower for the higher temperature near the body temperature as compared to the room temperature.

Polarization curve

Cyclic polarization curves were performed at pH=7.4 without albumin at 20°C and 37°C, as shown in Figure 4.20. Temperature increase should cause i_{corr} rise (there is a slight increase in the achieved plot, too). Variation in i_{corr} between the two curves is minor. Furthermore, passive region is almost the same in the both temperatures. One difference between the behavior of BMG and Co-Cr-Mo alloy is that there is a pitting potential for BMG (which was also visible by naked eyes after the experiment on the surface of the sample). Another difference is that there is no activation peak in this Figure, which was clear for Co-Cr-Mo alloy.

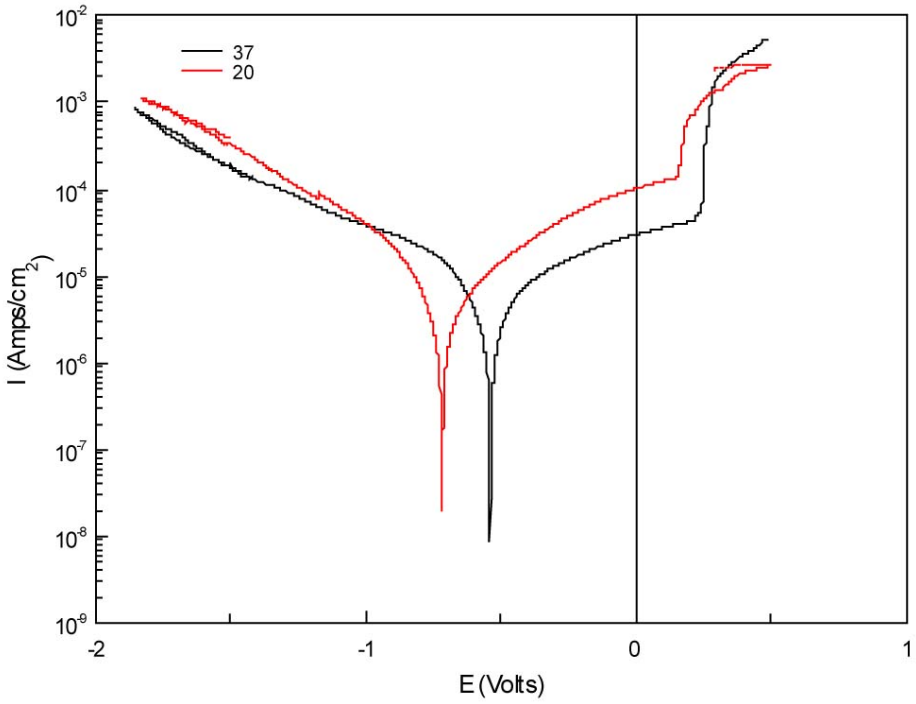

Figure 4.20: Effect of temperature on the polarization curve of Zirconium based bulk metallic glass. Experimental conditions: pH=7.4; PBS; T=20°C and T=37°C.

The experiment was also carried out in presence of protein, as shown in Figure 4.21.

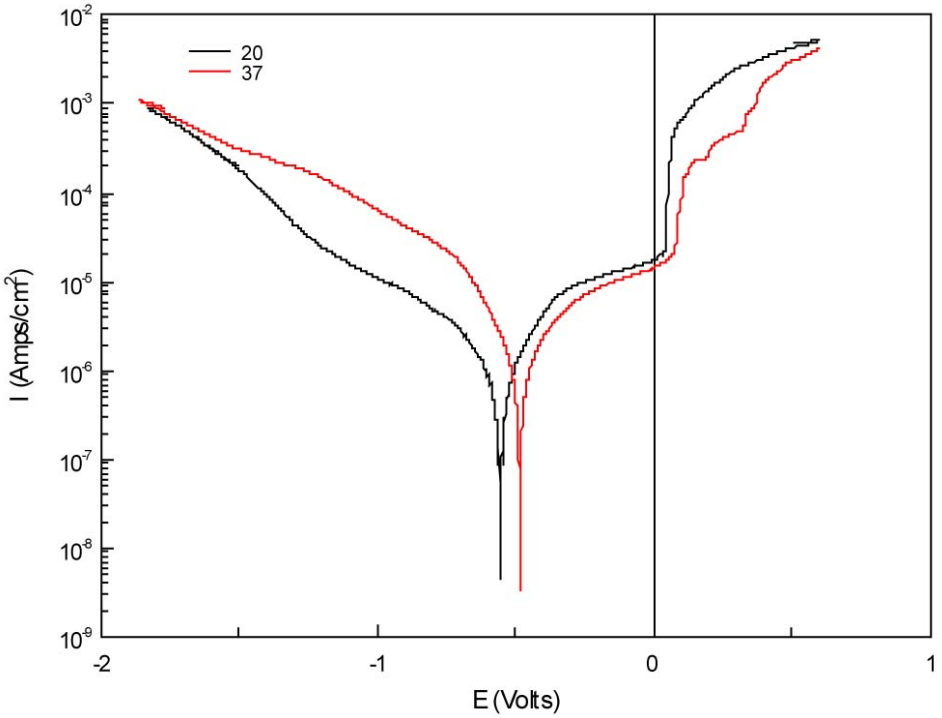

Figure 4.21: Effect of temperature on the polarization curve of zirconium based bulk metallic glass. Experimental conditions: pH=7.4; PBS with 2g/L albumin; T=20°C and T=37°C.

As a conclusion from Figures 4.20 and 4.21, it can be argued that increase in temperature results in increase in the corrosion potential and decrease in corrosion current density . It can Pitting corrosion potential was assessed between 0.05 to 0.28 volts.

4.2.1.3 Crystalline bulk metallic glass

Open circuit potential (OCP)

Figure 4.22 shows the curve of the OCP measurement for the crystalline zirconium based bulk metallic glass without albumin at 20°C and 37°C. The two curves were quite similar in exception of about 30 mV difference in the onset. In crystalline BMG, the curve for OCP are not smooth and similar to amorphous BMG. Also, It seems that the OCP value was slightly lower for temperature close to the body temperature.

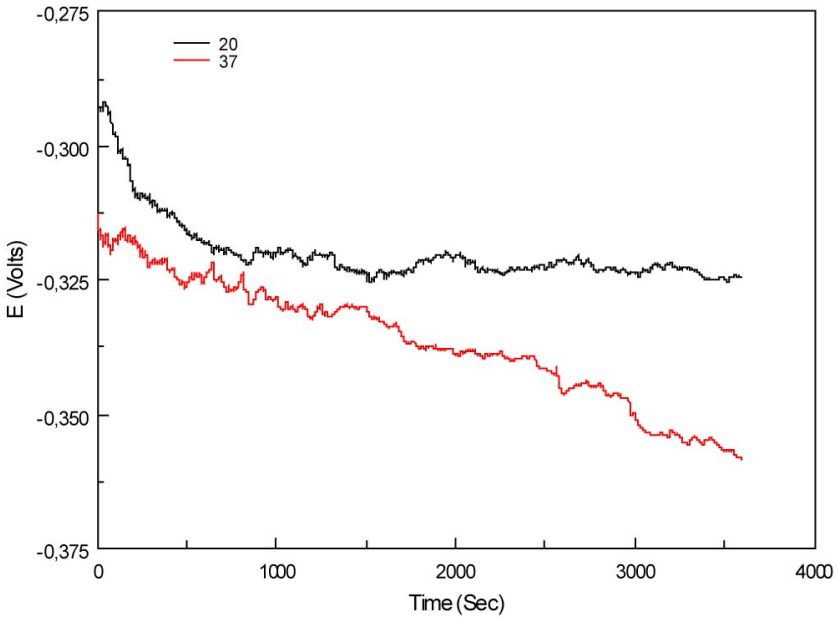

Figure 4.22: Effect of temperature on OCP value of crystalline bulk metallic glass. Experimental conditions: pH=7.4; PBS; T=20°C and T=37°C.

In order to confirm this trend about the temperature effect, the experiment was repeated with the presence of 2 g/L albumin in the electrolyte (Figure 4.23). According to the curves, the OCP value was lower for the experiment carried out at 37°C than the one done at room temperature.

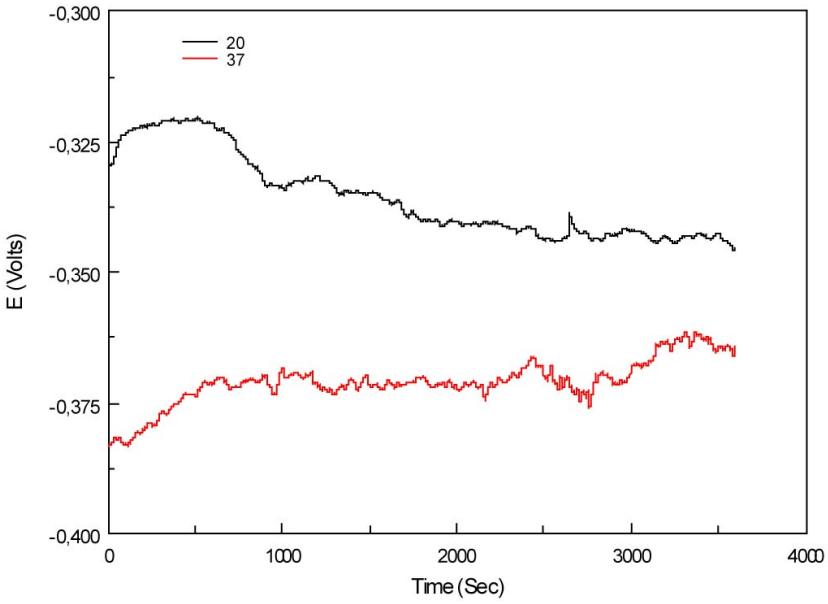

Figure 4.23: Effect of temperature on OCP value of crystalline bulk metallic glass. Experimental conditions: pH=7.4; PBS with albumin addition (2 g/L); T=20°C and T=37°C.

From Figures 4.22 and 4.23, it can be observed that for crystalline zirconium based bulk metallic glass, the OCP trend is almost constant with a small serration shape. Also with or without presence of albumin, OCP is lower for the higher temperature as compared to the room temperature.

Polarization curve

Cyclic polarization curves were performed at pH=7.4 without albumin at 20°C and 37°C, as shown in Figure 4.24. Passive region and pitting corrosion is almost the same in the both temperatures. One difference between the behavior of amorphous and crystalline BMG is that the pitting potential for crystalline BMG is lower than amorphous one and reason is that the crystalline one has defects and grain boundaries which are suitable places for the initiation of the corrosion while in the amorphous structure there is no such site. Because of decrease in the pitting potential, the passive region is quiet small. Generally it can be said that the corrosion behavior of crystalline BMG in PBS, pH 7.4 and in 37 °C and 20 °C is the same.

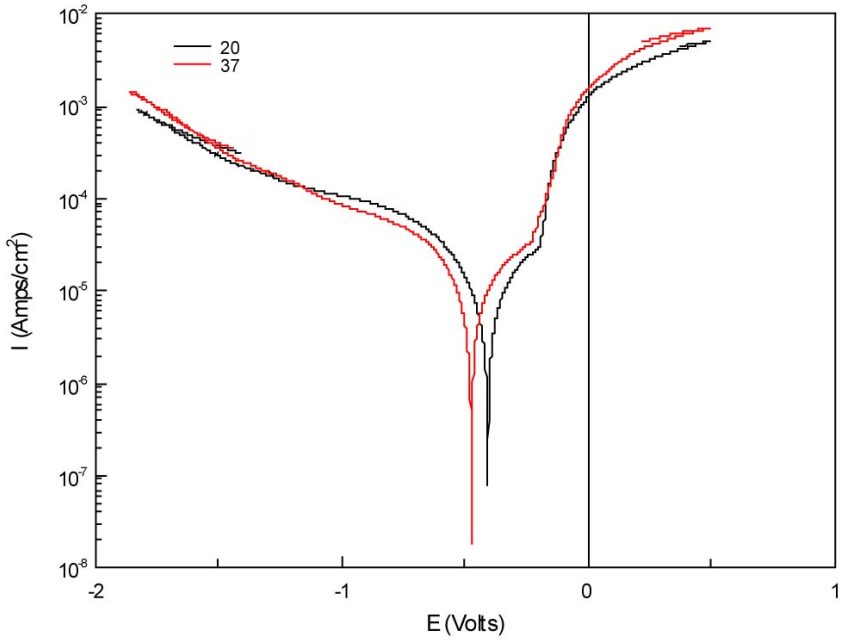

8

Figure 4.24: Effect of temperature on the polarization curve of crystalline Zirconium based bulk metallic glass. Experimental conditions: pH=7.4; PBS; T=20°C and T=37°C.

The experiment was also carried out in presence of protein, as shown in Figure 4.25. The patterns of the two curves are very similar to the previous one.

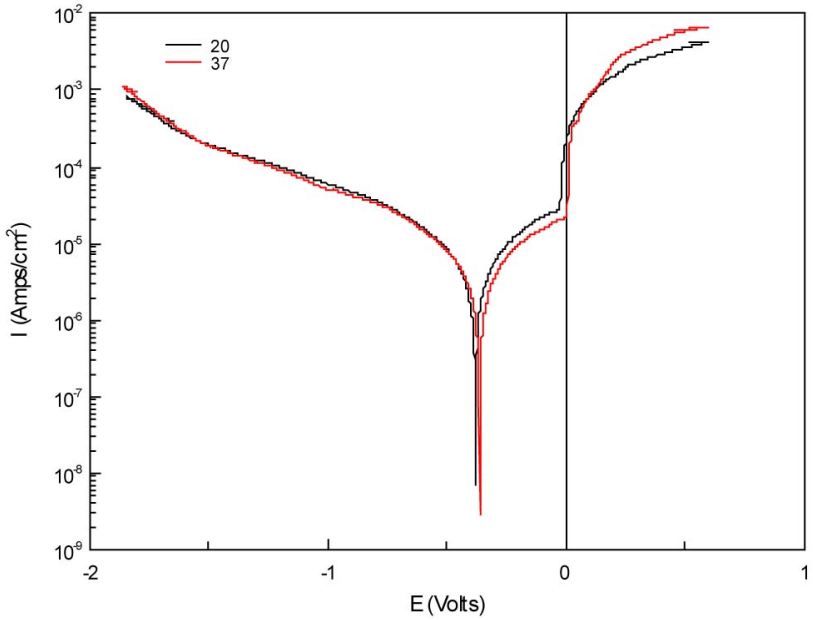

Figure 4.25: Effect of temperature on the polarization curve of crystalline zirconium based bulk metallic glass. Experimental conditions: pH=7.4; PBS with 2g/L albumin; T=20°C and T=37°C.

As conclusion from Figures 4.24 and 4.25, it can be said that presence of albumin increases the corrosion potential and also make the passive region a bit bigger. More importantly, it can be understood from these results that temperature dose not have that much effect on the corrosion behavior of the crystalline bulk metallic glass (with and without albumin).

4.2.2 pH effect

The pH value of the body decreases from 7.4 to 5.2 in case of infection. For this reason, to investigate the corrosion behavior of any implant material, it is important to examine it in different pH values to understand the material behavior in harsh environment. Generally, pH decrease causes a reduction of the corrosion resistance properties.

4.2.2.1 Co-Cr-Mo

Open circuit potential (OCP)

Figure 4.26 shows the results of the OCP measurements carried out for two pH values at 37°C. According to the curve, the pH seems to have a significant effect on the OCP. There is 15 mV difference in onset potential. Both curves look smooth and similar to each other.

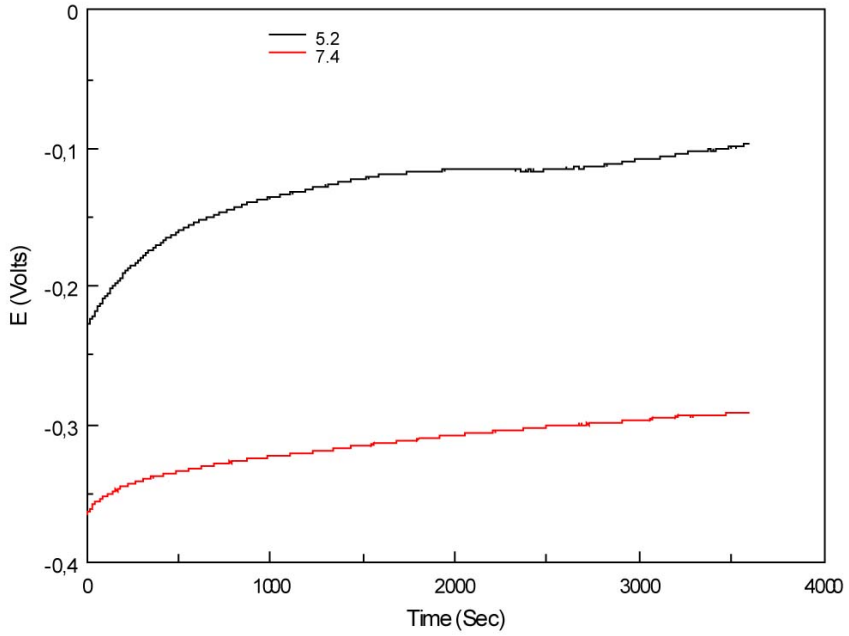

Figure 4.26: Effect of pH on OCP value of surgical grade Co-Cr-Mo grade F75. Experimental conditions: T=37°C; PBS; pH= 7.4 and 5.2.

The experiments were also performed with Co-Cr-Mo alloy with presence of albumin, as shown in Figure 4.27. The OPC looks similar to Figure 4.26. Comparing the result in Figure 4.27 with previous work [58] it can be seen that these results are in good agreement.

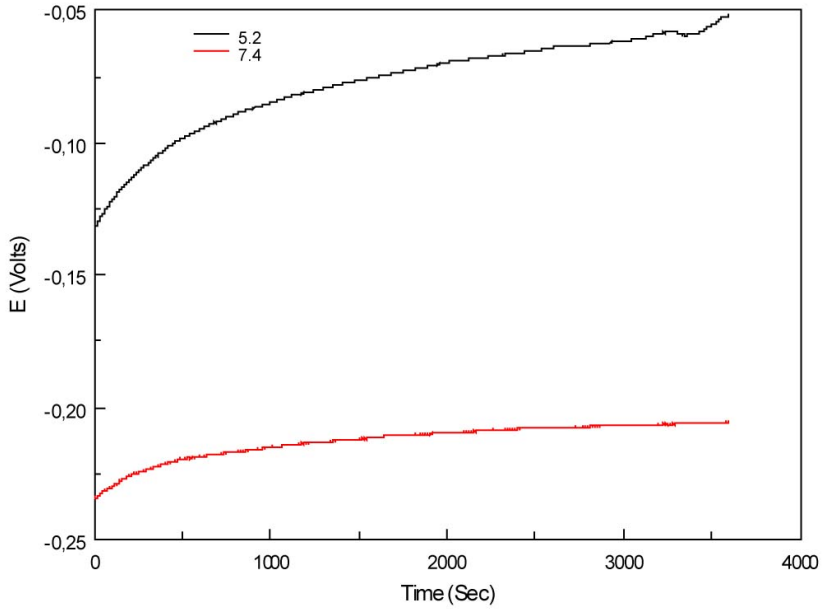

Figure 4.27: Effect of pH on OCP value of surgical grade Co-Cr-Mo grade F75. Experimental conditions: T=37°C; PBS with 2 g/L albumin; pH= 7.4 and 5.2.

Comparing Figures 4.26 and 4.27, it can be said that higher pH (7.4) has lower OCP than lower pH (5.2). Also, presence of albumin increases the onset potential for about 10 mV for both pH values.

Polarization curve

The results of the polarization curve acquisition with surgical grade Co-Cr-Mo grade F75 sample for two pH values are shown in Figure 4.28. The passive region is obvious and at pH=7.4 i_{pass} is lower. For theses curves, corrosion potential is very close but the corrosion current density is lower for the higher pH.

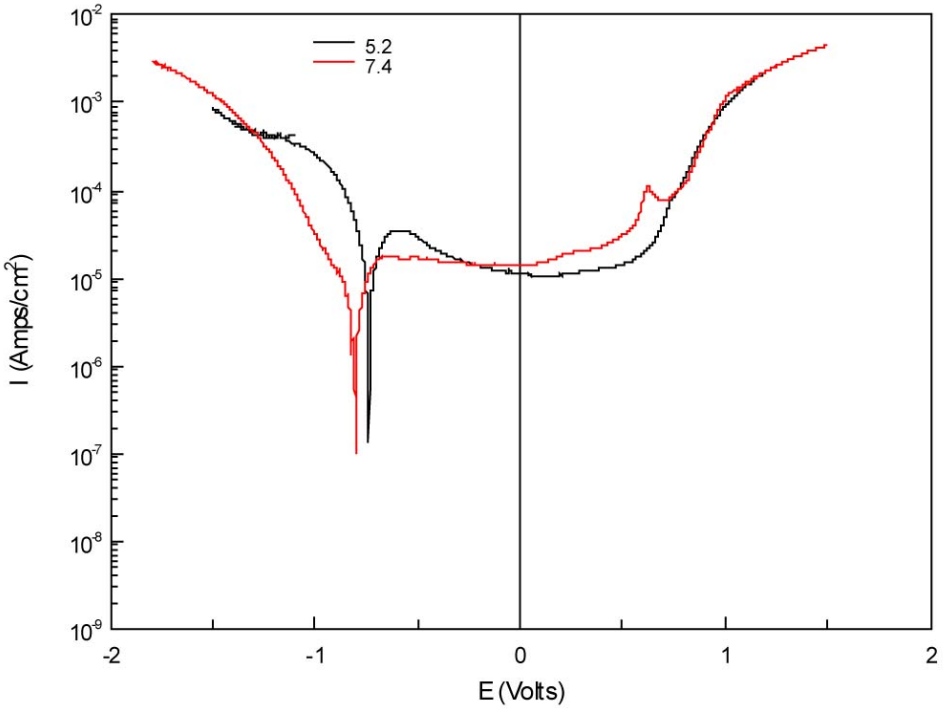

Figure 4.28: Effect of pH on the polarization curve of surgical grade Co-Cr-Mo grade F75. Experimental conditions: T=37°C; PBS; pH=7.4 and 5.2.

The same experiment was performed for Co-Cr-Mo alloy with the presence of 2 g/L albumin, as illustrated in Figure 4.29. The result shows that activation peak is bigger for the lower pH and the same as result in the Figure 4.28, for the pH 7.4, after reaching the transpassive region a peak can be seen which could be a result of oxidation of Cr^{3+} to Cr^{6+} in presence of phosphate ions in the electrolyte [69], while this peak disappears at lower pH. E_{corr} and i_{pass} in both cases are very similar but i_{corr} is smaller for the higher pH values.

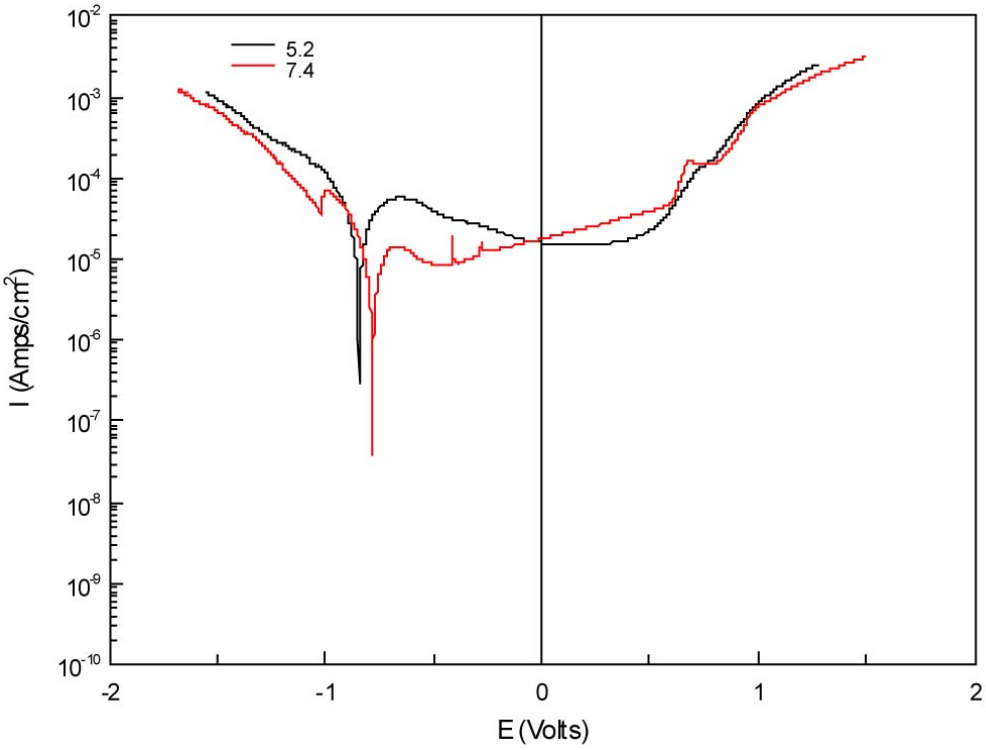

Figure 4.29: Effect of pH on the polarization curve of surgical grade Co-Cr-Mo grade F75. Experimental conditions: T=37°C; PBS with 2 g/L albumin; pH=7.4 and 5.2.

Generally, considering Figures 4.28 and 4.29, it can be said that the pH variation dose not have that much influence in corrosion potential and passive region but it has influence on corrosion current density and but i_{corr} is smaller for the higher pH values.

4.2.2.2 Amorphous bulk metallic glass (BMG)

Open circuit potential (OCP)

Figure 4.30 shows the curve of the OCP measurement for zirconium based bulk metallic glass without albumin at different pH values. The two curves were quite similar in exception of about 20 mV difference in the onset. In BMG, there is no smooth curve for OCP and curves are almost constant with very small variations. Also, It seems that without the presence of albumin, OCP for lower pH is lower than 7.4.

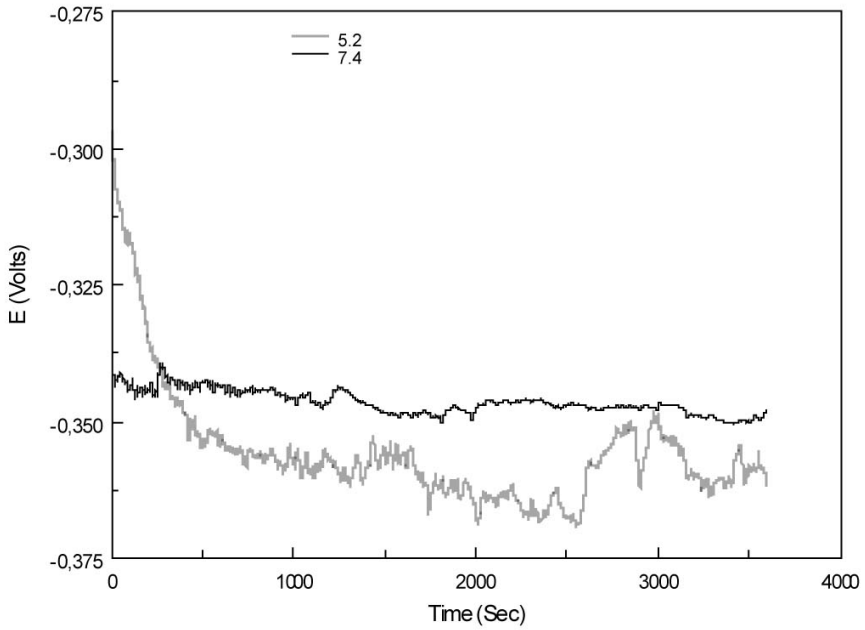

Figure 4.30: Effect of pH on OCP value of bulk metallic glass. Experimental conditions: Experimental conditions: T=37°C; PBS; pH=7.4 and 5.2.

Figure 4.31 is for the same experiment in presence of 2g/L albumin. As can be seen, the OCP is a bit lower for higher pH, otherwise the shape of the curves are the same.

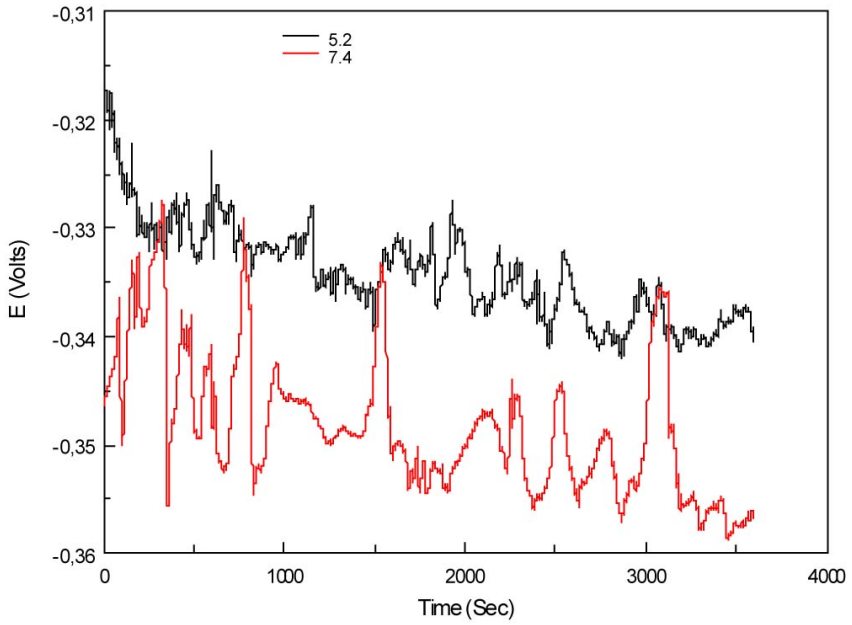

Figure 4.31: Effect of pH on OCP value of bulk metallic glass. Experimental conditions: Experimental conditions: T=37°C; PBS with 2 g/L albumin; pH=7.4 and 5.2.

Considering Figures 4.30 and 4.31, it can be said that addition of albumin has adverse effect on the OCP, while the variation is not that much and shapes are almost the same.

Polarization curve

The results of the polarization curve acquisition with zirconium based bulk metallic sample for two pH values are shown in Figure 4.32. They look the same as expected. The passive region is obvious and at pH=7.4 i_{pass} is lower. There is no activation peak and pitting corrosion is clear. Corrosion potential and pitting corrosion is higher for higher pH. On the other hand, the corrosion current density is the same for two different pH values.

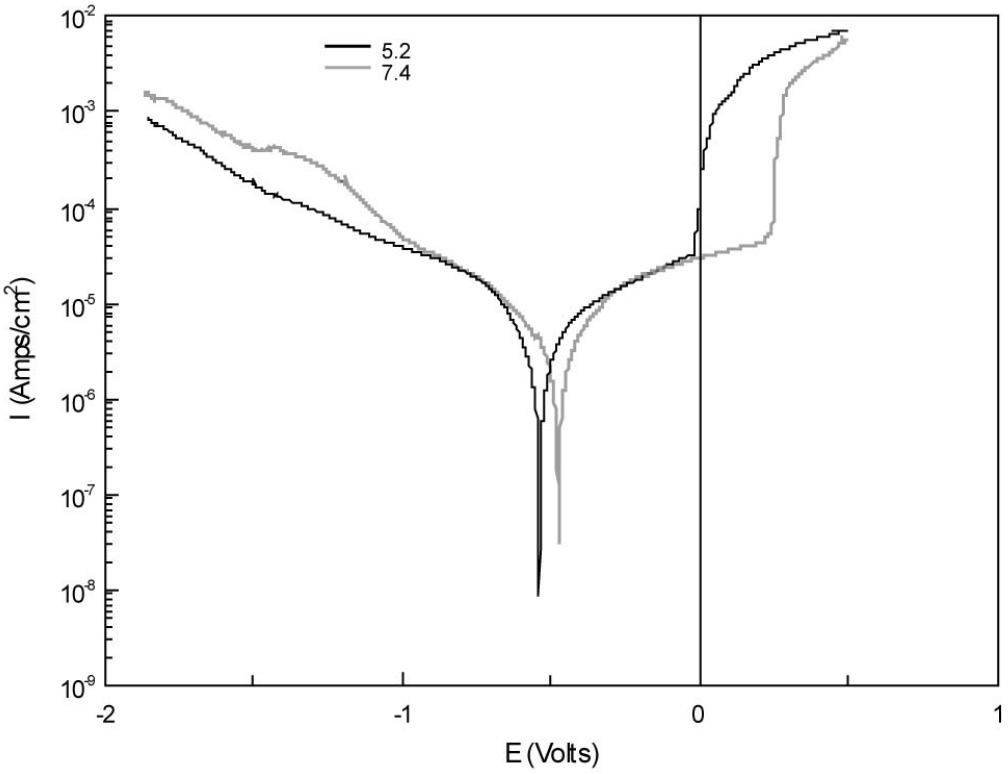

Figure 4.32: Effect of pH on the polarization curve of bulk metallic glass. Experimental conditions: T=37°C; PBS; pH=7.4 and 5.2.

The same experiment was performed for bulk metallic glass with the presence of 2g/L albumin, as illustrated in Figure 4.33.

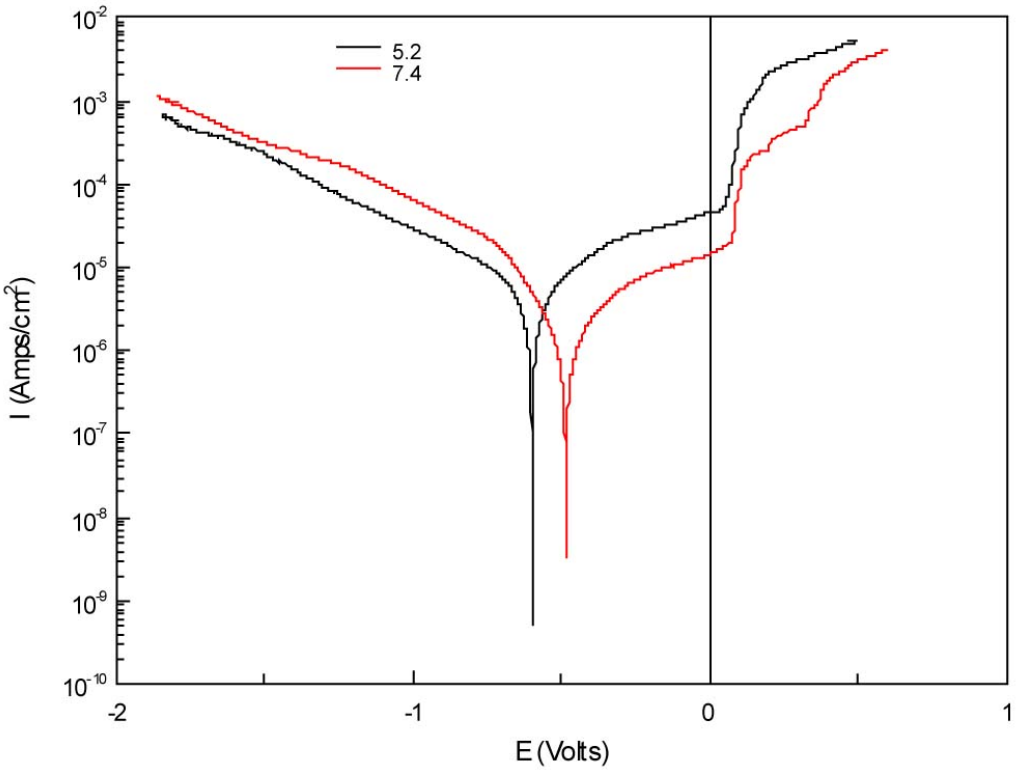

Figure 4.33: Effect of pH on the polarization curve of bulk metallic glass. Experimental conditions: T=37°C; PBS with 2 g/L albumin; pH=7.4 and 5.2.

From figures 4.32 and 4.33, corrosion potential and pitting potential is higher for higher pH value with and without albumin.

4.2.2.3 Crystalline bulk metallic glass

Open circuit potential (OCP)

Figure 4.34 shows the curve of the OCP measurement for crystalline zirconium based bulk metallic glass without albumin at different pH values. The two curves were quite similar in exception of about 20 mV difference in the onset. In crystalline BMG the curves are almost constant with very small variations. Also, It seems that without the presence of albumin, OCP for lower pH is lower than 7.4. This behavior is similar to the behavior of amorphous BMG under the same experimental conditions.

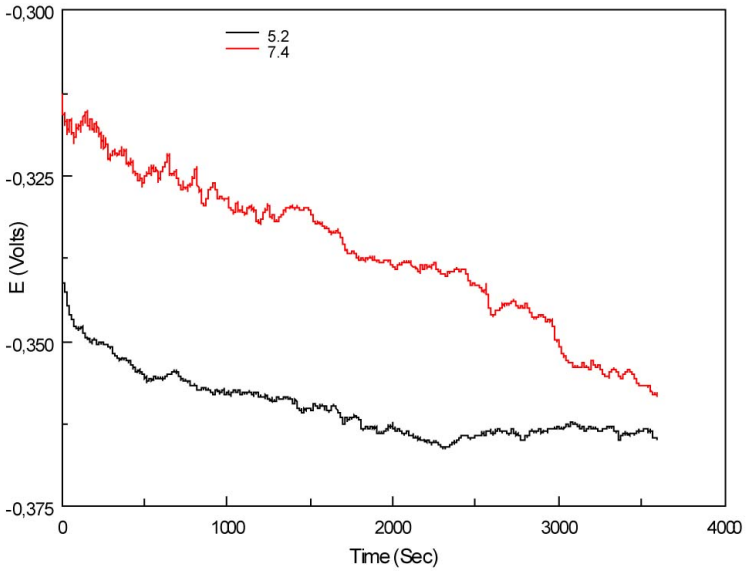

Figure 4.34: Effect of pH on OCP value of crystalline bulk metallic glass. Experimental conditions: Experimental conditions: T=37°C; PBS; pH=7.4 and 5.2.

Next Figure is for the same experiment in presence of 2g/L albumin. As can be seen in Figure 4.35, the OCP is a bit lower for higher pH.

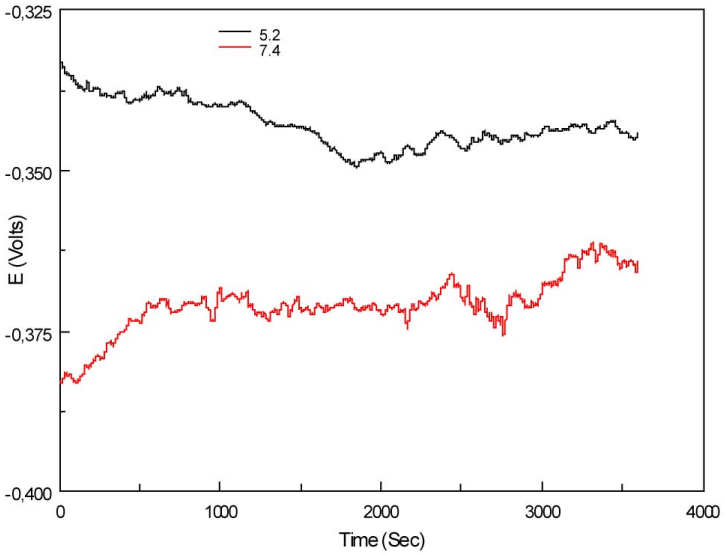

Figure 4.35: Effect of pH on OCP value of crystalline bulk metallic glass. Experimental conditions: Experimental conditions: T=37°C; PBS with 2 g/L albumin; pH=7.4 and 5.2.

Considering the information in Figures 4.34 and 4.35, it can be said that addition of albumin has adverse effect on the OCP. This behavior is the same as the behavior of amorphous bulk metallic glass, which was discussed in section 4.3.3.1.

Polarization curve

The results of the polarization curve acquisition with crystalline zirconium based bulk metallic sample for two pH values are shown in Figure 4.36. In this condition, the passive region is very small and pitting occurs before having a stable passive film on the surface. Corrosion potential in lower for the higher pH value and corrosion current density is almost the same for both curves. Also, pitting for both pH values occur in negative potential and the reason is the defects and grain boundaries present in the structure of crystalline BMG.

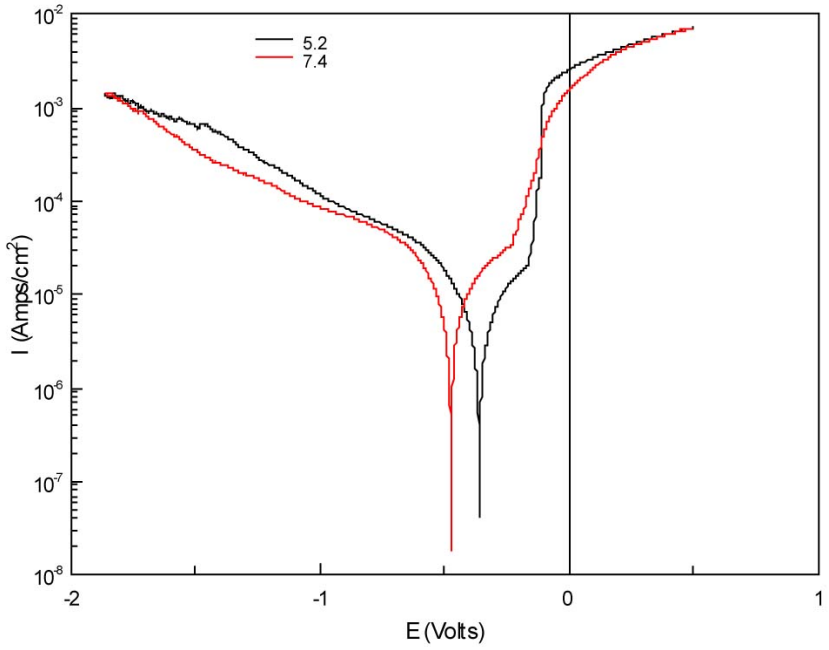

Figure 4.36: Effect of pH on the polarization curve of crystalline bulk metallic glass. Experimental conditions: T=37°C; PBS; pH=7.4 and 5.2.

The same experiment was performed for crystalline bulk metallic glass with the presence of 2g/L albumin, as illustrated in Figure 4.37.

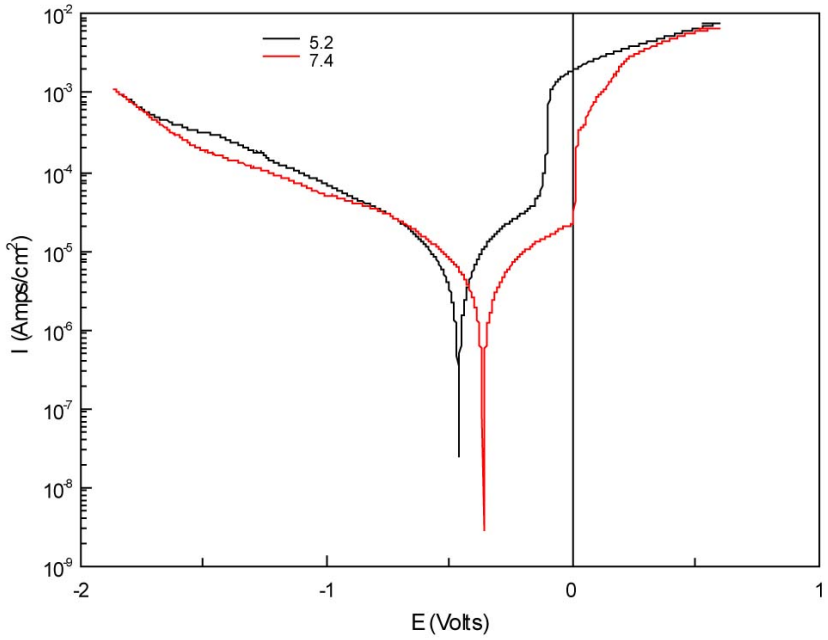

Figure 4.37: Effect of pH on the polarization curve of crystalline bulk metallic glass. Experimental conditions: T=37°C; PBS with 2 g/L albumin; pH=7.4 and 5.2.

From figures 4.36 and 4.37, albumin has adverse effect in the corrosion potential, however all the corrosion currents for both plots are very close.

4.2.2.4 Stainless steel 316

Open circuit potential (OCP)

Figure 4.38 shows the results of the OCP measurements carried out for two pH values at 37°C for stainless steel 316. There is 20 mV difference in onset potential. The curve for the pH 7.4 is not smooth, but the curve for pH 5.2 is smooth and almost constant. It can be seen that the OCP for both pH values get very close to each other.

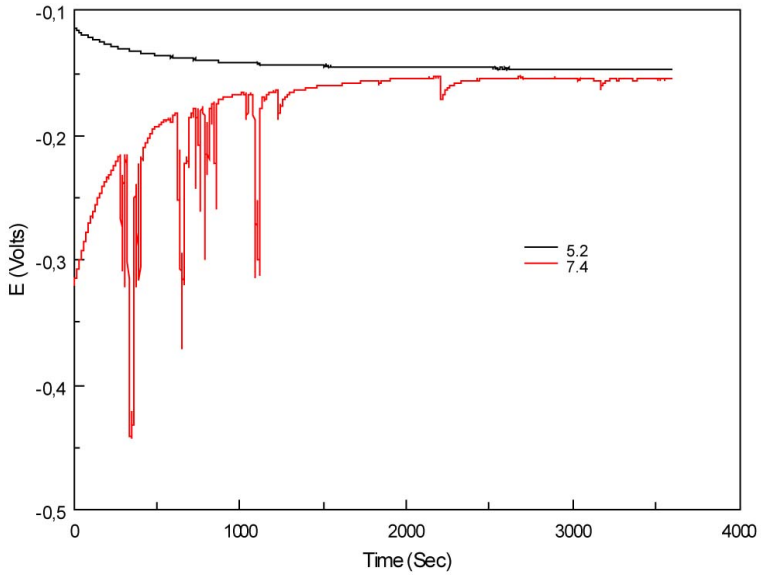

Figure 4.38: Effect of pH on OCP value of stainless steel 316. Experimental conditions: T=37°C; PBS; pH= 7.4 and 5.2.

The experiments were also performed with SS with presence of albumin, as shown in Figure 4.39. Here, curves are smooth and higher pH gets higher OCP.

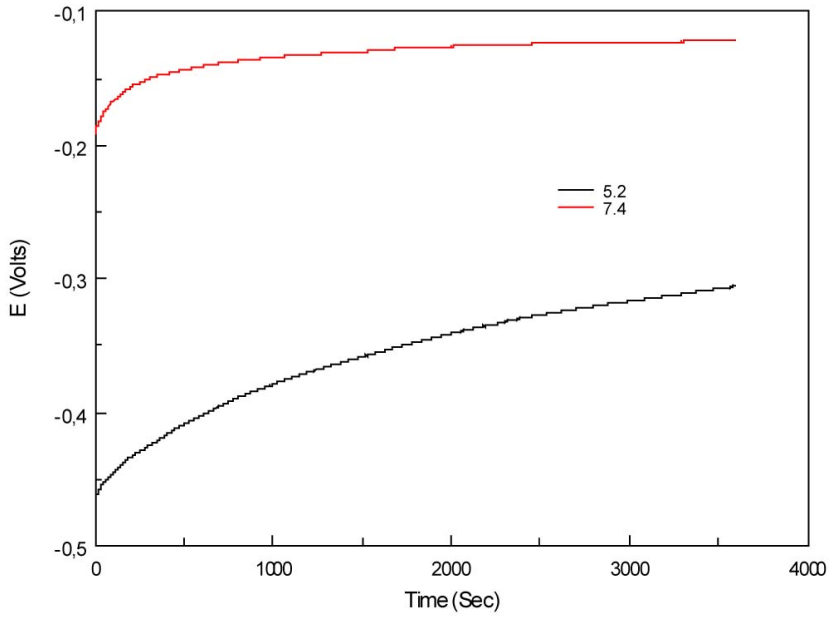

Figure 4.39: Effect of pH on OCP value of stainless steel 316. Experimental conditions: T=37°C; PBS with 2 g/L albumin; pH= 7.4 and 5.2.

Comparing Figures 4.38 and 4.39 is very tricky to interpret the effect of pH in SS, and further investigation is required to reach firm conclusion.

Polarization curve

The results of the polarization curve acquisition with stainless steel 316 sample for two pH values are shown in Figure 4.40. The passive region is obvious and at pH=5.2, i_{pass} is lower. Also, for lower pH, corrosion current density is lower and corrosion potential is higher.

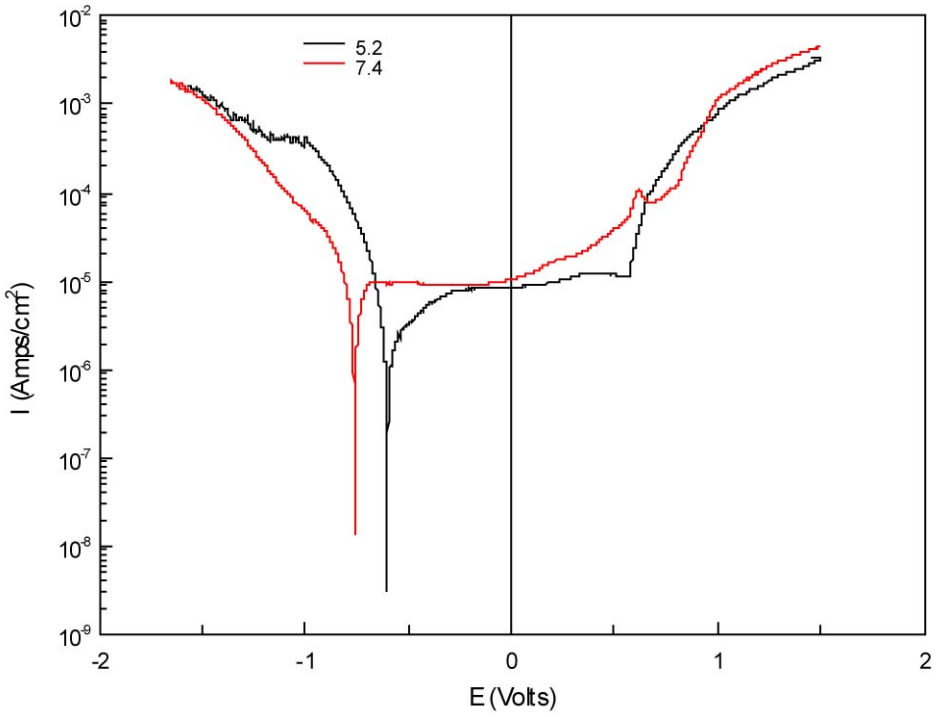

Figure 4.40: Effect of pH on the polarization curve of stainless steel 316. Experimental conditions: T=37°C; PBS; pH=7.4 and 5.2.

The same experiment was performed for SS with the presence of 2 g/L albumin, as illustrated in Figure 4.41. The result shows that activation peak is bigger and more obvious with the presence of albumin in both pH values. Also, after reaching the transpassive region a second peak can also be seen in pH 7.4.

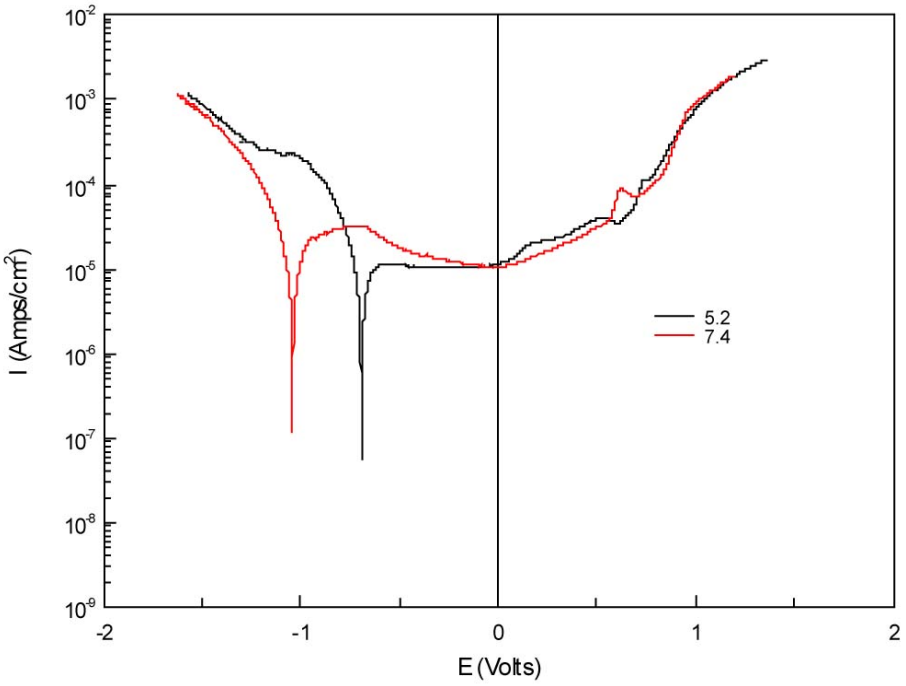

Figure 4.41: Effect of pH on the polarization curve of stainless steel 316. Experimental conditions: T=37°C; PBS with 2 g/L albumin; pH=7.4 and 5.2.

By considering the information in Figures 4.40 and 4.41, it can be said that the behavior is similar with and without albumin. In both Figures, there is an oxidation peak for pH 7.4. Also, presence of albumin makes the activation peak more visible. Furthermore, in both Figures, higher pH has higher corrosion current density and lower current potential.

4.2.3 Protein effect

The protein effect has to be studied because the biomaterials will be in contact with body fluids, which contains various types of proteins. Albumin is the most common protein present in the human body. For this reason, its impact was studied on the material corrosion behavior. According to Desroches, the adsorption of proteins on the metal surfaces [70], proteins have a bad influence on the corrosion resistance properties.

Detailed information about the effect of protein in different temperatures and pH values is given in Table 4.6 and in the sections 4.2.3.1 to 4.2.3.4, the effect of protein in 37°C and pH of 7.4 and 5.2 will be discussed.

4.2.3.1 Co-Cr-Mo

Open circuit potential (OCP)

To understand what could be the influence of protein, the measurements were done under various experimental conditions with and without protein addition. The results at pH=7.4 and at body temperature with and without protein are illustrated in Figure 4.42. It seems that albumin presence increases the OCP value. Nevertheless, a significant increase of the value is noted from the beginning of the measurement to 500s. After 500s, the value is constant to the end. In the previous work about electrochemical behavior of orthopedic material [58 and 66], the same comparison was made for the surgical grade Co-Cr-Mo alloy and the obtained result matches are in agreement with the reference [58].

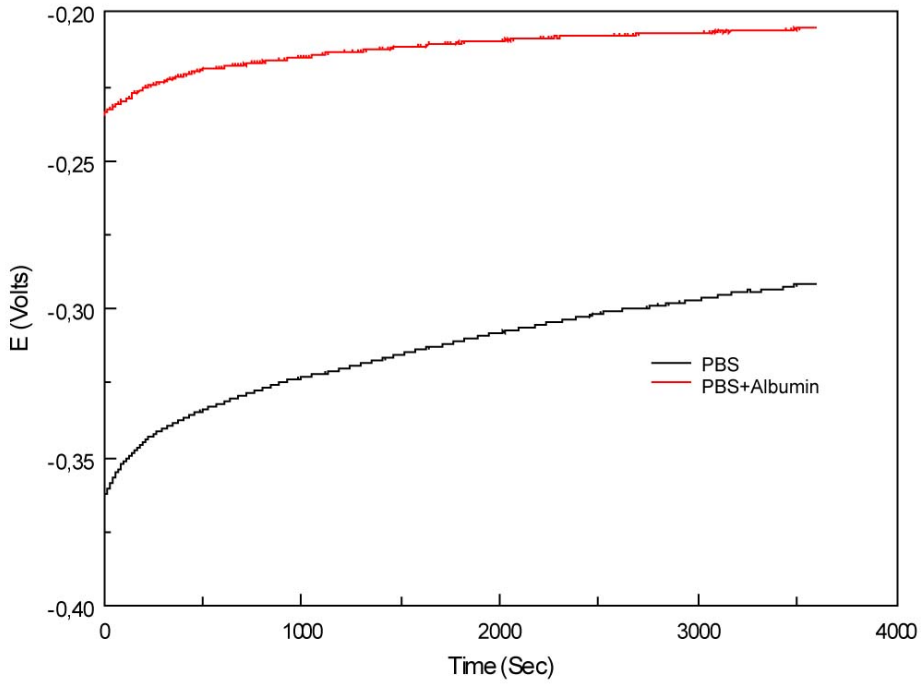

Figure 4.42: Effect of presence of 2 g/L Albumin on OCP value of surgical grade Co-Cr-Mo grade F75. Experimental conditions: T=37°C; pH=7.4; PBS with and without albumin addition

The same behavior was seen in lower pH, 5.2. As shown in Figure 4.43, in the body temperature and pH value of 5.2, the behavior of surgical grade Co-Cr-Mo grade F75 is the same as in pH 7.4.

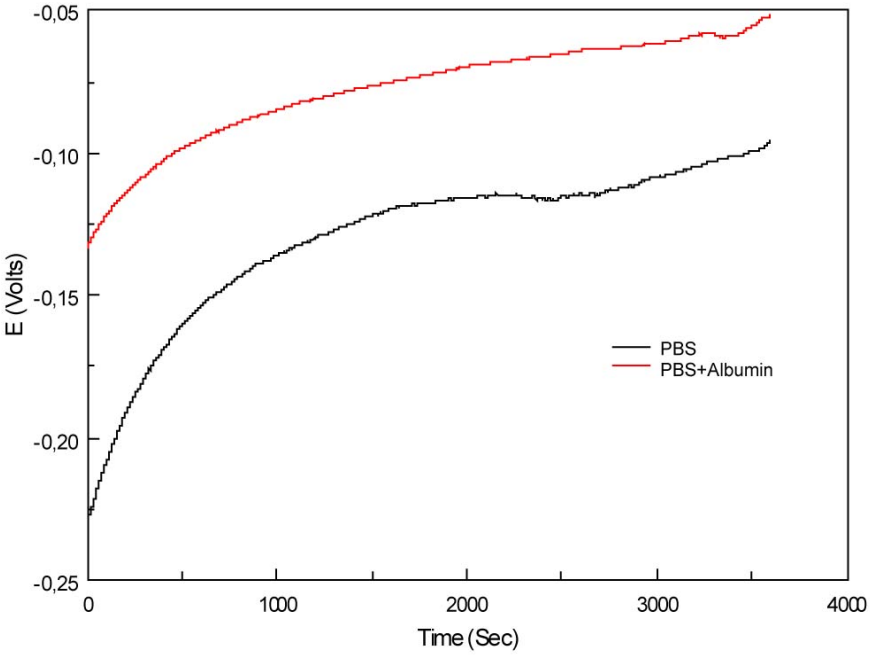

Figure 4.43: Effect of presence of 2 g/L Albumin on OCP value of surgical grade Co-Cr-Mo grade F75. Experimental conditions: T=37°C; pH=5.3; PBS without and with albumin addition.

These figures suggest that in Co-Cr-Mo alloy, presence of protein pushes the OCP to higher values.

Polarization curve

The protein effect was also investigated by polarization measurements. Figure 4.44 illustrates the experiments carried out at 37°C and pH of 7.4, with and without albumin addition. The passive region for with and without albumin is clear and the results are quite similar. In this case, the protein presence dose not have that much influence on the result except that the result with albumin has some noise.

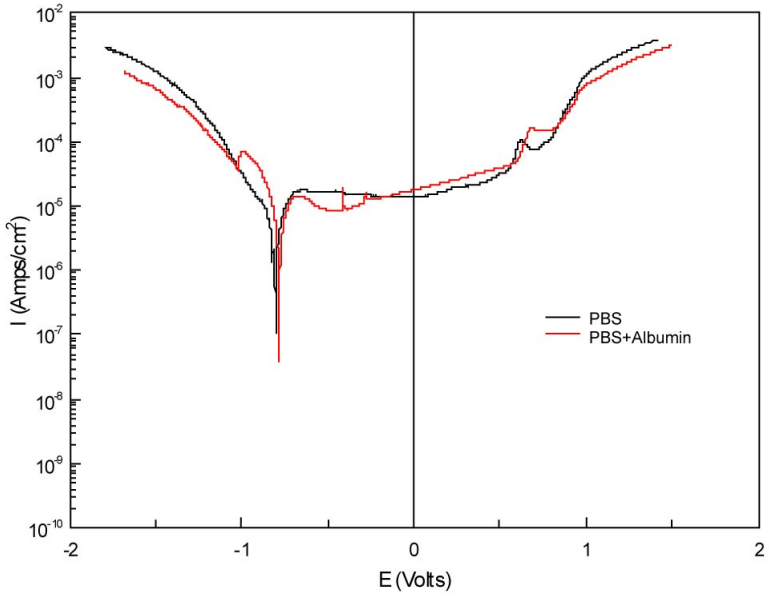

Figure 4.44: Effect of presence of 2 g/L Albumin on the polarization curves of surgical grade Co-Cr-Mo grade F75. Experimental conditions: T=37°C; pH=7.4; PBS without and with albumin addition.

Figure 4.45 shows that by decreasing the pH, activation peak becomes more clear and the oxidation peak disappears. Also, presence of albumin decreases the corrosion potential and increases the corrosion current density.

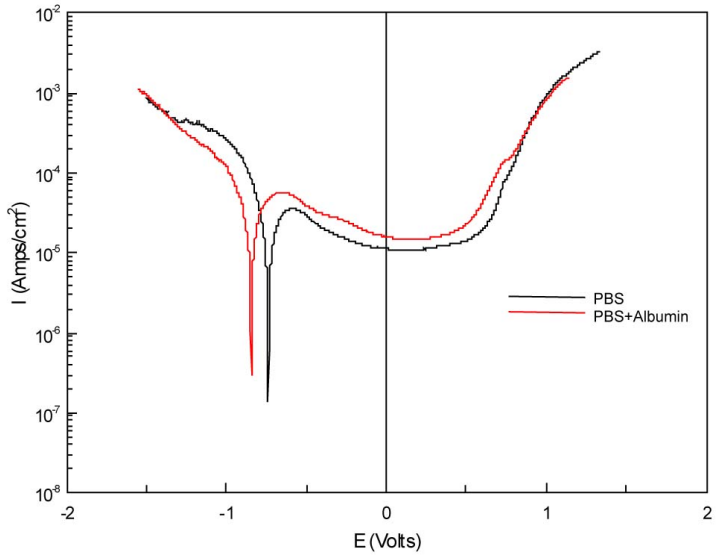

Figure 4.45: Effect of presence of 2 g/L Albumin on the polarization curves of surgical grade Co-Cr-Mo grade F75. Experimental conditions: T=37°C; pH=5.2; PBS without and with albumin addition.

Comparing the information in Figures 4.44 and 4.45, it can be said that the effect of protein is more severe in lower pH (5.2) than pH 7.4 and also there is not much difference with and without albumin additions.

4.2.3.2 Amorphous bulk metallic glass

Open circuit potential (OCP)

To understand what could be the influence of protein on bulk metallic glass, the measurements were done under various experimental conditions with and without protein addition. The results at pH=7.4 and at body temperature with and without protein are illustrated in Figure 4.46. It seems that albumin presence introduces more fluctuation to the result but at the end the change is not that much and both curves have almost the similar value.

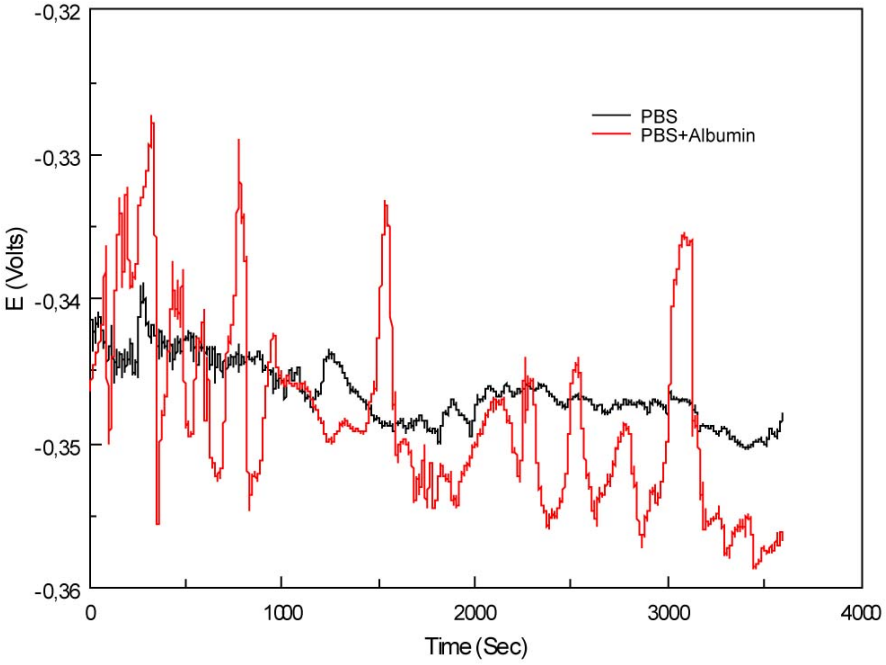

Figure 4.46: Effect of presence of 2 g/L Albumin on OCP value of bulk metallic glass. Experimental conditions: T=37°C; pH=7.4; PBS with and without albumin addition.

At lower pH with the same conditions, the result with albumin addition shows nearly a constant value with some small fluctuation (Figure 4.47).

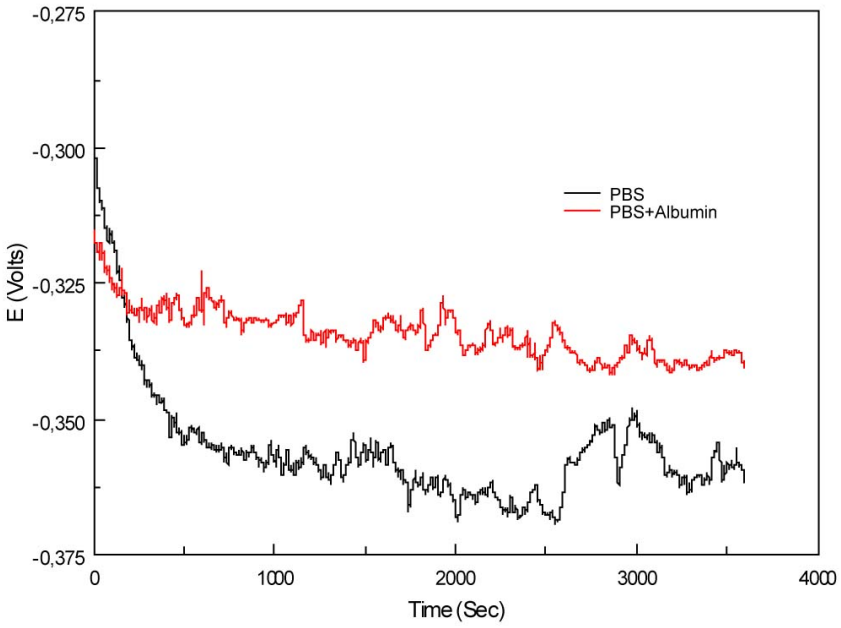

Figure 4.47: Effect of presence of 2 g/L Albumin on OCP value of bulk metallic glass. Experimental conditions: T=37°C; pH=5.2; PBS with and without albumin addition.

Here the values for two curves are different and without albumin, the OCP becomes lower, however it has high value at the start. It is hard to make a conclusion for the effect of albumin in OCP for amorphous BMG and it needs further tests.

Polarization curve

The protein effect was also investigated by polarization measurements for zirconium based bulk metallic glass. Figure 4.48 illustrates the experiments carried out at 37°C and pH of 7.4, with and without albumin addition. The passive region for both curves is clear. Presence of protein in this condition increases the corrosion potential and decreases the corrosion current density, passive region and pitting potential. Obtained result in the Figure 4.48 is very close to the result for Hiromoto et al. [72] and Nezafati's [66].

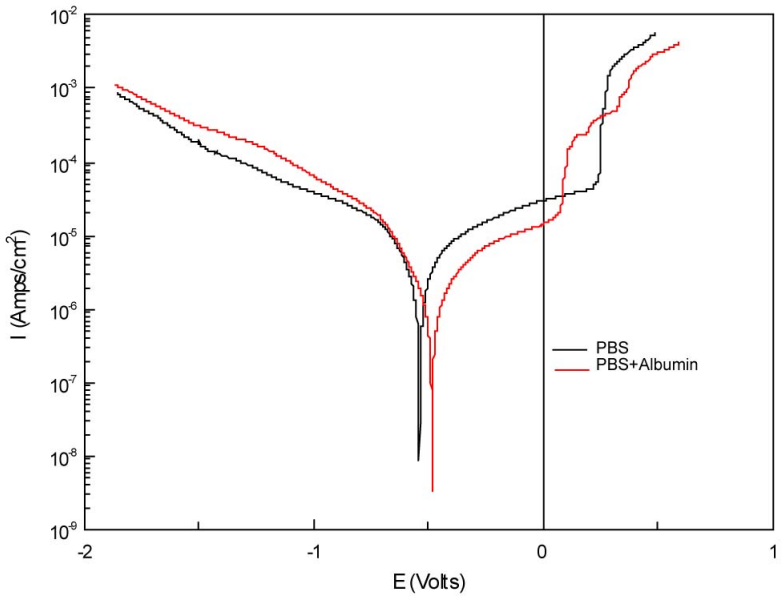

Figure 4.48: Effect of presence of 2 g/L Albumin on the polarization curves of zirconium based bulk metallic glass. Experimental conditions: T=37°C; pH=7.4; PBS without and with albumin addition.

Figure 4.49 shows that by decreasing the pH value, passive region becomes smaller and pitting potential decreases, however this effect is more for electrolyte without albumin. In pH 5.2, protein has adverse effect than in pH 7.4 in corrosion potential and corrosion current density.

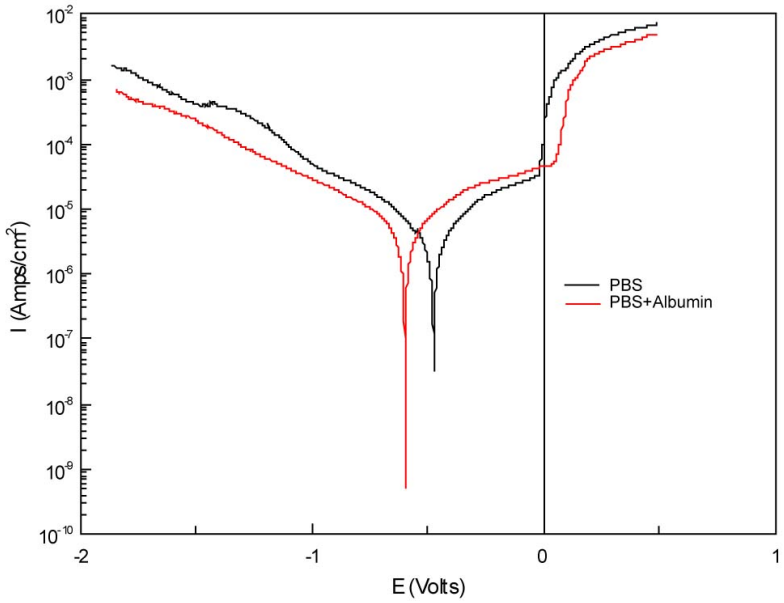

Figure 4.49: Effect of presence of 2 g/L Albumin on the polarization curves of zirconium based bulk metallic glass. Experimental conditions: T=37°C; pH=5.2; PBS without and with albumin addition.

Comparing the results taken from Figures 4.48 and 4.49, it can be said that albumin has adverse effect on E_{corr} and I_{corr} for different pH values.

4.2.3.3 Crystalline bulk metallic glass

Open circuit potential (OCP)

To understand what could be the influence of protein on crystalline bulk metallic glass, the measurements were done in various experimental conditions with and without protein addition. The results at pH=7.4 and at body temperature with and without protein are illustrated in Figure 4.50 that albumin presence decreases the OCP values.

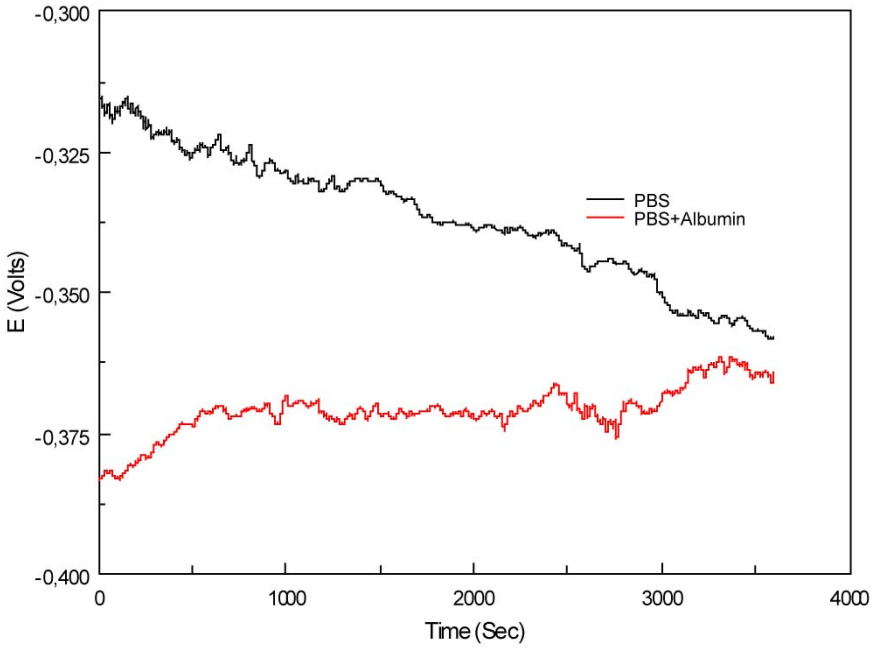

Figure 4.50: Effect of presence of 2 g/L Albumin on OCP value of crystalline zirconium based bulk metallic glass. Experimental conditions: T=37°C; pH=7.4; PBS with and without albumin addition.

In lower pH with the same conditions, it can be seen that the presence of albumin increases the OCP (Figure 4.51).

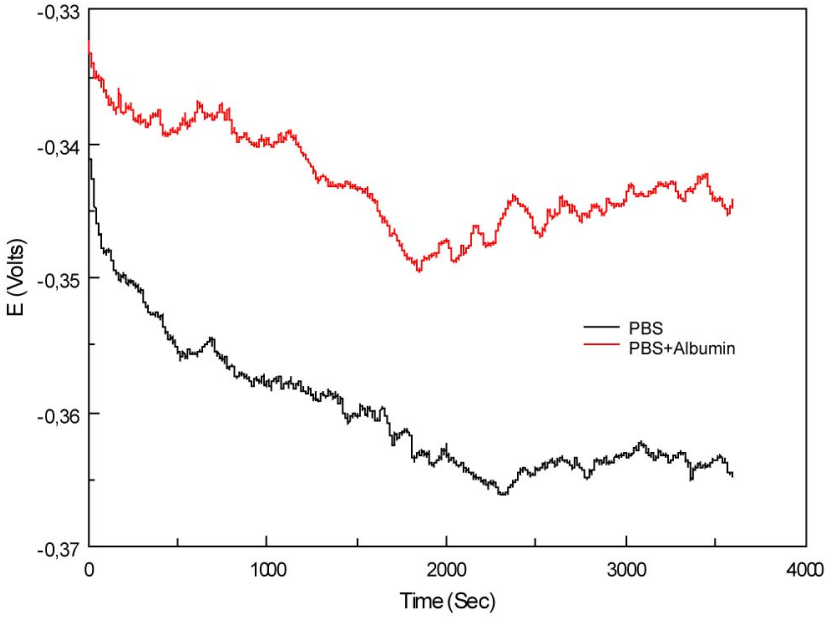

Figure 4.51: Effect of presence of 2 g/L Albumin on OCP value of crystalline zirconium based bulk metallic glass. Experimental conditions: T=37°C; pH=5.2; PBS with and without albumin addition.

Considering Figures 4.50 and 4.51, the effect of protein is adverse in different pH values on OCP.

Polarization curve

The protein effect was also investigated by polarization measurements for crystalline zirconium based bulk metallic glass. Figure 4.52 illustrates the experiments carried out at 37°C and pH of 7.4, with and without albumin addition. There is a very small passive region with albumin but without albumin there is no passive region and pitting occurs very fast at low potentials. Presence of protein in this condition increases the corrosion potential and decreases the corrosion current density.

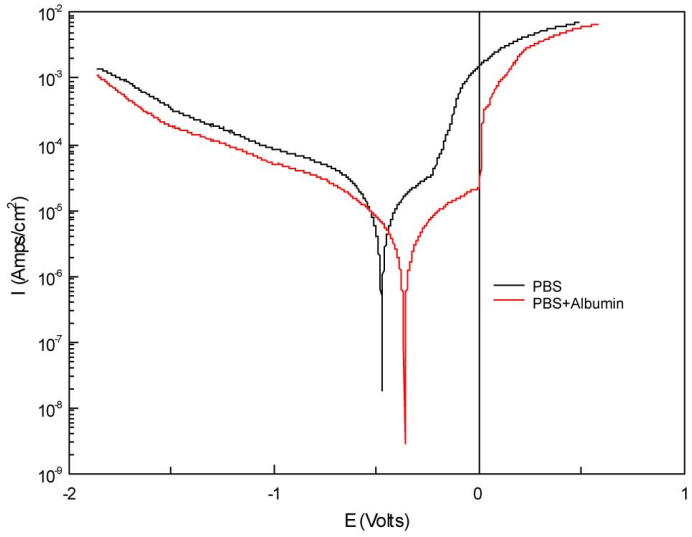

Figure 4.52: Effect of presence of 2 g/L Albumin on the polarization curves of crystalline zirconium based bulk metallic glass. Experimental conditions: T=37°C; pH=7.4; PBS without and with albumin addition.

Figure 4.53 shows that by decreasing the pH, passive region disappears for the curve with albumin and the corrosion potential is lower with protein addition.

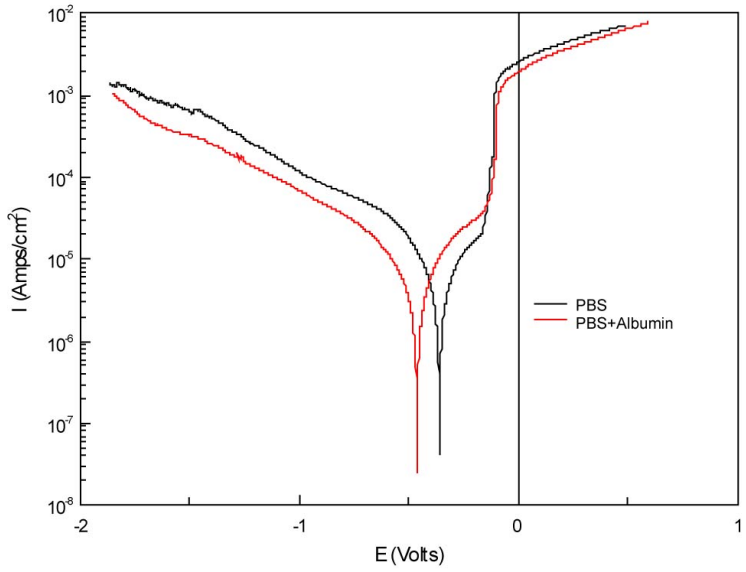

Figure 4.53: Effect of presence of 2 g/L Albumin on the polarization curves of crystalline zirconium based bulk metallic glass. Experimental conditions: T=37°C; pH=5.2; PBS without and with albumin addition.

Comparing the results taken from Figures 4.52 and 4.53, it can be said that albumin has adverse effect on E_{corr} and $I_{passive}$ in different pH values.

4.2.3.4 Stainless steel 316

Open circuit potential

To understand what could be the influence of protein on stainless steel, the measurements were done in various experimental conditions with and without protein addition. The results at pH=7.4 and at body temperature with and without protein are illustrated in Figure 4.54. It seems that without albumin there is more fluctuation in the result. As a conclusion, it can be said that with albumin, OCP is higher, however this result is in contrast with the previous work [66].

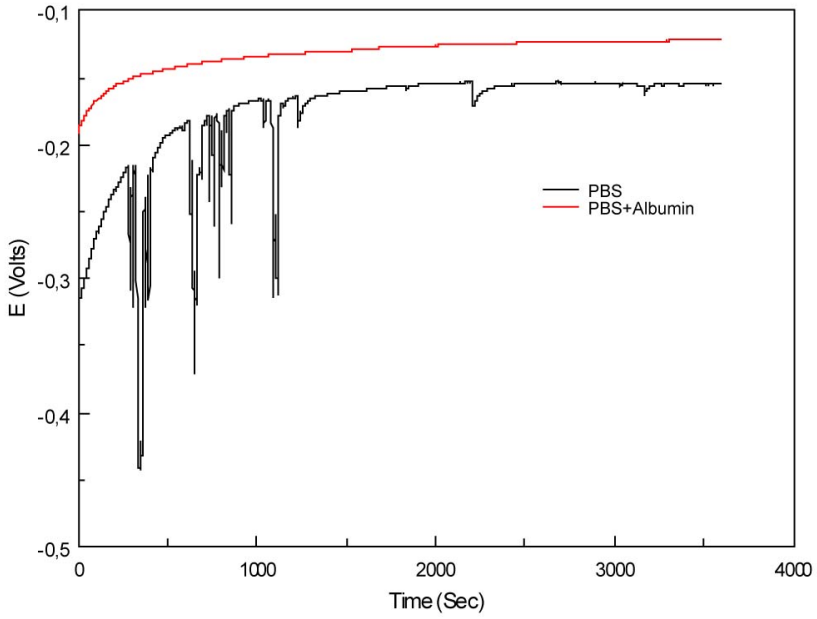

Figure 4.54: Effect of presence of 2 g/L Albumin on OCP value of stainless steel 316. Experimental conditions: T=37°C; pH=7.4; PBS with and without albumin addition.

In lower pH with the same conditions, it can be seen that the presence of albumin decreases the OCP and the onset potential is very low in comparison to other results (Figure 4.55).

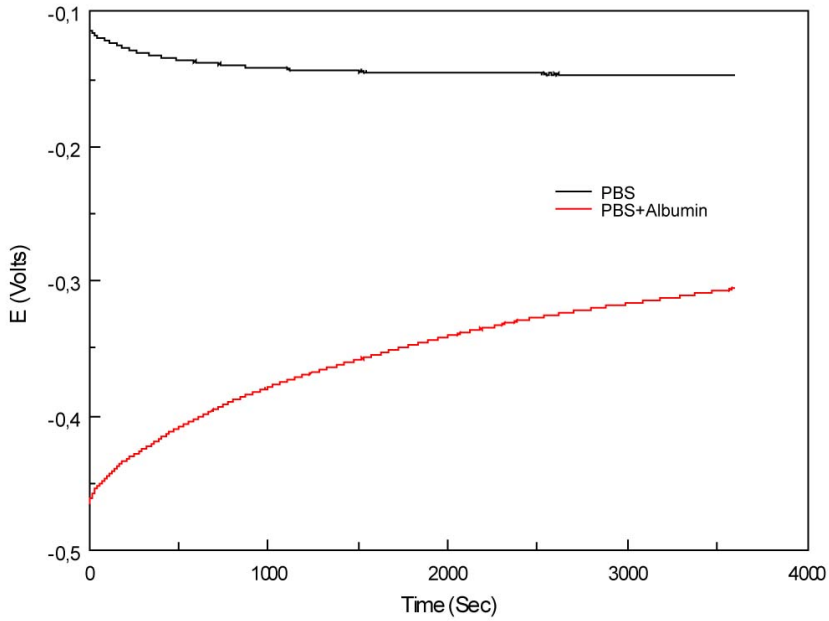

Figure 4.55: Effect of presence of 2 g/L Albumin on OCP value of stainless steel 316. Experimental conditions: T=37°C; pH=5.2; PBS with and without albumin addition.

Considering Figures 4.54 and 4.55, the effect of protein is adverse in different pH values on OCP. At higher pH, OCP is higher with albumin but is lower in pH 5.2

Polarization curve

The protein effect was also investigated by polarization measurements for SS. Figure 4.56 illustrates the experiments carried out at 37°C and pH of 7.4, with and without albumin addition. There is a clear passive region with and without albumin. Presence of protein increases the activation peak and has no effect on the oxidation peak. Also, it increases the I_{corr} and decreases the E_{corr}.

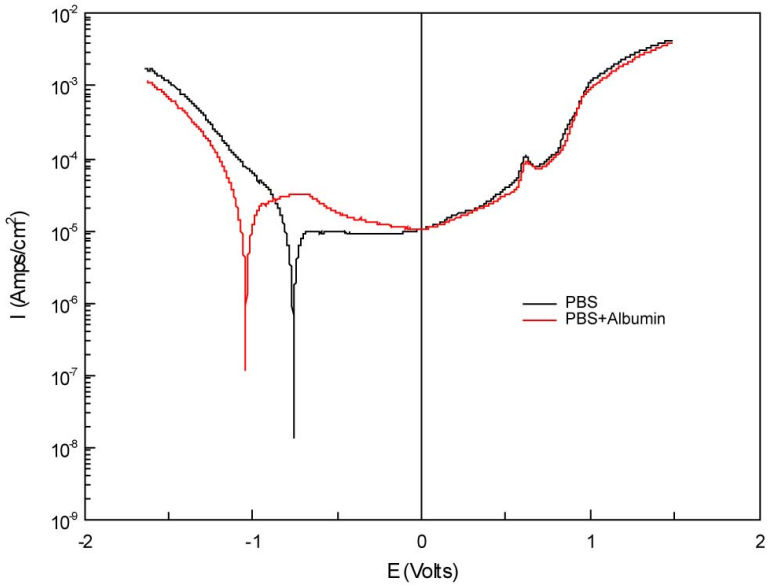

Figure 4.56: Effect of presence of 2 g/L Albumin on the polarization curves of SS. Experimental conditions: T=37°C; pH=7.4; PBS without and with albumin addition.

Figure 4.57 shows that by decreasing the pH, passive region dose not change that much. Also, in this condition, presence of protein increases the activation peak and has no effect on the oxidation peak and it also increases the I_{corr} and decreases the E_{corr}.

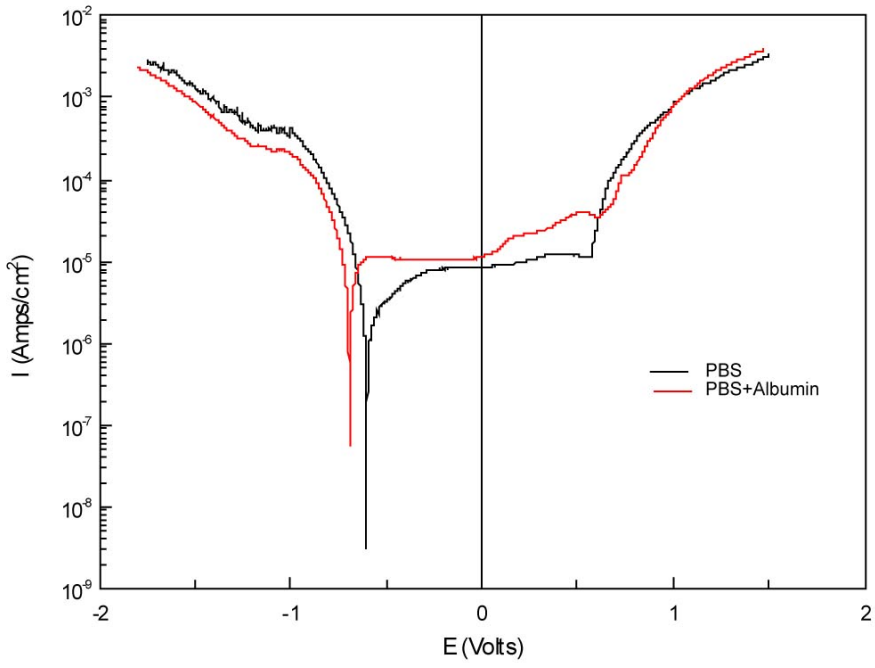

Figure 4.57: Effect of presence of 2 g/L Albumin on the polarization curves of SS. Experimental conditions: T=37°C; pH=5.2; PBS without and with albumin addition.

Comparing the results taken from Figures 4.56 and 4.57, it can be said that albumin has the same effect for both pH values, which results in higher I_{corr} and lower E_{corr}.

4.2.4 Comparison between all materials

In this section, all materials (Co-Cr-Mo, SS, and BMG) are compared together at body temperature (37^0C) and pH 7.4 with and without albumin addition.

Open circuit potential

An overview about behavior of CoCr, amorphous BMG and SS in 37°C and pH 7.4 without presence of albumin, is presented in Figure 4.58. It can be seen, SS has the highest OCP and BMG lowest. On the other hand, SS and Co-Cr-Mo have some increase in OCP while BMG has constant OCP.

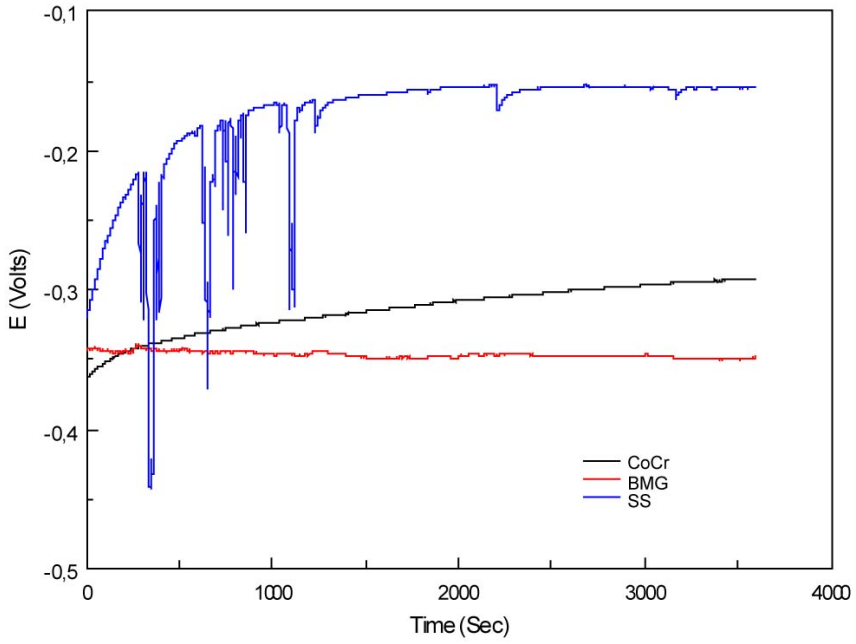

Figure 4.58: Comparison between corrosion properties of Zr-based bulk metallic glass, surgical grade Co-Cr- Mo and stainless steel 316 LVM in PBS. T=37°C; pH=7.4.

Figure 4.59 is the same as Figure 4.58 except the electrolyte has 2g/L albumin. It can be seen that the trend is the same as shown in previous Figure.

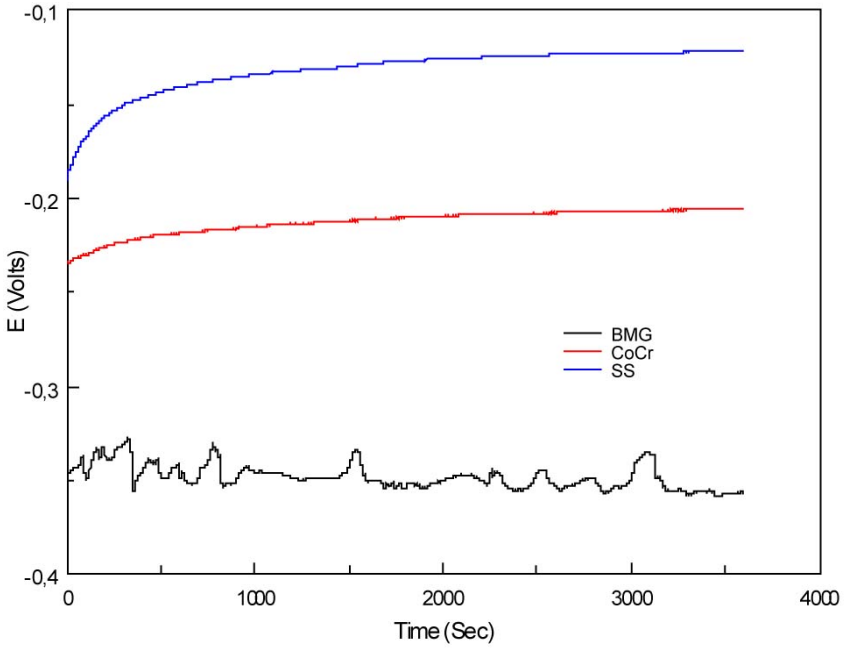

Figure 4.59: Comparison between corrosion properties of Zr-based bulk metallic glass, surgical grade Co-Cr-Mo and stainless steel 316 LVM in PBS with 2g/L albumin. T=37°C; pH=7.4.

As a conclusion, between mentioned alloys, SS has the highest OCP and BMG has the lowest one.

Polarization curve

Figure 4.60 gives an overview about behavior of Co-Cr-Mo, BMG and SS in 37°C and pH 7.4 without presence of albumin. As it can be seen, SS and Co-Cr-Mo have bigger passive region and both have oxidation peak at the same potential. On the other hand BMG has the lowest passive region and I_{corr} but E_{corr} and passive current is higher. Also, Co-Cr-Mo has the lowest E_{corr} and highest I_{corr}.

In general, finding a trend for these materials under different experimental conditions is very tricky and need further investigations.

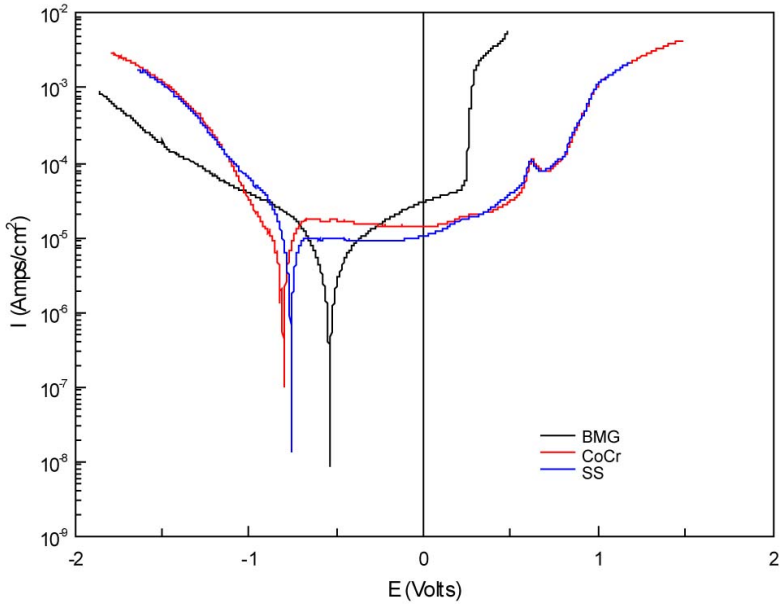

Figure 4.60: Comparison between corrosion properties of Zr-based bulk metallic glass, surgical grade Co-Cr-Mo and stainless steel 316 LVM in PBS. T=37°C; pH=7.4.

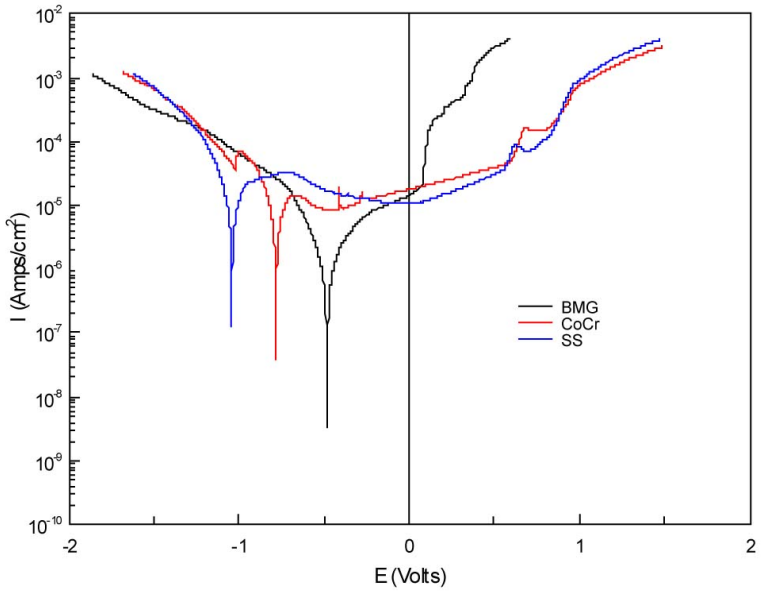

Figure 4.61: Comparison between corrosion properties of Zr-based bulk metallic glass, surgical grade Co-Cr-Mo and stainless steel 316 LVM in PBS with 2g/L albumin. T=37°C; pH=7.4.

Comparing the obtained results form Figures 4.60 and 4.61, effect of protein is clearer in SS rather than BMG or Co-Cr-Mo.

4.2.5 Detailed results for electrochemical measurements

Table 4.6: Detailed results for all electrochemical measurements.

T=37 °C pH=7.4

	I_{corr} (A/cm^2)	E_{corr} (V)	$I_{passive}$(A/cm^2)	OCP (V)	$E_{pitting}$ (V)
CoCr (PBS)	1.63E-05	-0.8	1.39E-05	-0.29±0.03	
CoCr (Albumin)	1.87E-05	-0.77	3.15E-05	-0.21±0.03	
SS (PBS)	1.49E-05	-0.76	1.75E-05	-0.15±0.01	
SS (Albumin)	3.75E-05	-1.04	1.82E-05	-0.12±0.01	
BMG (PBS)	4.15E-06	-0.53	3.33E-05	-0.35±0.01	0.28
BMG (Albumin)	1.58E-06	-0.48	1.30E-05	-0.35±0.03	0.12
CBMG (PBS)	8.28E-06	-0.47	2.54E-05	-0.36±0.01	-0.16
CBMG (Albumin)	6.64E-06	-0.36	1.63E-05	-0.35±0.03	0.02

T=37 °C pH=5.2

	I_{corr} (A/cm^2)	E_{corr} (V)	$I_{passive}$(A/cm^2)	OCP (V)	$E_{pitting}$ (V)
CoCr (PBS)	5.57E-05	-0.73	1.10E-05	-0.09±0.02	
CoCr (Albumin)	8.04E-05	-0.85	2.38E-05	-0.16±0.02	
SS (PBS)	1.95E-06	-0.51	1.22E-05	-0.14±0.01	
SS (Albumin)	1.68E-05	-0.69	1.53E-05	-0.33±0.03	
BMG (PBS)	4.00E-06	-0.49	2.75E-05	-0.36±0.02	0.01
BMG (Albumin)	1.08E-05	-0.59	3.20E-05	-0.36±0.02	0.07
CBMG (PBS)	9.95E-06	-0.35	1.73E-05	-0.36±0.01	-0.19
CBMG (Albumin)	3.74E-06	-0.46	3.09E-05	-0.34±0.02	0.17

T=20 °C pH=7.4

	I_{corr} (A/cm^2)	E_{corr} (V)	$I_{passive}$(A/cm^2)	OCP (V)	$E_{pitting}$ (V)
CoCr (PBS)	2.13E-05	-1.04	1.41E-05	-0.20±0.04	
CoCr (Albumin)	3.34E-05	-1.02	2.88E-05	-0.38±0.02	
BMG (PBS)	4.63E-06	-0.91	6.06E-05	-0.34±0.01	0.17
BMG (Albumin)	1.82E-06	-0.55	1.35E-05	-0.32±0.04	0.05
CBMG (PBS)	1.05E-05	-0.47	3.81E-05	-0.33±0.01	-0.19
CBMG (Albumin)	8.02E-06	-0.36	6.91E-05	-0.34±0.03	0.08

4.2.6 Typical cyclic polarization curves

In this section, the typical cyclic polarization curve for Co-Cr-Mo, BMG and SS are discussed. For this purpose, a cyclic polarization curve for each material is shown in the following figures.

4.2.6.1 Co-Cr-Mo

Comparing the results shown in the Figure 4.62, it can be seen that at the body temperature and high pH value (7.4), if there is albumin in the solution, the curve dose not experience repassivation. On the other hand, if there is no protein, there is a repassivation potential.

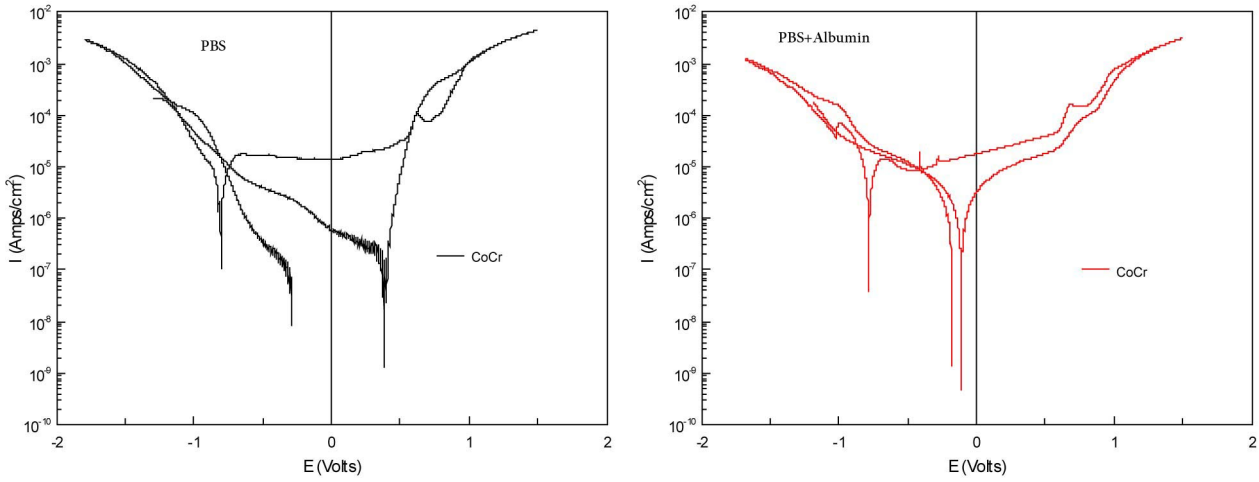

Figure 4.62: Effect of 2g/L albumin in the cyclic polarization curve for Co-Cr-Mo alloy. Experimental conditions: T=37°C; pH=7.4.

An overview of the behavior of Co-Cr-Mo in lower pH value solution, is presented in Figure 4.63.

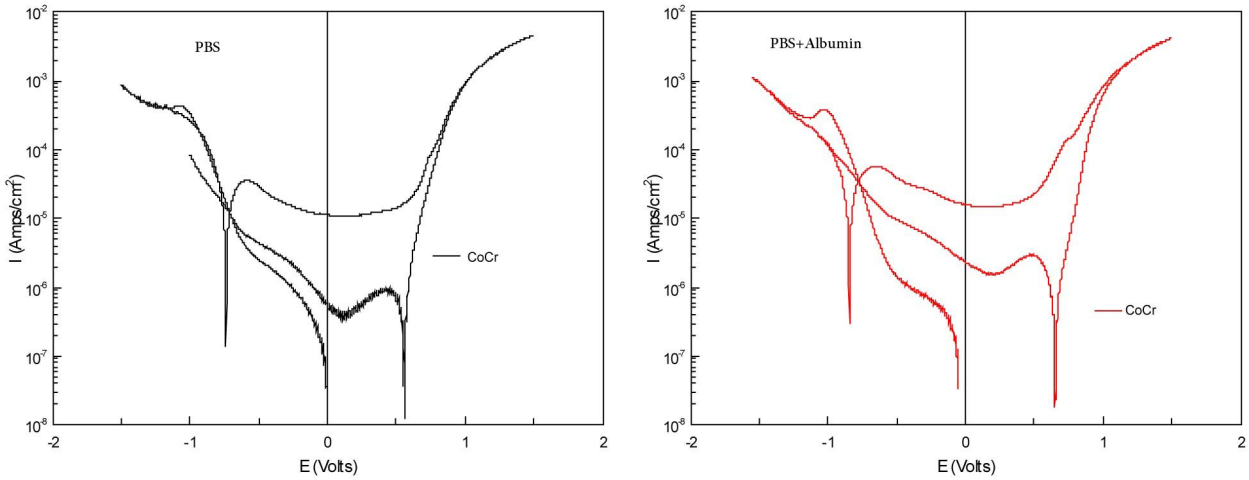

Figure 4.63: Effect of 2g/L albumin in the cyclic polarization curve for Co-Cr-Mo alloy. Experimental conditions: T=37°C; pH=5.2.

To make a conclusion for Co-Cr-Mo alloy it can be said that the alloy dose not undergo repassivation except in body temperature with pH 7.4 and without presence of albumin. Also, in the normal pH (7.4), oxidation peak is clear, which is not visible in lower pH.

4.2.6.2 Amorphous BMG

Behavior of bulk metallic glass is the same for all different conditions. First of all, BMG experience pitting by sudden increase of the current density and then it undergoes repassivation. Figure 4.64 is a typical behavior of BMG. Here there is no singe of activation or oxidation peak.

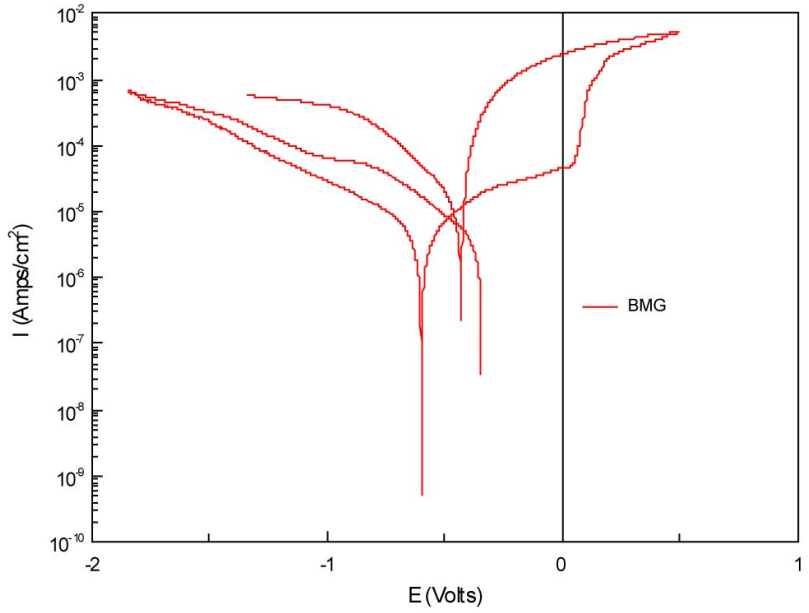

Figure 4.64: Typical cyclic polarization curve for amorphous Zr-based bulk metallic alloy.

4.2.6.3 Stainless steel 316

Stainless steel has the same behavior in different pH values (7.4 and 5.2). It can be seen that in presence of albumin in the electrolyte, stainless steel dose not experience repassivation while without presence of albumin repassivation occurs. Also, Stainless steel has an oxidation peak in the normal pH and body temperature.

Figures 4.65 and 4.66 shows stainless steel in different conditions

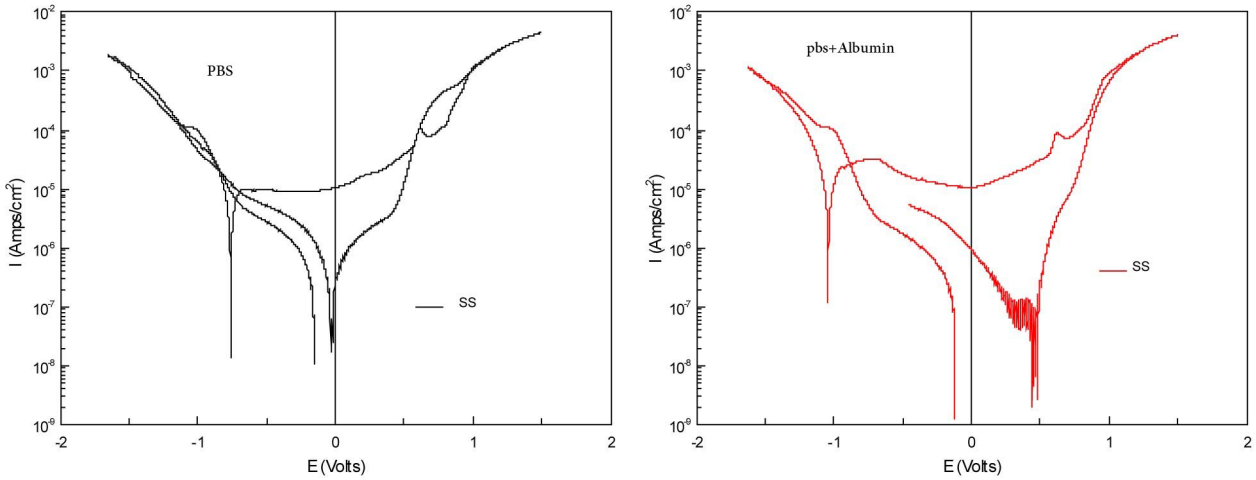

Figure 4.65: Effect of 2g/L albumin in the cyclic polarization curve for stainless steel 316. Experimental conditions: T=37°C; pH=7.4.

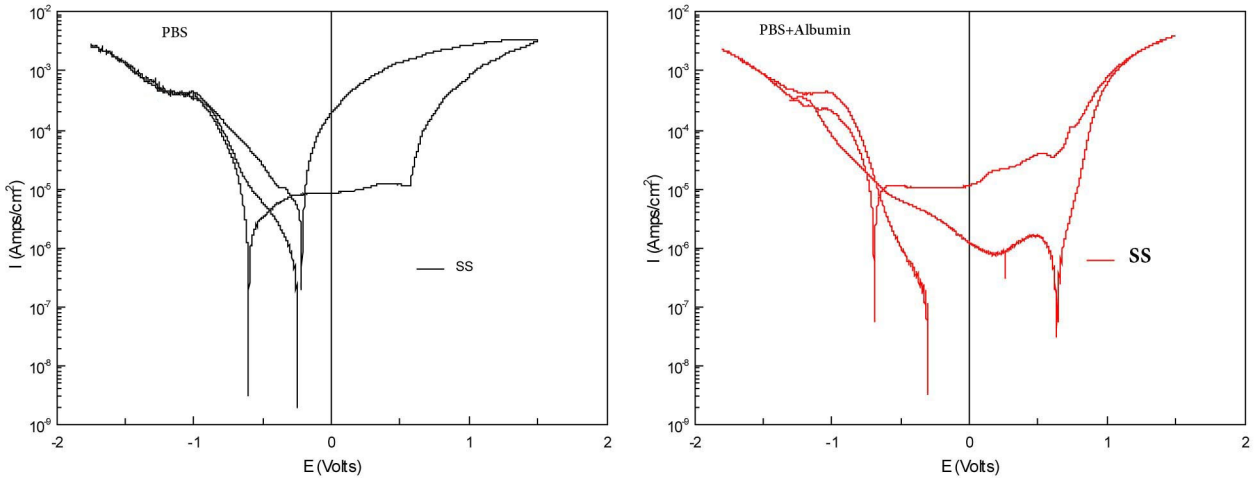

Figure 6.66: Effect of 2g/L albumin in the cyclic polarization curve for stainless steel 316. Experimental conditions: T=37°C; pH=5.2.

4.3 Pitting corrosion

By looking to electrochemical plots for different materials in different conditions, it can be understood that amorphous and crystalline bulk metallic glass undergo pitting corrosion. Based on this, pitting corrosion experiments were run for these materials.

4.3.1 Amorphous BMG

In all conditions for the electrochemical measurements, BMG undergoes pitting corrosion. Figure 6.67 and 6.68 show the pits on surface of the zirconium based bulk metallic glass after potentiodynamic measurements

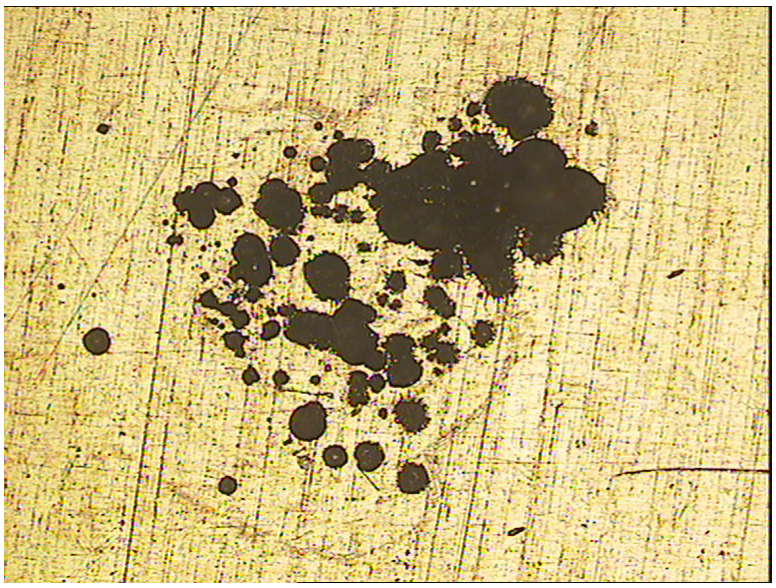

Figure 6.67: Pitting corrosion on the surface of the zirconium based bulk metallic glass in PBS solution. T=37°C; pH=7.4; Magnification 100X.

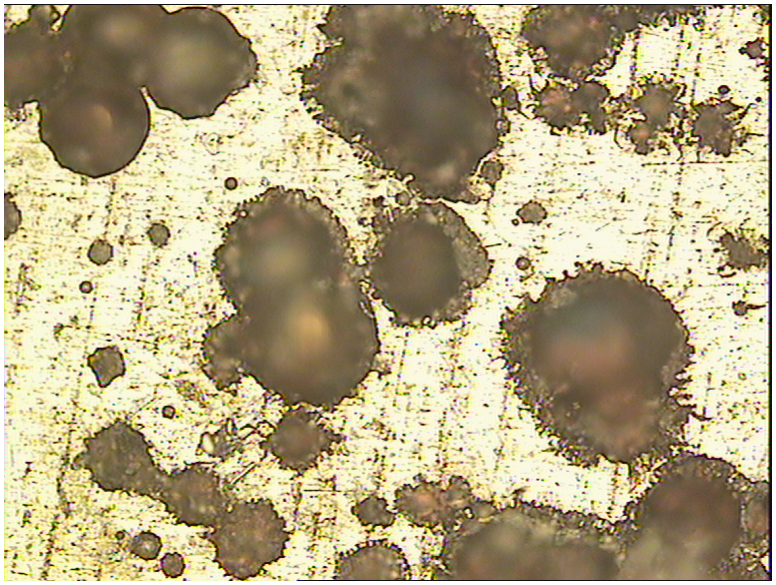

Figure 6.68: Pitting corrosion on the surface of the zirconium based bulk metallic glass in PBS solution. T=37°C; pH=7.4; Magnification 400X.

Pitting holes are clear in the images. In amorphous materials, there is no crystals or grain boundaries, so any kind of defects such as surface defects may cause the initiation of pitting corrosion. These images were taken by optical microscope (OM). By measuring the depth of pitting the pitting hole depth is estimated to be around 50 µm.

Considering the X-Ray diffraction obtained in Figure 4.4, it was seen that $CuZr_2$ and CuO crystals are present in the BMG received from Japan, which was not completely amorphous. So, and these crystals can be the initiation site for the pitting holes.

4.3.2 Crystalline BMG

The same as amorphous BMG, Crystalline BMG has a large increase in the current at a certain potential. Figure 6.69 and 6.70 show corrosion in surface of the crystalline zirconium based bulk metallic glass after potentiodynamic measurements.

Figure 6.69: Corrosion on the surface of the crystalline zirconium based bulk metallic glass in PBS solution. T=37°C; pH=7.4; Magnification 100X.

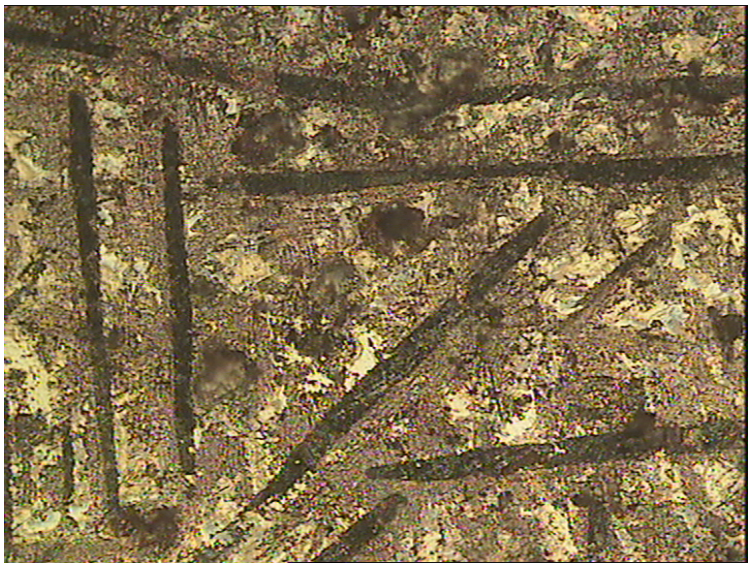

Figure 6.70: Corrosion on the surface of the crystalline zirconium based bulk metallic glass in PBS solution. T=37°C; pH=7.4; Magnification 400X.

By looking images it is concluded that the corrosion behavior of the crystalline BMG is different from the amorphous one. Figure 6.69 shows that in crystalline BMG, corrosion mostly occurs in dendrites and needles and deep pitting holes present in amorphous BMG cannot be seen here. Depth of corrosion spots is estimated not more than 5 μm.

Figure 6.71: Corrosion on the surface of the crystalline zirconium based bulk metallic glass in PBS solution. T=37°C; pH=7.4; Magnification 50X.

In the Figure 6.71 with low magnification, it can be seen that the corrosion looks like uniform corrosion attack rather than pitting corrosion, and it can be concluded that big needles and dendrites are sites for the corrosion attack.

4.4 FTIR-spectroscopy

The understanding of the protein adsorption on implant material is key issue to be studied for the biocompatibility point of view. This type of molecule could be adsorbed on almost every surface. Consequently, it could be interesting to characterize these interactions [59]. In this present work, experiments using infrared reflection absorption spectroscopy (IRRAS) were performed after that the materials were immersed into a liquid containing protein. Indeed, IRRAS was employed to get more data about the adsorption behavior of proteins and also to obtain information concerning the adsorbed layer structure after immersion time of 40 minutes in PBS solution with different concentrations of albumin at pH=5.2 and 7,4. This technique is very sensitive to the protein amount adsorbed.

The protein interfacial behavior with solid surfaces was characterized on surgical grade Co-Cr-Mo and amorphous Zr-based BMG by the spectra obtained. In this case of investigation, the domain spectral was focused on the 1400-1800 cm^{-1} region, where the amide I and the amide II vibrational modes appear. The material substrate, the albumin concentration and the pH value were chosen in order to understand their dependency with the amount of protein adsorbed on the material surface.

4.4.1 Effect of material substrate

The interaction of proteins on solid surface was characterized on Co-Cr-Mo and BMG alloys. In order to make some comparisons, all the experimental conditions were kept constant for the substrate materials. In fact, they were immersed for 40 minutes in 2g/L albumin in PBS solution. As expected, two different peaks are obtained around the same wavenumber than in the spectrum from the literature [70]. The first one is referred to amide I and the second one to amide II. Nevertheless, the BMG behavior seems to be different. The band around 1740 cm^{-1} is more pronounced compared Co-Cr-Mo alloy. This band could be due to carboxylic acid (–COOH) groups. This result is the same as obtained result from ref. 59.

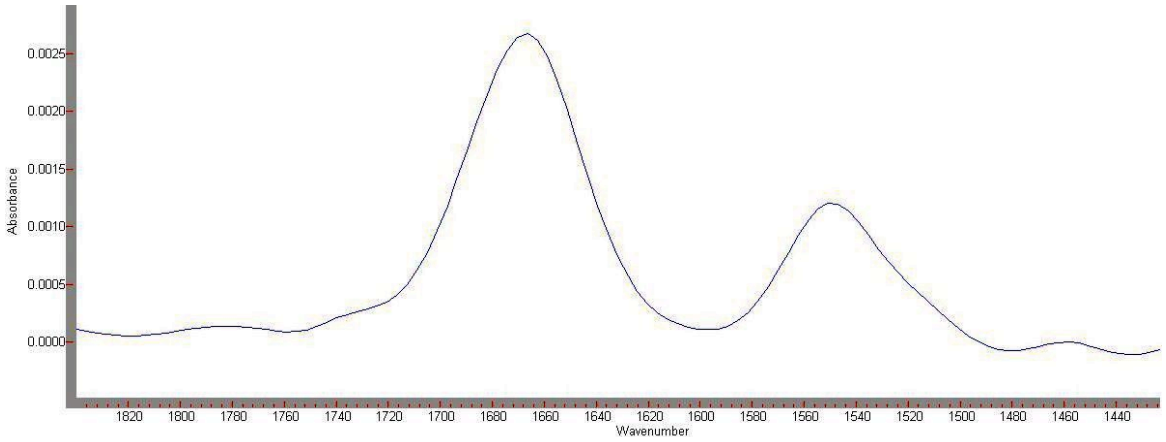

Figure 4.72: FTIR spectrum of Co-Cr-Mo. Experimental conditions: T=20°C; pH=7.4; PBS solution with 2 g/L of albumin.

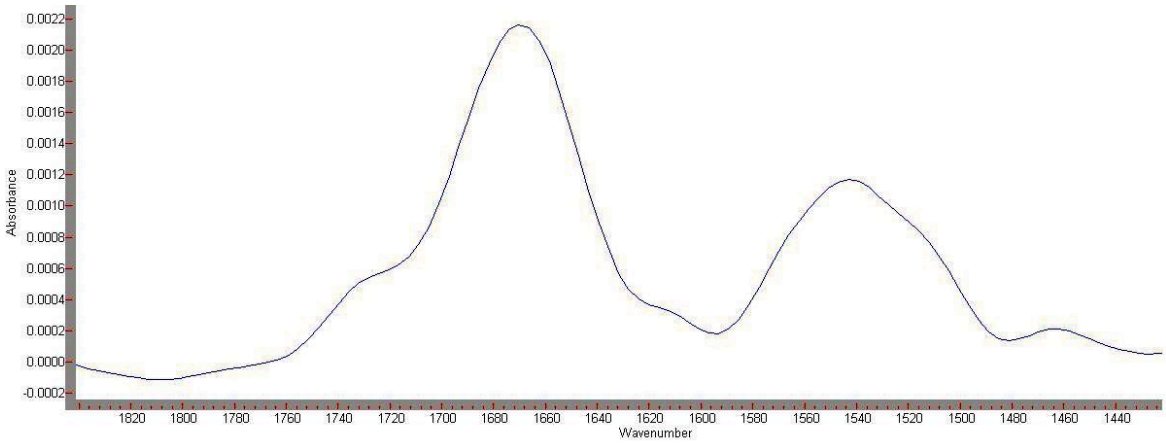

Figure 4.73: FTIR spectrum of Zr-based BMG. Experimental conditions: T=20°C; pH=7.4; PBS solution with 2 g/L of albumin.

The peak position is almost the same for both materials, amide I around 1670 cm^{-1} and amide II 1542 cm^{-1}. Furthermore, the intensity of the peak or peak height is higher for Co-Cr-Mo than BMG. This peak height is related to the protein adsorption on the surface.

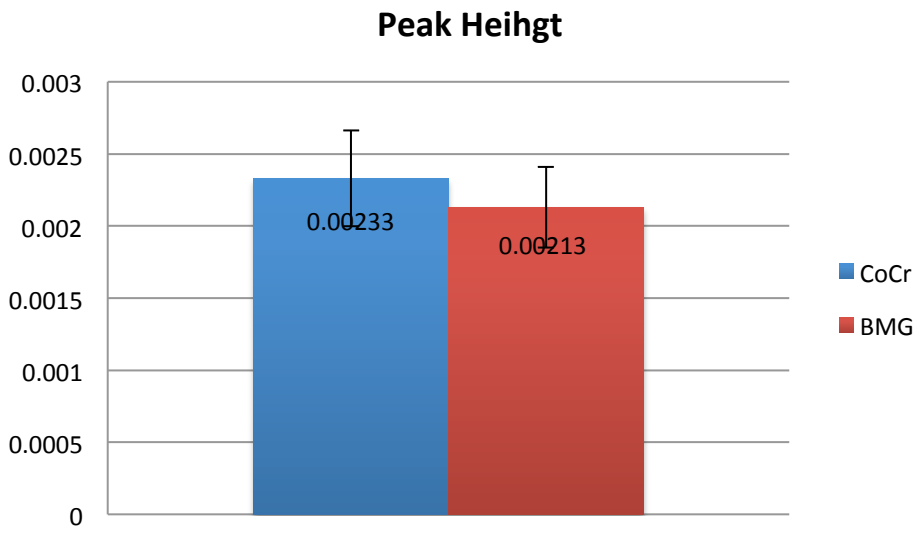

Figure 4.74: Intensity of the amide I band for Co-Co-Mo and BMG following 40 min exposure in PBS with 2 g / l albumin at pH=7.4 and T=20 °C.

4.4.2 Effect of pH

Studying the pH effect, it showed that adsorption of protein to the surface is dependent on pH. Figures 4.75 and 4.76 show that the tendency of protein adsorption becomes higher in lower pH values for both materials. This is related to the surface charge of the protein molecules which is higher at pH=7.4 compared to 5.2. The surface of the protein is negatively charged above the isolelectric point, which is at pH=4.8 for albumin. The repulsive interaction between the albumin molecules is smaller at pH=5.2 and leads to the formation of a more closed packed adsorbed layer on the surfaces.

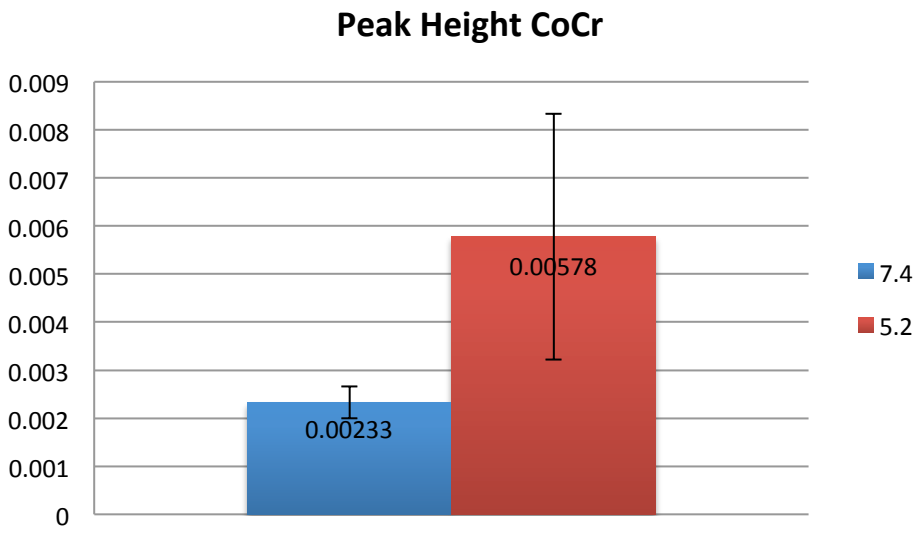

Figure 4.75: Intensity of the amide I band for CoCoMofollowing 40 min exposure in PBS with 2 g / l albumin at pH=5.2 and 7.4, T=20 °C.

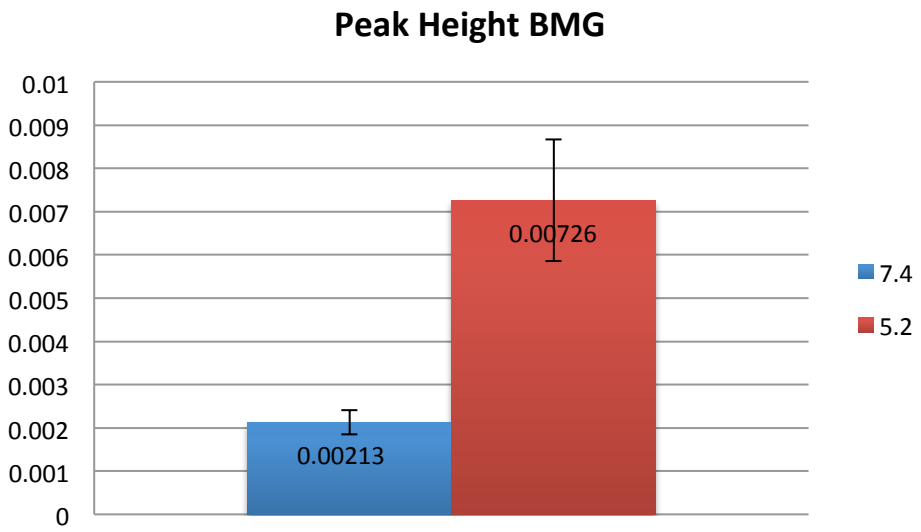

Figure 4.76: Intensity of the amide I band for BMG following 40 min exposure in PBS with 2 g /L albumin at pH=5.2 and 7.4, T=20 °C.

4.4.3 Effect of albumin concentration

It was interesting to know the effect of the albumin concentration on the adsorbed amount of albumin on the surface. Consequently, some experiments were carried out with Co-Cr-Mo BMG samples immersed for 40 minutes in PBS solution with various albumin concentrations. The

height of the amide I peak was measured for several concentrations of protein and in two different pH values.

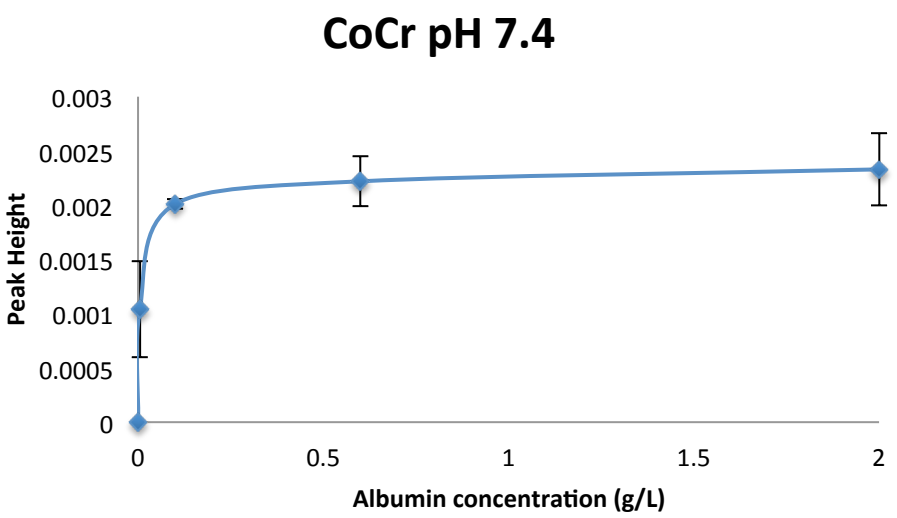

Figure 4.77: Intensity of the amide I band vs. albumin concentration for surgical grade Co-Cr-Mo grade F75. Experimental conditions: T=20°C, pH=7.4 and 40 minutes of immersion.

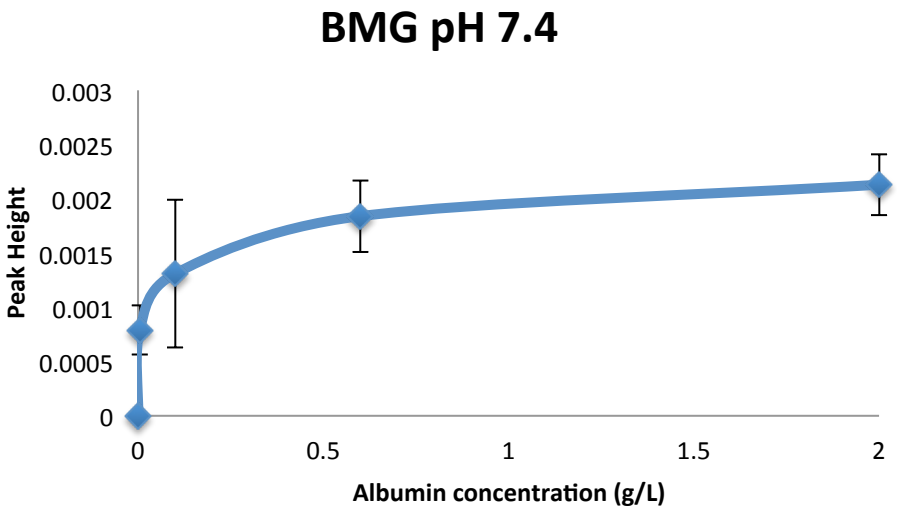

Figure 4.78: Intensity of the amide I band vs. albumin concentration for Zr-based BMG. Experimental conditions: T=20°C, pH=7.4and 40 minutes of immersion.

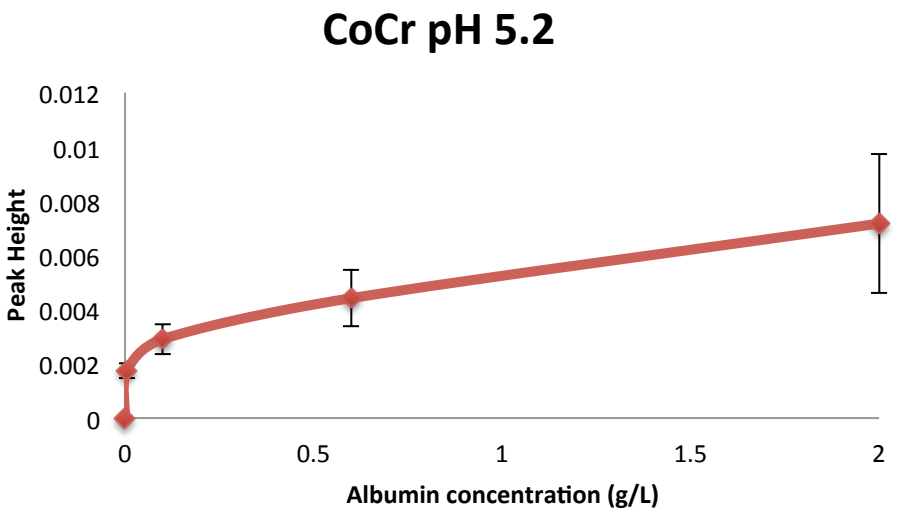

Figure 4.79: Intensity of the amide I band vs. albumin concentration for surgical grade Co-Cr-Mo grade F75. Experimental conditions: T=20°C, pH=5.2 and 40 minutes of immersion.

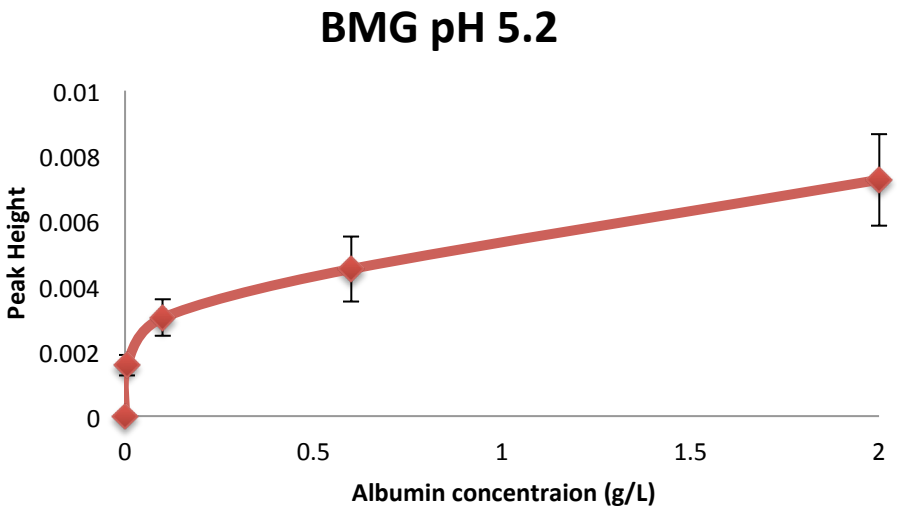

Figure 4.80: Intensity of the amide I band vs. albumin concentration for Zr-based BMG. Experimental conditions: T=20°C, pH=5.2 and 40 minutes of immersion.

The results from this set of experiments are in good agreement with the literature [59 and 70]. The adsorbed amount increases rapidly with increasing protein concentration in the onset of the curve. Nevertheless, a plateau could be noticed from 0.75 g/L and further increase of albumin concentration does not influence on the adsorbed amount so much. This means that from this concentration a saturated monolayer has formed on the material surface.

The surface of a metal after immersion should be composed of two layers. One is from the interaction with the body environment, which creates the formation of an oxide film on the metal surface, whereas the second one consists on a protein adsorption layer (Figure 4.81), although in real 2 layers may not be clearly separated.

Moreover, the albumin concentration in the body fluid (30-50 g/L) is higher than the one employed for the experiments (2 g/L maximum). Consequently, it is possible that there is more than one protein layer on the metal surface, but not necessary bonded together.

Figure 4.81: Surface structure of metal after immersion in solution containing proteins [71].

4.5 Electrochemical Impedance Spectroscopy (EIS)

Potentiodynamic polarization studies are fast and destructive and are not sufficient to completely explain the corrosion mechanism that takes place at the electrolyte/ metal interface [74]. Therefore, measurements using Electrochemical Impedance Spectroscopy was conducted to obtain a deeper understanding of the corrosion behaviour of the materials. In this section, three different materials, SS, Co-Cr-Co and amorphous BMG are compared together in two different temperatures (20 °C and 37 °C) and with or without presence of albumin.

Figure 4.82 shows a set of impedance data for above-mentioned materials in PBS solution and T=20 °C as a Nyquist diagram.

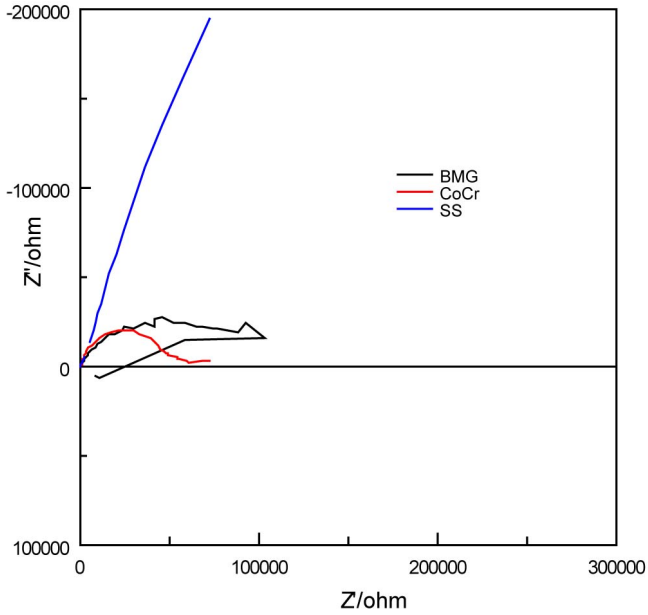

Figure 4.82: Experimental Nyquist plot in PBS, T=20 °C, pH 7.4, after holding the samples at open circuit potential for 1 h.

It can be seen in Figure 4.82 ,Co-Cr-Mo is less corrosion resistance than SS and BMG and SS is the most corrosion resistance. The achieved result matches obtained result from polarization curves data, which was presented in Table 4.6.

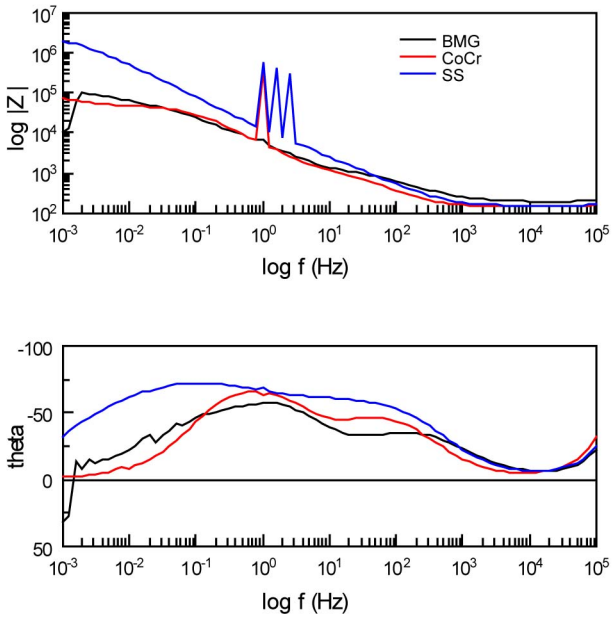

Figure 4.83: Bode plots of EIS data for SS, CoCr and BMG in PBS solution, T=20 °C, pH 7.4.

From the phase angle plot in figure 4.83 it can be seen clearly that CoCr and BMG show two time constant for the corrosion process at the solution metal interface. On the other hand, SS shows broader peak two time constants less clearly detectable. The results indicated that by forming a self-protective oxide layer, SS is has high resistance against corrosion attack.

Next two Figures are the same as 4.82 and 4.83, except experiments were carried out at body temperature (37 °C).

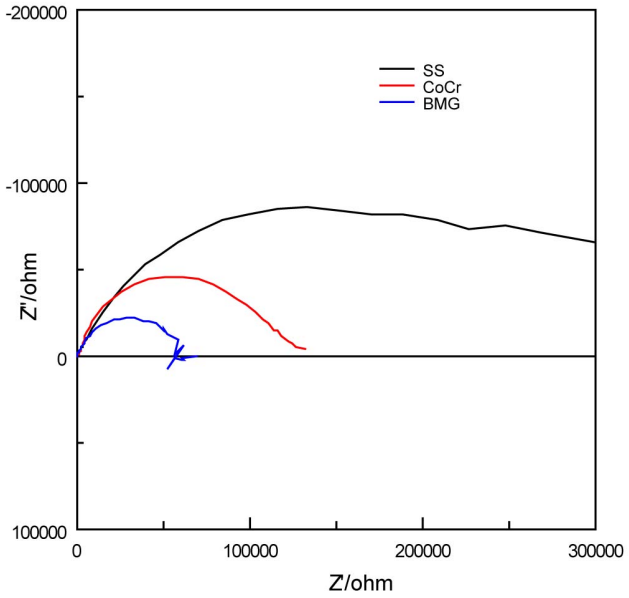

Figure 4.84: Experimental Nyquist plot in PBS, T=37 °C, pH 7.4, after holding the samples at open circuit potential for 1 h.

Above Figure shows that SS is the most corrosion resistive and BMG is the less resistive one. These results shows good co-relation with the result from polarization curves, which was presented in Table 4.6.

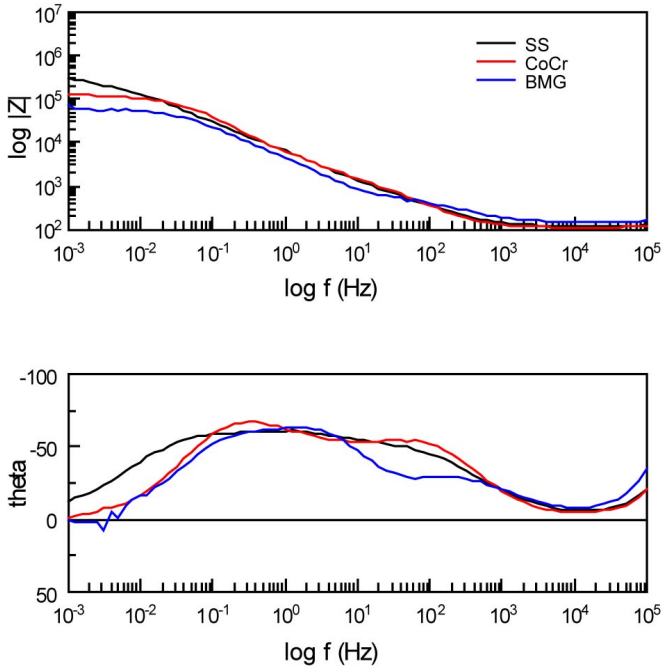

Figure 4.85: Bode plots of EIS data for SS, Co-Cr-Mo and BMG in PBS solution, T=37 °C, pH 7.4.

Considering Figures for three materials in PBS solution, it can be concluded that the behavior of SS, Co-Cr-Mo and BMG does not change much in the narrow range of temperature.

Figure 4.86 and 4.87evaluate the corrosion properties in the electrolyte metal interface with presence of 2g/L albumin in the solution.

Figure 4.86 shows a set of impedance data for above-mentioned materials in PBS with albumin and T=20 °C as a Nyquist diagram.

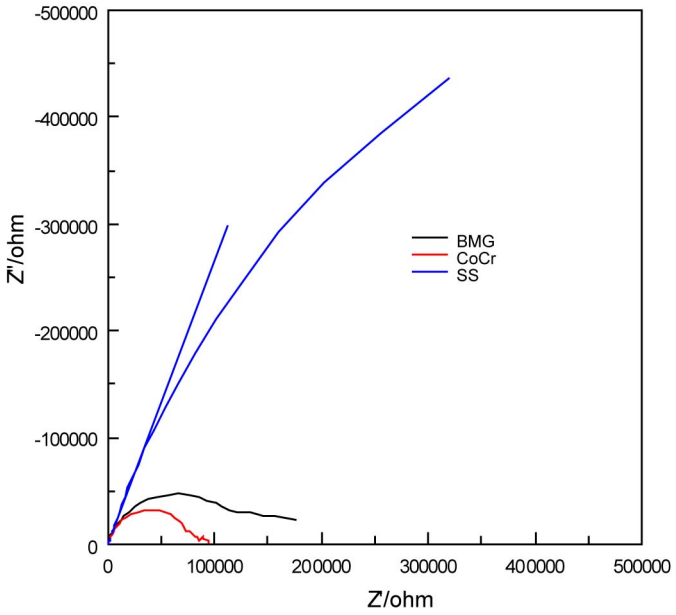

Figure 4.86: Experimental Nyquist plot in PBS with 2g/L albumin, T=20 °C, pH 7.4, after holding the samples at open circuit potential for 1 h.

In the Figure 4.86 it can be seen that SS is the most resistive on against corrosion and Co-Cr-Mo is the weakest on in this conditions. However there is a big shift in the Z' axis, which can be explained by the absorption of protein to the surface, which prohibits electron exchange.

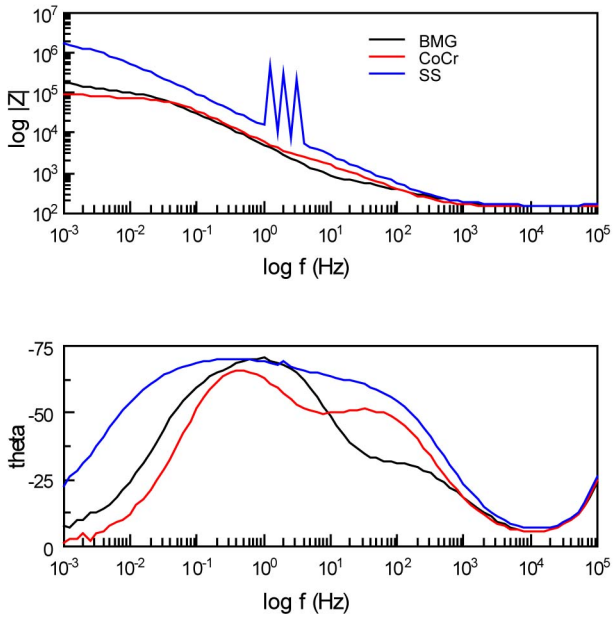

Figure 4.87: Bode plots of EIS data for SS, CoCr and BMG in PBS with 2g/L albumin, T=20 °C, pH 7.4, after holding the samples at open circuit potential for 1 h.

Figure 4.87 also shows that SS has one single broad peak and Co-Cr-Mo and BMG have two time constant.

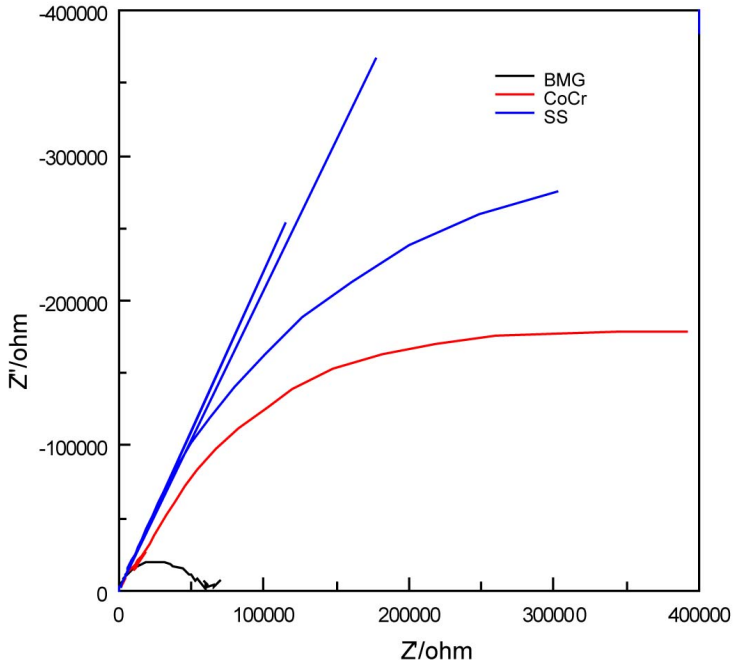

Figure 4.88: Experimental Nyquist plot in PBS with 2g/L albumin, T=37 °C, pH 7.4, after holding the samples at open circuit potential for 1 h.

Considering the above Figure, it can be seen that BMG has the lowest corrosion resistance while SS has the highest one, but the behavior of Co-Cr-Mo has changed a lot in comparison to previous conditions either with albumin or without albumin. It can be assumed that the adsorption of protein to the surface acts like a barrier against electron exchange and increases the corrosion resistivity.

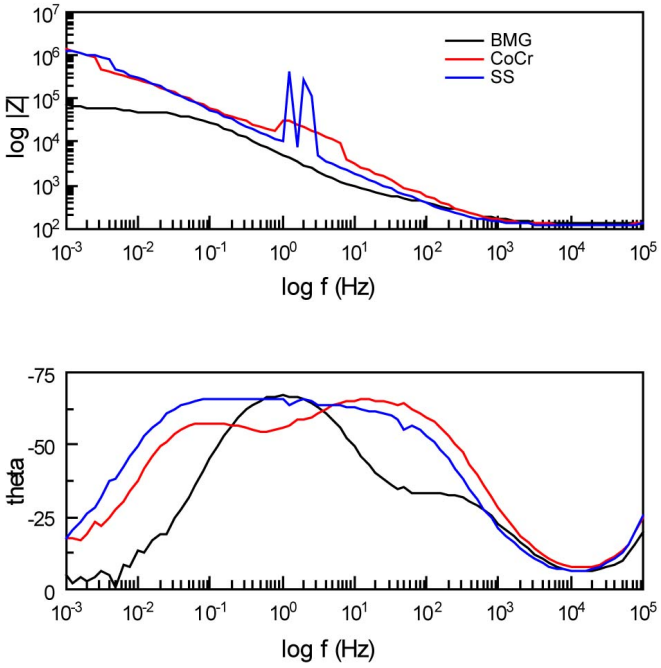

Figure 4.89: Bode plots of EIS data for SS, Co-Cr-Mo and BMG in PBS with 2g/L albumin, T=37 °C, pH 7.4, after holding the samples at open circuit potential for 1 h.

To have an overall overview in this part, it can be said that in the presence of albumin in the electrolyte, the adsorption of protein lead to changes of the electrochemical behaviour and in some cases also an increase in the corrosion resistance.

5. Conclusion

The main objective of this study was to develop the methodology of investigation of bulk metallic glasses for the use of these materials in medical applications. Firstly, there was an attempt to synthesis of BMG in a controlled atmosphere with a resistance vertical furnace. Secondly, the corrosion behavior of common orthopedic material, Co-Cr-Mo and SS 316 LVM was studied and compared with Zr-based BMG in media which simulating a body environment. Moreover, FTIR measurements were performed in order to study the adsorption of the protein albumin on surfaces of Co-Cr-Mo and BMG.

Synthesis of BMG was not successful due to several reasons. A major obstacle is the sensitivity of the BMG to oxygen and there was oxide layer on the surface of preliminary materials. Experiment should be made in a smaller crucible with higher quality raw materials and higher vacuum.

Electrochemical experiments, including OCP measurements, potentiodynamic measurements and electrochemical impedance were performed in simulated biological environments to study the effects of temperature, pH and albumin on the corrosion behavior of Co-Cr-Mo alloy, stainless steel 316 and Zr-based BMG. Each experiment was repeated at least three times to ensure reproducibility of the obtained result. Results varied for different conditions, but generally it can be concluded that BMG showed passive behavior under these conditions. However the passive film on the BMG seems to be less protective compared to SS 316 LVM and Co-Cr-Mo and BMG material was susceptible for pitting corrosion. Variation in temperature between 20 to 37 °C had little effect for all materials while a decrease in pH form 7.4 to 5.2 had minor effects on the passive region for Co-Cr-Mo, increased the tendency for pitting on stainless steel and lowered the breakdown potential significantly for amorphous BMG. A comparison between the BMG and the same material with a crystalline structure showed that the passive region was significantly reduced for the crystalline material.

The presence of albumin in the solution leads to the formation of an adsorbed layer of protein molecules, which affects the electrochemical behavior of the materials. An interesting observation was that the presence of the protein layer decreased the tendency for pitting corrosion of SS316 LVM and crystalline BMG.

The FT-IRRAS technique was employed to study the protein adsorption on the surfaces of BMG and Co-Cr-Mo. In these experiments, substrate material and albumin concentration were varied. By increasing the albumin concentration the amount of adsorbed protein rapidly increased reaching a plateau corresponding to an adsorbed monolayher of albumin. The

amount of adsorbed albumin was similar on the both materials and increases when the pH is decreased from pH = 7.4 to pH = 5.2. The effect of pH is related to the difference in the net electrical charge of the protein acquires above the isoelectric point (pH = 4.8). Due to weaker electrostatic interaction between the albumin molecules is the amount adsorbed on the surface larger at pH=5.2.

There are some suggestions for the future works related to this area. Synthesis of BMG was not that much successful due to many reasons, because BMG is really sensitive to oxygen and there was oxide layer on the surface of preliminary materials. It should be tried to run the experiment in smaller crucible with higher quality raw materials and better vacuum environment.

BMG showed promising properties in this work but more investigations should be done to satisfy all demands for its application as a biomaterial. Since BMG is sensitive to oxygen and oxide layer on the surface of the preliminary materials experiment should be run in a smaller crucible with higher quality raw materials and higher vacuum. The susceptibility for pitting corrosion, the effect of processing parameters, surface conditions and the effect of wear resistant coating the surface are issues which should be addressed in order replace the conventional ones with BMG in biomedical applications.

6. Reference:

1. http://www.hipsurgery.co.il/english/introduction.htm, December 2010.
2. "Total hip replacement, guide for patients", The Evarts Joint Center, Highland Hospital, 1000 south Avenue, Rochester, New York 14620.
3. http://www.eorthopod.com/sites/default/files/images/hip_oa_anatomy01.jpg, December 2010.
4. National Center for Health Statistics, "Health, United States, 2009: In Brief—Medical Technology." Hyattsville, MD. (2010).
5. Canadian Joint Replacement Registry (CJRR), "2005 ReportóTotal Hip and Total Knee Replacements in Canada", Ottawa, Ontario (2005).
6. http://www.patient.co.uk/doctor/Hip-Joint-Replacements-What-a-GP-Needs-to-Know.htm, December 2010.
7. O. Furnes, L. I. Havelin, B. Espehaug, K. Steindal, T. E. Sørås "Annual report 2009, The NorwegianArthroplasty Register" http://www.haukeland.no/nrl/Rapporter/aarsrapporter.htm (2009).
8. J. Kärrholm,G. Garellick,C. Rogmark,P. Herberts "Swedish Hip Arthroplasty Register, Annual Report 2007" http://www.jru.orthop.gu.se/ Department of Orthopedics Sahlgrenska University Hospital (2008).
9. N.J. Hallab, J.J. Jacobs, and J.L. Katz," Biomaterials Science, An Introduction to Materials in Medicine", 2nd ed., ed. B.D. Ratner et al., Amsterdam: Elsevier Academic Press, pp. 526–555 (2004).
10. Furnes, S. A. Lie, L. I. Havelin, L. B. Engesaeters, and S. E. Vollset, "The economic impact of failures in total hip replacement surgery.", Acta Orthop Scand, 67(2):115–121 (1996).
11. A. Bandyopadhyay and S. Bose, "Materials and design of orthopedic devices", In John G. Webster, editor, Encyclopedia of Medical Devices and Instrumentation, pages 187-192, John Wiley & Sons, 2nd edition (2006).
12. L. Zou ,X. Zou ,H. Li, Q. Xue, C. Bünger, "The Influence of Bone Graft Volume and Alendronate Treatment on Spine Fusion" *European Musculoskeletal Review,69-71 (2008).*
13. M. D. Demetriou, A. Wi est, D. C. Hofmann, W. L. Johnson, B. Han, N. Wolfson, G. Wang, P. K. Liaw, "Amorphous Metals for Hard-tissue Prosthesis", JOM, 83-91 (2010).
14. A. L. Greer, "Metallic glasses... on the threshold", Materials Today, 12(1-2), p.14–22 (2009).
15. G. Kumar, H. X. Tang, and J. Schroers, "Nanomoulding with amorphous metals", Nature, 457(12):868–873 (2009).

16. A. Gebert, K. Buchholz, A. Leonhard, K. Mummert, J. Eckert, and L. Schultz, “Investigations on the electrochemical behavior of Zr-based bulk metallic glasses”, Materials Science and Engineering A 267,294– 300 (1999).
17. S. Zhang, T. Ichitsubo, Y. Yokoyama, T. Yamamoto, E. Matsubara, A. Inoue, “Crystallization Behavior and Structural Stability of $Zr_{50}Cu_{40}Al_{10}$ Bulk Metallic Glass”, Materials Transactions, Vol. 50 No. 6, pp. 1340-1345 (2009).
18. Y. Yokoyama, K. Fujita, A.R. Yavari, A. Inoue, “Malleable hypoeutectic Zr–Ni–Cu–Al bulk glassy alloys with tensile plastic elongation at room temperature”, Philosophical Magazine Letters, Vol. 89, No. 5, 322–334 (2009).
19. R. Boyer, G. Welsch, and E. W. Collings,” Materials Properties Handbook: Titanium Alloys”, ASM International (1994).
20. W. Rostoker and J. 0. Galante, ”Materials for human implantation,” J. Biomech. Eng., 101, 2-14 (1979).
21. J. D. Witt, M. Swann, “Metal wear and tissue response in failed titanium alloy total hip replacements”, Journal of Bone and Joint Surgery - British Volume, Vol 73-B, Issue 4, 559-563 (1991).
22. *M*. *Kawahara*, “Effects of aluminum on the nervous system and its possible link with neurodegenerative diseases”, *J*. *Alzheimer Disease*, vol. *8*, *pp*. *171-182* (*2005).*
23. D. A. Basketter, L. I. Lea, J. K. Cooper, C. A. Ryan, G. F. Gerberick, R. J. Dearman, I. Kimber, “Identification of metal allergens in the local lymph node assay”, American Journal of Contact Dermatitis Vol. 10, issue 4, pp. 207-212 (1999).
24. G.F. Nordberg, B.A. Fowler, M. Nordberg, L. Friberg, “Handbook on the Toxicology of Metals”, 3rd edition, Elsevier Academic Press, pp. 84-86 (2007).
25. W. KLEMENT JUN., R. H. WILLENS, POL DUWEZ, “Non-crystalline Structure in Solidified Gold–Silicon Alloys”, Nature 187, 869 – 870 (1960).
26. A. Inoue, K. Ohtera, K. Kita, and T. Masumoto, “New amorphous Mg–Ce–Ni alloys with high-strength and good ductility”, Jpn. J. Appl. Phys. Part 2 27(12), L2248–L2251 (1988).
27. A. Inoue, T. Zhang, and T. Masumoto, “Al–La–Ni amorphous-alloys with a wide super cooled liquid region”, Mater. Trans. JIM 30(12), 965–972 (1989).
28. A. Inoue, T. Zhang, and T. Masumoto, “Zr–Al–Ni amorphous-alloys with high glass transition temperature and significant super cooled liquid region”, Mater. Trans. JIM 31(3), 177–183 (1990).
29. M. Miller, P. Liaw, “Bulk Metallic Glasses: An Overview”, Springer, pp. 1-2 (2008).
30. D. Turnbull, “The Liquid State and The Liquid-Solid Transition”, Trans. AIME vol.221 pp.422 (1961).

31. D. Turnbull, “Liquids: Structure, Properties, Solid Interactions”, T. J. Hughel, ed.), pp.6-24, Elsevier Publishing Co., New York (1965).
32. A. L. Greer, “Confusion by Design”, Nature vol.366 pp.303 (1993).
33. A. Inoue, N. Nishiyama, H. M. Kimura, “Preparation and Thermal Stability of Bulk Amorphous $Pd_{40}Cu_{30}Ni_{10}P_{20}$ Alloy Cylinder of 72 mm in Diameter”, Master. Trans., JIM (38)179-183 (1997).
34. X. H. Lin, W. L. Johnson, “ Formation of Ti-Zr-Cu-Ni bulk metallic glasses”, J. Appl. Phys. 78 (11) (1995).
35. A. Inoue, A. Takeuchi, “ Recent progress in bulk glassy, nanoquasicrystalline ans nanocrystalline alloys”, Materials Science and Engineering A 375-377, pp. 16-30 (2004).
36. J. D. Bernal, J. Mason, “Packing of Spheres: Co-ordination of Randomly Packed Spheres”, Nature 188, 910 – 911 (1960).
37. M. D. Demetriou, M. E. Launey, G. Garrett, J. P. Schramm, D. C. Hofmann, W. L. Johnson, R. O. Ritchie, “A damage tolerant glass”, Nature Materials 10, 123-128 (2011).
38. W. L. Johnson, K. Samwer, “A Universal Criterion for Plastic Yielding of Metallic Glasses with a $(T/T_g)^{2/3}$Temperature Dependence”, Physical Review Letters 95, 195501 (2006).
39. J.R. Davis, “Handbook of Materials for Medical Devices”, Materials Park, OH: ASM International, pp. 106 - 111 (2003).
40. M. L. Morrison, R. A. Buchanan, P. K. Liaw, B. A. Green, G. Y. Wang, C. T. Liu, J. A. Horton, “Corrosion–fatigue studies of the Zr-based Vitreloy 105 bulk metallic glass”, Materials Science and Engineering, A 467, pp. 198–206 (2007).
41. J.J. Lewandowski, W.H. Wang, A.L. Greer,” Intrinsic plasticity or brittleness of metallic glasses”, Philosophical Magazine Letters, 85, pp. 77–87 (2005).
42. J. Black, “Biological Performance of Materials: Fundamentals of Biocompatibility”, 4th Edition, Boca Raton, FL: CRC Press, (2006).
43. http://bagofbirds.files.wordpress.com/2008/02/20080219_102_350x263.jpg, February 2011.
44. R. Huiskes H. Weinans, B. Vanrietbergen, “Clinical Orthopedics and Related Research” 274, pp. 124-134, (1992).
45. K.J. Bundy, C.J. Williams, R.E. Luedemann, “Stress-enhanced ion release - The effect of static loading“, *Biomaterials* Volume 12, Issue 7, pp. 627–639 (1991).
46. N. Homazava, A. Shkabko, D. Logvinovich, U. Krähnenbühl, A. Ulrich, “Element-specific in situ corrosion behavior of Zr-Cu-Ni-Al-Nb bulk metallic glass in acidic media studied using a novel mcrocapillary flow injection inductively coupled plasma mass spectrometry technique”, Intermetallics, 16:1066–1072, (2008).
47. L. Liu, C. L. Qiu, C. Y. Huang, Y. Yu, H. Huang, S. M. Zhang, “Biocompatibility of Ni-free Zr-based bulk metallic glasses”, Intermetallics,17:235–240, 2009.

48. http://www.chem1.com/acad/webtext/elchem/EC-images/corrosion_iron.gif, February 2011.
49. ASM Handbook online, Volume 13A, "Corrosion: fundamentals, Testing and Protection", (2010).
50. C. -O. A. Olsson, D. Landolt, "Passive film on stainless steel- chemistry, structure and growth", Electrochimica Acta 48, pp.1093-1104, (2003).
51. J. A. Helsen, Y. Missirlis, "Biomaterials: A Tantalus Experience (Biological and Medical Physics, Biomedical Engineering)", Springer; 1st Edition, (2010).
52. *Z. Ahmad, "*Principles of Corrosion Engineering and Corrosion Control", Elsevier, (2006).
53. P. Sury, "Corrosion behavior of cast and forged implant materials for artificial joints, particularly with respent to compound designs", Corrosion science Vol. 17, pp. 155-169, (1977).
54. http://www.corrosion-doctors.org/, March 2011.
55. M. Traisnel, D. le Maguer, H. F. Hildebrand, A. Iost, "Corrosion of Surgical Implants", Clinical Materials 5, 309-318, (1990).
56. http://www.corrosion-club.com/intergr.htm, March 2011.
57. O. E. M. Pholer,"Failure of orthopedic metallic implants", ASM handbook on failure analysis and prevention, 9th ed. (Metals Park, OH: ASM International) vol. 11, p 670, (1986).
58. C. Martin, "Electrochemical study of alloys for implants", Master degree project, Royal Institute of Technology, (2010).
59. http://searchwarp.com/UserImages/180983/jointdiagram.jpg, March 2011.
60. http://www2.hawaii.edu/~chungeun/hsa5.jpg, April 2011.
61. Fuss C., Palmaz J. C., Sprague EA., "Fibrinogen: structure, function, and surface interactions", J Vasc InterV.Radiol. 12, Pages: 677-682, (2001).
62. http://www.umcutrecht.nl/subsite/respiratorymedicine/Research/Inflammation-The-role-of-the-lung-and-neutrophil-margination.htm, May 2011.
63. S. Hiromoto, A.-P. Tsai, M. Sumita, T. Hanawa, "Effect of pH on the polarization behavior of Zr65Al7.5Ni10Cu17.5 amorphous alloy in a phosphate-buffered solution", Corrosion Science 42, pp. 2193-2200, (2000).
64. R. W. Revie, N. D. Greene, "Corrosion behaviour of surgical implant materials II. Effects of surface preparation", Corrosion Science 9, pp. 763-770, (1969).
65. D. Sharnan, "The Problem of Corrosion in Orthopedic Implant Materials", Orthopaedic Update (India), Vol. 9, No. 1, (1999).
66. M. Nezafati, "Study over Corrosion properties and ion release of Zr55Cu30Ni5Al10 Bulk Metallic Glass for hip joint implants", Master degree project, Royal Institute of Technology, (2010).

67. Biological evaluation of medical devices Part 15: Identification and quantification of degradation products from metals and alloys, ISO 10993-15:2000.
68. M. Skjellerudsveen, “Zr55Cu30Ni5Al10 Bulk Metallic Glass –Preparation of amorphous metal and the possibility of its application as articulating surface material in an artificial hip joint”, Master degree project, Norwegian University of Science and Technology, Trondheim (2010).
69. A.W.E. Hodgson, S. Kurza, S. Virtanen, V. Fervel, O.A. Olsson, S. Mischler. Electrochimica Acta vol.49 pp.2167–2178 (2004).
70. M. J. Desroches, N. Chaudhary, “PM-IRRAS Investigation of the interaction of serum Albumin and Fibrinogen with a biomedical-grade stainless steel 316LVM surface”, Biomacromolecules, 8, 2836-2844, (2007).
71. A.Igual Munoz, S. Mischler, “Interactive Effects of Albumin and Phosphate Ions on the Corrosion of CoCrMo Implant Alloy”, J. Electrochem. Soc., Volume 154, Issue 10, pp. C562-C570 (2007).
72. S. Hiromoto, A.-P. Tsai, M. Sumita, and T. Hanawa, “Effect of chloride ion on the polarization behavior of the Zr65Al7.5Ni10Cu17.5 amorphous alloy in phosphate buffered solution”, *Corrosion Science*, 42, 1651-1660 (2000).
73. U.K. Mudali, S. Baunack, J. Eckert, L. Schultz, A. Gebert, “Pitting corrosion of bulk glass-forming zirconium-based alloys”, Journal Of Alloys & Compounds, Vol. 377, pp.290-297, (2004).
74. F.X. Qin, X.M. Wang, G.Q. Xie, K. Wada, M. Song, K. Furuya, K. Asami, A. Inoue, “Microstructure and electrochemical behavior of Ti-coated$Zr_{55}Al_{10}Ni_5Cu_{30}$ bulk metallic glass”,Intermetallics, Volume 17, Issue 11, Pages 945-950, (2009).